Somatotopic Precision of Whisker Tuning in Layer 2/3 of Rat Barrel Cortex

by

Samuel Harding Forrester

A dissertation submitted in partial satisfaction of
the requirements for the degree of

Doctor of Philosophy

in

Neuroscience

in the

Graduate Division

of the

University of California, Berkeley

Committee in charge:

Professor Daniel Feldman, Chair
Professor Hillel Adesnik
Professor Linda Wilbrecht
Professor Terrence Deacon

Spring 2017

ABSTRACT

Somatotopic Precision of Whisker Tuning in Layer 2/3 of Rat Barrel Cortex

by

Samuel Harding Forrester

Doctor of Philosophy in Neuroscience

University of California, Berkeley

Professor Daniel Feldman, Chair

Chapter 1: Somatosensory maps in rodents & primates—a review

This chapter reviews basic principles and recent findings in primate, human, and rodent somatosensory maps. Topographic maps of the body surface are a major feature of somatosensory cortex. In primates, parietal cortex contains four somatosensory areas, each with its own map, with the primary cutaneous map in area 3b. Rodents have at least three somatosensory areas, and the whisker map in rodent primary somatosensory cortex is a canonical system for studying cortical microcircuits, sensory coding, and map plasticity.

Maps are not isomorphic to the body surface, but magnify behaviorally important skin regions, which include the hands and face in primates, and the whiskers in rodents. Within each map, intracortical circuits process tactile information, mediate spatial integration, and support active sensation. Functional representations are more overlapping than suggested by textbook depictions of map topography. Maps may also contain fine-scale representations of touch sub-modalities, or direction of tactile motion. In addition, somatosensory maps are plastic throughout life in response to altered use or injury.

Chapter 2: Somatotopic precision of whisker tuning in layer 2/3 of rat barrel cortex

Although cortical maps of the sensory periphery are topographically organized at a large scale, the fine-scale precision of the map at the level of neighboring cells varies between species, sensory modalities, and cortical layers. In rodent somatosensory cortex, where each whisker is mapped to a dedicated cortical column, cells in layer 4 of each column are predominantly tuned to the appropriate whisker (columnar whisker; CW). However, in mice, cells in the upper cortical layers display locally heterogeneous "salt-and-pepper" tuning. It remains unclear whether the same heterogeneity is found in the upper layers of the rat whisker map. To address this question, we examined whisker tuning in regular-spiking (RS) and fast-spiking (FS) units recorded from layer 2/3 whisker columns in anesthetized rats. Among RS units, we observe a narrow majority (59%) best tuned to the CW; a clear majority (88%) with the CW among a statistically comparable group of "equal best" whiskers; and a small number (12%) of units best driven by one or more surround whiskers and poorly responsive to the CW. CW-tuned units display

sharper tuning and faster responses to their best whisker than non-CW-tuned units, but are distributed evenly along vertical and horizontal dimensions of the column. These results demonstrate tuning in rat L2/3 that is more homogeneous than in mouse layer 2, but less so than in rat or mouse layer 4. FS units are tuned to the CW more frequently (78%) than RS units, consistent with broadly sampled input from local excitatory cells most responsive, as a group, to the columnar whisker.

ACKNOWLEDGEMENTS

Thanks first to Dan Feldman, who has been a patient, dedicated, and gifted mentor—and an excellent P.I., which involves doing a diverse assortment of jobs very well, all at once. I am profoundly glad, right now more than ever, that labs like Dan's continue to ask and answer questions with unflagging rigor and creativity. I will always be grateful, and better off, for the privilege of working in the Feldman lab these past six years. Thanks are also due to the members of my thesis committee—Linda Wilbrecht, Hillel Adesnik, and Terrence Deacon—and, before them, my qualifying exam committee and rotation supervisors (Rich Kramer, Yang Dan, Kristin Scott, Polina Lishko). Each provided unfailingly constructive feedback over the course of my time at Berkeley.

In the Feldman lab, I had the honor of working with the most fun and gifted labmates I could have hoped for: Melanie Gainey, Justin Elstrott, Kelly Clancy, Dave House, Joe Goldbeck, Amy LeMessurier, Olivia Pourzia, Leah McGuire, Tomer Langberg, Joe Aman, Michelle Antoine, Han Chin Wang, Toshio Miyashita, Ray Shao, Renna Wolfe, Lu Li, and our incomparable manager Katie Dorsch—not to mention the wonderful people in Marla Feller's lab next door. I was especially fortunate to work alongside Brian Isett, who was a brilliant and supportive friend throughout my time in the lab, and the kind of colleague any workplace is lucky to have. And I owe a deep debt of gratitude to Keven Laboy and Phil Schnepel, whose good company and tireless problem-solving made inestimable contributions to my own project. Thanks also to Mochi Lu, Michael Nemeh, Deborah Yip, and Suchetana Dutta, for their skillful assistance with key technical aspects of my work.

Outside of lab, I was lucky to arrive at Berkeley with the entering neuroscience class of 2010—notably Levi Gadye, Sam Israel, and Tyler Lee, who each helped make teaching neuroscience a rewarding part of my graduate experience. I'm particularly grateful to Mike Levy, for endless hours of good conversation and good food, and to Vanessa Carels, for leavening so many days on campus with wit and decency and insight. And I will always appreciate the help and support I received from Kati Markowitz—our dynamite program administrator during my first couple of years—and from her successor, Candace Groskreutz.

Thanks also to Dan Higgins, Travis Curtis, Maria Elena Frias, Nathan Rausch, Nathan Fredrickson, Austin Gillison, Eric Garcia, and Micah Ludeke, for keeping my life in San Francisco full of laughter and drama and storytelling. To Mark Tanaka, for the great gift of a roof over my head, and to my vibrant and considerate housemates Nikki Vezina, Julia Whistler, Hana Haber, and Jaan Shenberger. To Benjamin Clegg, for being a consummate friend and a model naturalist and teacher. And to Esteban Ortiz, for being unassumingly extraordinary, and everything I hoped for, which was a great deal.

Finally, thanks above all to my parents, Margaret and Jeshel; my step-parents, Keziah and Mark; and my siblings Joe, Lucy, Georgette, Charlotte, Haz, and Ella. I am forever grateful for all their love and support during my many years spent far away, and delighted to find them as generous and creative as ever now that I've returned.

For Louis Ward IV

TABLE OF CONTENTS

Chapter 1: Somatosensory maps in primates & rodents—a review 1
Introduction 1
1.1. Somatosensory maps in primates 2
1.1.1. Multiple somatotopic maps in parietal cortex 2
1.1.2. Summary of ascending pathways for cutaneous stimuli in primates 3
1.1.3. Somatotopic discontinuities and the genital representation 4
1.1.4. Somatotopy of the trigeminal representation 4
1.1.5. Somatotopy of the hand and foot representations 5
1.1.6. Spatial precision and integration in cortical sensory coding of touch 6
1.1.7. Segregation of RA and SA responses into distinct columns 7
1.2. Somatosensory maps in rodents 8
1.2.1. Overview of rodent somatotopic maps 8
1.2.2. The column as a modular unit of cortical organization 9
1.2.3. Ascending pathways for whisker input to S1 10
1.2.4. Cortical circuitry in whisker columns 11
1.2.5. Functional organization of the whisker map 11
1.2.6. Response dynamics and multi-whisker integration 12
1.2.7. Maps of whisker deflection direction and other parameters 13
1.3. Determinants of cortical magnification in somatosensory maps 13
1.4. Plasticity of somatosensory maps 14
1.4.1. Overview of map plasticity 14
1.4.2. Somatosensory map plasticity in non-human primates 15
1.4.3. Somatosensory map plasticity in humans 16
1.4.4. Somatosensory map plasticity in rodents 17
1.4.5. Mechanisms of somatosensory map plasticity 18
1.4.6. Relevance to recovery of function after stroke or peripheral injury 19
1.5. Conclusion 20
1.6. Figures for Chapter 1 21

Chapter 2: Somatotopic precision of whisker tuning in layer 2/3 of rat barrel cortex 31
Introduction 31
2.1. Materials and Methods 32
2.1.1. Surgery, anesthesia, and whisker mapping 32
2.1.2. Whisker stimuli 33
2.1.3. Extracellular recording 33
2.1.4. Histology 33
2.1.5. Spike sorting 34
2.1.6. Data analysis 34
2.2. Results 35
2.2.1. Tuning does not differ systematically under caudal and rostral stimuli 36
2.2.2. The columnar whisker is usually among the best whiskers for regular-spiking units, but often not the absolute best 37
2.2.3. Whisker tuning curves reveal regular-spiking units sharply tuned to the columnar whisker or to surround whiskers 38
2.2.4. CW- and non-CW regular-spiking units: comparison of whisker latencies, depth, and location within the column 39
2.2.5. Fast-spiking units are more frequently tuned to the columnar whisker 40
2.3. Discussion 41
2.3.1. Laminar and species differences in local tuning heterogeneity of regular-spiking cells 41
2.3.2. Homogeneous columnar whisker tuning among fast-spiking cells 43
2.3.3. Conclusion and future questions 43
2.4. Figures & Tables for Chapter 2 45

References 73
Chapter 1 73
Chapter 2 99

LIST OF FIGURES

Figures for Chapter 1

Figure 1.1: Somatosensory pathways and maps in primates.

Figure 1.2: Somatotopic maps in humans.

Figure 1.3: Somatosensory maps in rats and mice.

Figure 1.4: Map plasticity in primates and rodents.

Figures & Table for Chapter 2

Figure 2.1: Whisker stimuli and recording from verified whisker columns.

Figure 2.2: Single-unit sorting and identification of regular- and fast-spiking units.

Figure 2.3: Whisker tuning and onset latency under rostral versus caudal stimuli.

Figure 2.4: Best whisker identity in regular-spiking units.

Figure 2.5: Nine-whisker tuning curves of regular-spiking units.

Figure 2.6: Tuning curves for all regular-spiking units.

Figure 2.7: CW vs. BW onset latencies in regular-spiking units.

Figure 2.8: Regular-spiking unit tuning properties by location within the whisker-column.

Figure 2.9: Fast-spiking units are tuned to the CW more frequently than regular-spiking units.

Table 2.1: Tuning properties and recording parameters for all analyzed units, by tuning group.

Supplemental Figure 1: Tuning properties of regular-spiking units under minimal-amplitude (0.5°) stimuli only.

Supplemental Figure 2: BW and CW tuning scores for regular-spiking units as a function of mean BW-evoked spikes per stimulus.

Supplemental Figure 3: Tuning properties of regular-spiking units from upper L2/3 and from lower L2/3.

CHAPTER 1:
SOMATOSENSORY MAPS IN PRIMATES & RODENTS—A REVIEW

INTRODUCTION

A fundamental feature of primary somatosensory, visual, and auditory cortex is the topographic mapping of the peripheral sensory epithelium and other sensory parameters. Sensory maps develop from a combination of molecular cues and activity-dependent developmental processes, and co-localize neurons that have similar functions. This is thought to provide an adaptive minimization of wiring costs, both within a brain region (by arranging functionally connected cells proximally) and across regions in a processing hierarchy (by facilitating connections between cells that process the same sensory parameters) (reviewed in Kaas, 1997; Chklovskii & Koulakov, 2004; Wilson & Bednar, 2015; Bednar & Wilson, 2016). The somatosensory areas of human parietal cortex contain multiple topographic maps of the body surface, famously depicted by Penfield and colleagues as the "homunculus" (Penfield & Rasmussen, 1950). Knowledge of the layout and wiring of somatotopic maps is key to understanding normal somatosensory processing. Maps are also plastic in response to experience and injury, and the study of map plasticity holds promise for therapeutic interventions to improve somatosensory recovery after injury.

Critical early evidence for somatotopic maps came from Jackson's observation that the sensations and movements associated with epileptic seizures followed orderly progressions over the body surface, reflecting the spatial spread of neural activity across maps in the originating brain regions (Jacksonian march; Hughlings Jackson, 1868, 1873; Charcot, 1887). Maps in motor cortex were then confirmed by Sherrington and colleagues in non-human primates (Leyton & Sherrington, 1917). Penfield and Boldrey subsequently demonstrated a somatotopic map for tactile sensation in the human anterior parietal cortex, based on percepts elicited in epileptic patients by cortical stimulation during surgery (1937; cf. Cushing, 1909); this map was later schematized as the homunculus. At the same time, Woolsey, Adrian and others recorded cortical potentials in anterior parietal cortex of anesthetized monkeys elicited by tactile stimuli, and suggested a similar somatotopy common across primates (Marshall et al., 1937, 1941; Adrian, 1941; Woolsey, 1952). Subsequent studies confirmed the existence of somatotopic maps in the primary somatosensory cortex of other mammals, most notably rodents (Woolsey & van der Loos, 1970; reviewed in Krubitzer et al., 2011).

The modern study of primate somatosensory maps began with the discovery that anterior parietal cortex contains not one but four complete representations of the body, each following the mediolateral layout described by Penfield and Woolsey but contributing distinctly to somatosensory processing (Paul et al., 1972; Merzenich et al., 1978; Kaas et al., 1979). Equally important was the finding that even the mature brain exhibits robust map plasticity in response to injury (Merzenich et al., 1983a, 1983b) or changes in sensory use (Jenkins et al., 1990). In addition to primate studies, the cortical map of the whiskers in rats and mice has proved an invaluable model for studying both the neural circuits underlying normal somatotopy and the mechanisms of map plasticity. More recent work in primates and rodents has examined the

dynamics of map activation in awake animals. This review will survey current knowledge of the organization, function, and plasticity of somatosensory maps in primates and rodents.

1.1. SOMATOSENSORY MAPS IN PRIMATES

1.1.1. Multiple somatotopic maps in parietal cortex

In primates, four adjacent areas in the anterior parietal cortex (cytoarchitectonic areas 3a, 3b, 1, and 2) comprise the first stages in cortical somatosensory processing. Each area contains a separate, topographically organized representation of the contralateral body and face (Kaas et al., 1979; Krubitzer et al., 2004) (Figure 1B). Area 3a mainly represents deep (muscle) inputs (Iwamura et al., 1983a). By contrast, areas 3b, 1, and 2 are thought to represent successive stages in the early cortical processing of cutaneous stimuli (reviewed in Qi et al., 2008). Area 3b is the main recipient of cutaneous tactile input ascending from the ventro-posterior thalamus, and thus contains the primary cutaneous map in cortex; it is the homologue of the primary somatosensory cortex (S1) of lower mammals (Kaas, 1983). Area 3b sends output to area 1 (Garraghty et al., 1990a), establishing a second cutaneous map. Areas 3b and 1 both project to area 2, which thus contains a third cutaneous map, and integrates it with a representation of deep inputs. Adjacent to the four anterior parietal areas are two additional somatosensory areas in lateral parietal cortex: the secondary somatosensory cortex (S2; Burton et al., 1995; Ruben et al., 2001, in humans) and the parietal ventral area (PV; Krubitzer & Kaas, 1990; Krubitzer et al., 1995; Qi et al., 2002; Disbrow et al., 2000, in humans). These areas contain less precise somatotopic maps, and are thought to mediate higher-order and inter-hemispheric somatosensory processing (Krubitzer et al., 1995; Disbrow et al., 2001, 2003), which depends on input from the anterior parietal areas (Pons et al., 1987a; Burton et al., 1990; Garraghty et al., 1990b).

The somatotopy of tactile maps in all four anterior parietal areas (3a, 3b, 2, and 1) is known in detail, primarily from extracellular unit recordings in anesthetized monkeys. These studies mapped receptive fields using near-threshold indentation of the skin with hand-held probes, in both macaques (Nelson et al., 1980; Pons et al., 1985a, 1985b, 1987b; Rothemund et al., 2002; Krubitzer et al., 2004) and New World monkeys (Merzenich et al., 1978; Kaas et al., 1979; Sur et al., 1980, 1982; Felleman et al., 1983; Carlson et al., 1986; Cusick et al., 1989). Three major features of somatotopic maps are evident (Figure 1.1B; Figure 1.2A), consistent with Penfield and Woolsey's early recordings. First, each area maps tactile input in a mediolateral progression of foot, hindlimb, trunk, neck, forelimb, hand, face, and oral features. Second, adjacent maps roughly mirror each other across area borders, such that rostro-caudal somatotopy is reversed in adjacent areas (Kaas et al., 1979; Krubitzer et al., 2004); this same mirrored organization occurs between adjacent S2 and PV (Krubitzer & Kaas, 1990; Krubitzer et al., 1995; Qi et al., 2002). Finally, hand, foot, and lower face/mouth/oral structures are magnified within the map, relative to other inputs, and magnification across body regions is inversely correlated with the receptive field size of cortical cells (Sur et al., 1980; see section 1.3).

The somatotopic map in area 3b includes anatomically distinct modules corresponding to specific body regions. This is evident from myelin staining in cortical layers (L) 3 and 4, which

reveals modules as myelin-rich regions bounded by myelin-poor septa. These modules are present at infancy (Qi & Kaas, 2004), and correspond to the representations of individual digits (Jain et al., 1998a; Qi & Kaas, 2004), as well as orofacial features (Kaas et al., 2006; Iyengar et al., 2007) (Figure 1.1C). Boundaries between the modules correspond to discontinuities in the cutaneous receptor distribution. Cortical modules are even clearer in rats and mice (see section 1.2.1).

Many of the basic features of somatotopic maps described in non-human primates have also been observed in humans, using measures of hemodynamic activation in response to stimuli (e.g., intrinsic signal optical imaging (ISOI) and functional magnetic resonance imaging (fMRI)). In the next sections, we summarize the ascending pathways that bring tactile input to cortex, and review areas of recent discovery in map topography and function.

1.1.2. Summary of ascending pathways for cutaneous stimuli in primates

The cutaneous afferent pathways to cortex are well described, and contain somatotopic maps at each subcortical processing stage (Figure 1.1A). Glabrous skin contains a range of morphologically, functionally, and molecularly distinct low-threshold tactile afferents. These are classified into four functional types: rapidly adapting (RA) types 1 and 2 (RA1, RA2), and slowly adapting (SA) types 1 and 2 (SA1, SA2). Hairy skin contains distinct afferents associated with the follicles (reviewed in Abraira & Ginty, 2013). From the body, cutaneous primary afferents run in the spinal nerves, enter the spinal cord, and ascend via the dorsal columns to synapse onto cells in the ipsilateral dorsal column nuclei. These second-order cells project across the midline to synapse in the contralateral ventro-posterior lateral nucleus of the thalamus (VPL), which in turn projects to the body representation in areas 3b and 1 of somatosensory cortex. From the face, afferent axons run in the trigeminal nerve, and enter the brainstem to synapse in the principal trigeminal nucleus (PrV). These second-order cells project across the midline to the thalamic ventro-posterior medial nucleus (VPM), which projects to the face representation in areas 3b and 1 (Rausell et al., 1998; Padberg et al., 2009). In area 3b, thalamo-cortical axons from VPL and VPM principally target L4, the main input layer (Jones, 1975; Nelson & Kaas, 1981). In area 1, VPL and VPM axons target L3, and are thought to modulate the stronger driving input to L4 received from area 3b (Nelson & Kaas, 1981; Garraghty et al., 1990a). VPL and VPM project less extensively to other areas in somatosensory cortex, such that relays between cortical areas establish serial processing of cutaneous stimuli along a 3b $\rightarrow$ 1 $\rightarrow$ 2 $\rightarrow$ S2/PV pathway (Randolph & Semmes, 1974; Pons et al., 1992; Eskenasy & Clarke, 2000, in humans). Receptive field sizes generally increase at successive stages of this pathway (Sur et al., 1985; Fitzgerald et al., 2006). In area 1, this reflects broader intra-areal connectivity (Ashaber et al., 2014), in addition to a minority of non-homotopic projections from area 3b (Wang et al., 2013).

Orderly somatotopic maps exist at each stage of subcortical processing (dorsal column and trigeminal nuclei; VPL and VPM; Figure 1.1A). Each of these subcortical maps contains magnified representations of the hand and mouth, and discrete, bounded anatomic modules representing individual digits, or specific body and face regions (in brainstem, Florence et al., 1991; Qi & Kaas, 2006; in thalamus, Mountcastle & Henneman, 1952; Jones & Friedman, 1982; Kaas et al., 1984; Qi et al., 2011; Sawyer et al., 2015; reviewed in Kaas, 2008). Therefore, the

magnification and modules apparent within the maps in areas 3b and 1 are inherited from subcortical representations and refined in cortex, rather than being synthesized de novo.

1.1.3. Somatotopic discontinuities and the genital representation

Penfield's homunculus contained two substantial discontinuities: the representation of the face and hand adjacent to each other (Figures 1.1B, 1.2A), and the representation of the genitals immediately ventral to the foot on the medial wall of the cortex. The face–hand discontinuity is common across primates and some other mammals, derives from the segregation of VPL and VPM inputs to the cortex (Krubitzer & Kaas, 1987; Parpia, 2011), and is reflected in the "Jacksonian march" of somatic sensations in some cases of epilepsy (e.g., from face to fingers; Mauguiere & Courjon, 1978). Neural tracing studies in monkeys have demonstrated extensive horizontal connections within the hand, and other cervical nerve dermatome representations, as well as internally within the face representation, but few horizontal connections crossing between the hand and face regions (Manger et al., 1997; Fang et al., 2002). Thus, hand and face representations are neighboring, but not heavily interconnected.

The location of the genital representation has been called into doubt by several mapping studies. Microelectrode recordings in macaques of both sexes revealed a small representation of the genitals and gluteal skin between the leg and lower trunk representations on the postcentral gyrus—that is, in the expected homuncular location (Rothemund et al., 2002; cf. Woolsey et al., 1979). Several human fMRI and PET studies found the same result using tactile or electrical genital stimuli (Kell et al., 2005; Georgiadis et al., 2006, 2009, 2010; Michels et al., 2010; reviewed in Cazala et al., 2015). Thus, the genitals have a small cutaneous representation at the correct homuncular position on the postcentral gyrus, plus a possible second representation in the medial wall. Divergent findings across studies may reflect individual differences, conflation of representations for tactile stimuli and arousal, and technical difficulties in recording from the medial wall.

Other regions of the sacral dermatomes, apart from the genitals, are clearly localized to the medial wall (e.g., posterior leg, gluteal region, and tail) (Pubols & Pubols, 1971; Merzenich et al., 1978; Nelson et al., 1980; Felleman et al., 1983) (Figure 1.1B). Historically, these observations—and the apparent genital discontinuity—led to the idea that dermatomes are mapped mediolaterally in cortex, by the order in which their spinal nerves join the ascending dorsal columns (Whitsel et al., 1971). The revised mapping of the genitals, as well as other deviations from the dermatomal sequence found in primate maps (Merzenich et al., 1978; Nelson et al., 1980), suggests that somatotopic maps do not strictly follow either a homuncular or a dermatomal layout, but rather reflect elements of both these schemes—in addition to other influences arising from differential magnification and powerful use-dependent plasticity (see sections 1.3 and 1.4).

1.1.4. Somatotopy of the trigeminal representation

Somatotopic organization has been examined in most detail for the face (trigeminal) and hand representations. The mapping of trigeminal inputs in area 3b is largely consistent across species (Jain et al., 2001; but see Cusick et al., 1986). From medial to lateral, the contralateral upper

face, nose, upper lip, and lower lip are mapped along the caudal 3b border, and the chin and buccal cavity are mapped on the rostral border. Large representations of the contralateral teeth and tongue each span the rostro-caudal extent of 3b (Dreyer et al., 1975; Nelson et al., 1980; Cusick et al., 1986, 1989; Jain et al., 2001). More laterally, the *ipsilateral* tongue, teeth, and buccal cavity are represented, in contrast with the typical contralateral mapping scheme; these same structures also receive some ipsilateral representation in VPM (Jones et al., 1986). Ipsilateral structures occupy less than 5% of the total trigeminal representation in area 3b of New World monkeys, but occupy 40% in macaques; this may reflect the macaque's use of cheek pouches for food storage and manipulation (Manger et al., 1995, 1996). In New World monkeys, the lateral half of area 3b includes seven myelin-rich anatomic modules—one each for the upper face (F1), upper lip region (F2), and lower face and lip (F3) (all contralateral), and for the contralateral teeth (O1), contra- and ipsilateral tongue (O2), ipsilateral teeth (O3), and ipsilateral tongue (O4) (Jain et al., 2001; Kaas et al., 2006; Ingeyar et al., 2007) (Figure 1.1C). Area 1 contains a similar map of the face, flipped rostro-caudally to mirror the 3b representation. By contrast, area 2, which lacks the full lateral extent of 3b and 1, seems to lack a complete map of the oral cavity (Krubitzer et al., 1995; Jain et al., 2001).

Trigeminal map topography in humans is similar. In area 1, intrinsic signal optical imaging (ISOI) during electrical skin stimulation has revealed that the face is mapped lateral to the hand in a roughly upright orientation, with the contralateral ophthalmic, maxillary, and mandibular divisions of the trigeminal nerve represented in mediolateral sequence, with some degree of overlap (Sato et al., 2002, 2005; Schwarz et al., 2004). In area 3b, fMRI during tactile stimulation has shown that the contralateral lower lip, teeth, and tongue are mapped in mediolateral sequence, as in monkeys (Miyamoto et al., 2006). Putative area 2 appears to contain a less precise map in which distinct facial loci activate largely overlapping cortical domains (e.g., Sato et al., 2002; Miyamoto et al., 2006).

1.1.5. Somatotopy of the hand and foot representations

The hand and foot representations have been investigated in both microelectrode recordings in monkeys and fMRI studies in humans. In areas 3b and 1 of monkeys, the glabrous hand and foot have a magnification factor (i.e., ratio of cortical area to body area) 100 times greater than the trunk or upper limbs (Sur et al., 1980). The glabrous surfaces of hand digits 1 (thumb) through 5 are represented in an orderly latero-medial sequence in areas 3b and 1, and similarly, but less precisely, in areas 3a and 2 (Pons et al., 1985b; Krubitzer et al., 2004). In area 3b, each finger is oriented with its base toward the caudal (3b/1) border, and its tip at the rostral (3a/3b) border (Jain et al., 1998a; Qi & Kaas, 2004). The glabrous palm is mapped next to the base of the fingers, whereas the dorsal skin of the hand is represented by small regions interspersed with the glabrous representation (Paul et al., 1972; Sur et al., 1982; Pons et al., 1985b, 1987). The orientation of the hand maps is reversed across the 3a/3b border, the 3b/1 border, and the 1/2 border, consistent with the mirror reversals of the overall body maps. Within each finger representation, receptive field size decreases linearly from finger base to tip, correlated with an increase in peripheral receptor density and cortical magnification (Sur et al., 1980; see section 1.3).

Finger maps in humans, measured with ISOI and fMRI, are consistent with those in monkeys. Human finger maps feature mirror-image reversals in all four anterior parietal areas (Blankenburg et al., 2003; Sanchez-Panchuelo et al., 2012, 2014) and a lateromedial sequence of fingers 1 through 5 in areas 3b, 1, and 2 (e.g., Kurth et al., 2000; Sato et al., 2005; Besle et al., 2013; Kolasinski et al., 2016) (Figures 1.2B, 1.2C). In area 3b, the within-finger map organization is consistent across subjects for fingers 5 and 4, but not for fingers 1 to 3, which may be subject to greater use-dependent plasticity (Schweisfurth et al., 2014). Finger representations are less discrete in areas 1 and 2, consistent with a hierarchical progression of spatial integration across these areas (Krause et al., 2001; Stringer et al., 2011, 2014; Besle et al., 2014; Martuzzi et al., 2014).

1.1.6. Spatial precision and integration in cortical sensory coding of touch

Classical map topography reports only the dominant skin position represented at each cortical point, not the full shape of tactile receptive fields. Receptive field size is a key determinant of the spatial precision of sensory coding, and also reveals how neurons integrate across skin locations to compute important features of tactile stimuli. Studies in both anesthetized and awake macaques have reported that most neurons in the glabrous hand digit representations of area 3b have receptive fields confined to a single finger, and usually to a single phalanx. These receptive fields include both a focused excitatory center and a broader inhibitory surround (Sur, 1980; Sur et al., 1985; DiCarlo & Johnson, 2002; Sripati et al., 2006; cf. Thakur et al., 2012). In area 1, neuronal receptive fields have similar excitatory/inhibitory structure but are nearly an order of magnitude larger, and sometimes include foci on multiple pads on a single finger (~ 40% of cells) or across multiple fingers (~25%) (Sur, 1980; Iwamura et al., 1983a, 1983b; Sur et al., 1985; Sripati et al., 2006). Area 2 cells are more likely again to have multi-finger receptive fields (Pons et al., 1985b), and in some cases have bilateral receptive fields (Taoka et al., 2000).

However, it is clear that cortex spatially integrates neural responses over areas well beyond the average minimal receptive field size. Anatomic studies in New World monkeys and macaques have shown that intracortical projections in area 3b can span several hundred microns, exceeding the width of a finger representation (Garraghty et al., 1989; Garraghty & Sur, 1990; Rausell & Jones, 1995; DeFilipe et al., 1986). Such studies have also demonstrated that horizontal projections provide extensive cross-connectivity between fingerpad representations within area 3b, and even more so in area 1 (Négyessy et al., 2013; Ashaber et al., 2014), despite largely homotopic connectivity between the two areas (Wang et al., 2013). Feedback connections from other cortical areas to 3b are also broadly targeted, and may further support multi-finger integration (Liao et al., 2013). Consistent with these anatomic findings, pharmacologic blockade of cortical inhibition within an area 3b finger representation in anesthetized macaques unmasks horizontal excitatory drive that expands receptive fields to include adjacent fingers, revealing broad subthreshold spatial integration (Alloway & Burton, 1991). Strengthening of these excitatory connections, induced by lesions or altered behavior, may provide a substrate for map plasticity (see section 1.4.5).

Several imaging and electrophysiological studies in area 3b suggest that spatial integration is broader in awake than in anesthetized animals, possibly due to reduced lateral

inhibition in the awake state. In awake squirrel monkeys, ISOI activations in L2/3 of area 3b by fingerpad stimuli are several times larger in amplitude and area than under anesthesia, such that even representations of nonadjacent fingers can overlap (Chen et al., 2005, 2009). It is unclear how much spiking, rather than subthreshold, responses contribute to this greater activation. However, recording sites across cortical layers in awake macaques demonstrate population spiking responses not just to the somatotopically corresponding finger, but also to each other finger on the hand, with a clear predominance of the expected finger seen mainly in the input layer, L4 (Lipton et al., 2010). These studies, and similar work in rodent S1 (e.g., Ferezou et al., 2006; Frostig et al., 2008), demonstrate that single-point stimuli activate broader regions in awake cortex than is suggested by classical somatotopic maps derived under anesthesia, because those maps only represent the average receptive field center of neurons. In awake animals, tactile stimuli initially activate the corresponding somatotopic location, but activation then spreads to neighboring cortical locations, presumably via intracortical connections. Thus, widespread activation and accurate somatotopy coexist in cortical maps (Reed et al., 2010b).

Spatial integration likely serves not only to expand receptive fields, but also to nonlinearly modulate neuronal responses to contextual stimuli. In area 3b of awake macaques, single-unit spiking to tactile stimulation of the dominant fingerpad is significantly modulated by subthreshold input from adjacent or even non-adjacent pads (Thakur et al., 2012). This modulation is predominantly suppressive, and occurs in both awake and anesthetized monkeys (Lipton et al., 2010; Reed et al., 2010a). Co-stimulation of fingerpads can also synchronize spiking between neuron pairs up to 2 mm apart in L2/3 of area 3b, an effect that may be driven by lateral excitatory connectivity (Reed et al., 2008, 2012). Therefore, circuits for spatial integration exist within somatotopic maps, and may support contextual processing of tactile information across fingers and during active sensing with the whole hand. Cross-finger suppression may underlie the funneling illusion, in which simultaneous tactile stimulation at multiple sites elicits the false percept of a single spatially intermediate stimulus. Consistent with this idea, stimulation of two adjacent fingerpads activates a single cortical area at an intermediate location in the finger map (Chen et al., 2003; Friedman et al., 2008; cf. Gardner & Costanzo, 1980).

1.1.7. Segregation of RA and SA responses into distinct columns

An ongoing question regarding primate somatosensory maps is to what degree, in addition to their somatotopic arrangement, neurons are organized at a finer scale according to other receptive field parameters. In 1957, Mountcastle and colleagues proposed that somatosensory cortex is subdivided into columns of cells with receptive fields tuned to the same somatotopic location and tactile submodality (Mountcastle et al., 1957, 1969; see section 1.2.2). Consistent with this model, early studies of owl monkeys and macaques found that in the middle layers of area 3b (presumptive L4), the glabrous finger representations contained alternating, rostro-caudally oriented domains that differentially represent RA and SA afferent inputs (Paul et al., 1972; Sur et al., 1981, 1984; neurons in superficial and deep layers responded only to RA input). This organization is similar to the ocular dominance columns in the monkey's visual cortex, and suggested fine-scale columnar RA and SA input streams. Functional independence of RA and SA columns is supported by microstimulation experiments in macaques trained to discriminate

flutter stimuli on the fingerpad, which primarily activate RA neurons. In these animals, microstimulation of RA columns, but not of SA columns, can substitute for tactile stimulation, suggesting that higher cortical areas decode flutter stimuli specifically from activation of RA columns (Romo et al., 1998, 2000).

However, although the early studies defined SA neurons in cortex as having sustained firing to step indentations, and RA neurons as having onset/offset responses, most "SA" neurons recorded also displayed an RA-like offset (Sur et al., 1981, 1984). Recent studies indicate that "SA" neurons in 3b and 1 actually integrate independent SA1 and RA1 components (Pei et al., 2009; cf. Sakurai et al., 2013, in rodent whisker columns). Therefore, "RA" and "SA" columns may represent modules with differential convergence from each submodality, and thus different selectivity for vibrotactile frequency, rather than exclusive RA and SA streams (reviewed in Saal & Bensmaia, 2014). The existence of fine-scale modules for vibrotactile frequency is supported by recent findings in squirrel monkeys, where low, medium, and high frequencies of vibrotactile stimulation of the fingerpads activate distinct but overlapping patches of 250-µm diameter in areas 3b and 1 (Chen et al., 2001; Friedman et al., 2004). These patches may be defined by predominant input from SA1, RA1, and RA2 afferent inputs, respectively, or may reflect more complex submodality convergence. Because these studies used ISOI, which predominantly reports L2/3 activity, the relationship between these patches and classical RA and SA columns in L4 remains unclear.

1.2. SOMATOSENSORY MAPS IN RODENTS

1.2.1. Overview of rodent somatotopic maps

The primary somatosensory cortex (S1) of rats and mice—like its primate homologue, area 3b—contains a somatotopic map of the contralateral body and face (Figures 1.3A–C, 1.3G). Rodent maps do not contain major discontinuities as in primates. The caudo-rostral body axis is mapped from medial to lateral in S1, with the limb representations extending anteriorly from the trunk and the face representation continuous with the neck and body (Welker, 1976; Chapin & Lin, 1984); the lower incisor and tongue are mapped lateral to the lower and upper jaws, respectively (Remple et al., 2003). The genitals are mapped in their somatotopically appropriate location between the hindlimb and trunk (Lenschow et al., 2016). The forepaw and hindpaw representations are highly magnified, occupying 15% and 4% of the total map in rats, versus just 14% devoted to the trunk, limbs, and tail (Dawson & Killackey, 1987).

The somatotopic map can be visualized histologically in L4 by staining for markers of thalamo-cortical axon terminals, or for mitochondrial enzymes enriched in highly active neurons, such as cytochrome oxidase (CO) (Figure 1.3G). These stains reveal distinct CO-rich anatomic modules in L4, which represent the individual pads and digits of each paw (Waters et al., 1995) and the individual whiskers (vibrissae) within the facial map (Woolsey & Van der Loos, 1970). The whisker modules are known as "barrels" due to their ovoid shape. Rodent whiskers include small tactile hairs on the upper and lower lips (microvibrissae) that passively sense object features, and larger tactile hairs on each side of the face (macrovibrissae) that are actively moved, using specialized muscles, to detect and palpate objects ("whisking"; Brecht et al., 1997; reviewed in

Diamond et al., 2008a). In the rat, representations of the upper-lip and lower-lip microvibrissae account for 25% and 9% of the entire S1 map, respectively, whereas the macrovibrissae representation occupies 34% (Dawson & Killackey, 1987). This extreme magnification also occurs in mice and several other muridae, and reflects the behavioral salience of the whiskers as local object detectors (Woolsey et al., 1975; reviewed in Krubitzer et al., 2011).

The whisker barrels have been extensively studied. Rat and mouse macrovibrissae (henceforth, "whiskers") are organized on the face into five rows (denoted A–E), and four or more arcs (denoted by numbers; thus, A1–A4; B1–B5, etc.) (Figure 1.3A). Each whisker is represented by a barrel in contralateral L4, with the barrels arranged isomorphically with the whiskers on the face, forming a precise topographic map (Figure 1.3C). Each L4 barrel is a cluster of neurons that receives thalamo-cortical axonal input predominantly representing the corresponding whisker, and forms the center of a radial S1 column that processes this input (Figure 1.3D). L4 barrels are closely apposed in mice, but in rats are separated by septal regions with lower cell density (Land & Simons, 1985). Thus, the S1 whisker map exhibits a clear modular columnar structure, with an orderly somatotopy evident in the arrangement of barrel columns. These features make the whisker map a powerful model system for studying tactile representation, circuits, processing, and plasticity in cerebral cortex (reviewed in Feldmeyer et al., 2013). In rats, CO staining often shows 2–3 subdomains within each barrel (Land & Erickson, 2005). These may correspond to distinct termination zones of VPM axons (Furuta et al., 2011), but the functional correlates of these domains remain unknown.

S1 projects intracortically to two adjacent somatosensory areas, the secondary somatosensory cortex (S2) and parietal ventral area (PV) (Fabri & Burton, 1991; Remple et al., 2003; Benison et al., 2007), both homologous to the synonymous regions in primates (Qi et al., 2008) (Figure 1.3C). S2 lacks separate columns for each whisker, instead containing striplike domains each comprising a continuous representation of the whiskers of one row (e.g., A1–A4) in caudo-rostral order. These strips are arrayed isomorphically with the whisker rows on the face, and the mediolateral order of the strips is a mirror reversal of the whisker rows in S1 (Hoffer et al., 2003). PV lacks detailed facial and whisker representations, but contains a body map mirroring that in S2. Thus, integrative processing through successive, mirrored representations is seen in rodent somatosensory cortex, as in primates.

1.2.2. The column as a modular unit of cortical organization

The radial column is classically regarded as the modular unit of cortical circuitry and processing (Mountcastle, 1957). In the textbook view, columns have strong internal connectivity and weaker external (cross-columnar) connectivity, and in sensory areas, each receives a distinct type of sensory input. As a result, neurons within a column are thought to represent similar sensory information. However, this strong view of columnar organization is debated (Rockland, 2010), based on several lines of argument. Extensive horizontal connections exist across columns, particularly in L2/3 and L5 (see section 1.2.4), and co-columnar cells can be tuned for different sensory features (see sections 1.2.5–1.2.7). The anatomic definition of a column varies between cortical areas, and rigid anatomic divisions between columns (e.g., the septa between digit modules or whisker barrels) are the rare exception, rather than the rule. In S1, the somatotopic

organization of whisker receptive fields is identical between mouse strains that have barrels and strains that do not (Welker et al., 1996). In primary visual cortex (V1), closely related species may have ocular dominance columns or may not, and binocular visual ability is independent of the presence of defined ocular dominance columns (Horton & Adams, 2005). Given such findings, some researchers argue that cortical columns are not a distinct modular building block of cortical maps, or are too interconnected or variably defined to be a useful concept (Horton & Adams, 2005; cf. Ghazanfar & Nicolelis, 2001).

Despite these reservations, it is clear that modular, stereotyped, radially organized microcircuits exist in cortex, suggesting that each radial domain in a given cortical area performs a similar computation on its inputs (Fox, 2008; Roe et al., 2015). In addition, there are examples of clearly modular organization in primary somatosensory maps—including digit modules in primates, whisker columns in rats, and modules for each ray of the tactile star of the star-nosed mole (Catania, 2011; see section 1.3)—that strongly indicate functional columnar processing. Microcircuits share a broadly similar organization across sensory areas, although region-specific differences do exist. Thus, columnar processing is a reasonable model of cortical function, though it may be substantially modified by dense cross-columnar or feedback connections.

1.2.3. Ascending pathways for whisker input to S1

Subcortical pathways for cutaneous and vibrissal tactile sensation in rodents are similar to those in primates. Here, we focus on pathways for whisker sensation. Information from the whiskers reaches cortex via pathways that ascend through the ipsilateral brainstem trigeminal nuclei then cross to contralateral thalamic nuclei, which project to S1 and S2 (reviewed in Bosman et al., 2011). Most information about whisker contact onto objects is relayed through the main lemniscal pathway, via the principal trigeminal nucleus of the brainstem (PrV) and the VPM nucleus of the thalamus (Yu et al., 2006). This pathway generally exhibits receptive fields dominated by single whiskers, suggesting a role in object localization (Minnery & Simons, 2003; Minnery et al., 2003; Haidarliu et al., 2008), although subcomponents of the pathway exhibit multi-whisker receptive fields (reviewed in Deschênes & Urbain, 2016). A distinct paralemniscal pathway conveys weaker multi-whisker signals, via the rostral-interpolar trigeminal nucleus of the brainstem (SpVir) and the posterior medial nucleus of the thalamus (POm). This pathway is active only during whisking, and may provide integrative information about whisker kinematics (Yu et al., 2006). Whereas the lemniscal pathway includes orderly maps of the whiskers with associated barrel-like modules at each level of processing—"barrelettes" in PrV (Ma & Woolsey, 1984), "barreloids" in VPM (Van der Loos, 1976; Land et al., 1995; Haidarliu & Ahissar, 2001), and barrels in S1—the paralemniscal pathway relays (SpVir and POm) lack somatotopic whisker maps. VPM provides the main source of feedforward input to L4 barrels in S1 whisker columns, whereas POm projects to L5 and L1 in S1 septa and whisker columns, as well as to S2 (Lu & Lin, 1993; Ahissar et al., 2001; Furuta et al., 2009). In addition to its role in feedforward information flow, POm may also provide a thalamic relay for cortico-cortical information flow between sensory areas (reviewed in Guillery & Sherman, 2011).

1.2.4. Cortical circuitry in whisker columns

The lemniscal whisker input arriving via a VPM barreloid to an L4 barrel in S1 flows through the canonical cortical excitatory circuit, running from L4 up to L2/3 then down to L5 and L6 (the main cortical output layers) (reviewed in Douglas & Martin, 2004, and Feldmeyer, 2012) (Figure 1.3D). Columnar segregation of single-whisker information is largely maintained in the initial stages of this circuit. First, despite limited multi-whisker integration in the brainstem, most individual lemniscal thalamo-cortical afferents carry signals dominated by a single whisker (reviewed in Deschênes & Urbain, 2016), and synapse mainly in the corresponding L4 barrel (Jensen & Killackey, 1987; Arnold et al., 2001; Oberlaender et al., 2012). Second, L4 barrels are largely independent, with few cross-columnar excitatory projections (Feldmeyer et al., 1999; Petersen & Sakmann, 2000; Egger et al., 2008). Finally, ~70% of L4 axon arbor in L2/3 is within the home column (Lübke et al, 2000; Brecht & Sakmann, 2002; Bender et al., 2003; Shepherd et al., 2005). As a result, VPM barreloid $\rightarrow$ L4 barrel $\rightarrow$ L2/3 circuits largely preserve narrow receptive fields and orderly somatotopy (Petersen & Sakmann, 2001). Recently, it has been shown that L5 and L6 neurons within whisker columns also receive strong and direct input from VPM, providing a distinct processing pathway for lemniscal signals, independent of the higher layers (Constantinople & Bruno, 2013; Pluta et al., 2015).

Columnar segregation becomes less strict in the projections from L2/3 $\rightarrow$ L5 and L4 $\rightarrow$ L5 and L6, which have more cross-columnar spread. Strong cross-columnar excitatory projections exist within and between L2/3 and L5, in general running preferentially along column rows rather than arcs (Hoeflinger et al., 1995; Kim & Ebner, 1999; Lübke at al., 2003; Larsen & Callaway, 2006; Adesnik & Scanziani, 2010). In addition, multi-whisker paralemniscal inputs target upper L5 (L5A) in both columns and septa, and are further relayed to columnar L2/3 in mice (Bureau et al., 2006; Kichula & Huntley, 2008) and to septal L2/3 in rats (Ahissar et al., 2001; Shepherd et al., 2005; de Kock & Sakmann, 2009; but see Staiger et al., 2014). Each of these circuits provides non-topographic or multi-whisker inputs that may shape the overall whisker map (Figure 1.3D). Besides these excitatory microcircuits, inhibitory circuits exist that modulate synaptic integration, spike timing, response gain, and receptive field size, via both local and long-distance connections (reviewed in Isaacson & Scanziani, 2011, and Gentet, 2012).

1.2.5. Functional organization of the whisker map

Most single neurons in S1 whisker columns have receptive fields focused on a single whisker (called the "principal" or "best" whisker), with weaker spiking responses to neighboring whiskers (Moore & Nelson, 1998). Receptive field tuning to the best whisker is strongest in L4 neurons (Brecht & Sakmann, 2002), and classical single-unit recordings suggest that in a clear majority of L4 cells the best whisker is the one corresponding anatomically to the cortical column (Simons, 1978; Armstrong-James & Fox, 1987). This is consistent with the largely topographic input from VPM thalamus to L4 barrels and limited cross-barrel excitation in L4 (detailed above). Receptive fields in L2/3 and especially in L5 are broader, consistent with the greater cross-columnar and paralemniscal inputs in these layers (Brecht et al., 2003; Manns et al., 2004; Wright & Fox, 2010; Le Cam et al., 2011). However, the best whisker matches the anatomic columnar whisker in ~70% of L5 cells (Wright & Fox, 2010). In all layers, whisker-evoked spiking responses are

composed of relatively few spikes (typically < 1 spike per whisker deflection), indicating a highly sparse sensory code (de Kock et al., 2007; reviewed in Barth & Poulet, 2012).

In mice, each cortical column contains ~10,000 neurons, and occupies a 150 × 150 µm tangential area in the whisker map. Whereas single-cell electrophysiology only reveals average map topography at ~50–100 µm resolution, precise subcolumnar topography, at single-cell resolution, is measurable using two-photon calcium imaging of cell populations. This method has shown that in rodents, unlike carnivores and primates, L2/3 of visual cortex contains locally intermixed neurons tuned for different orientations, spatial frequencies, and retinotopic positions, termed "salt-and-pepper" organization (Ohki et al., 2005; Bonin et al., 2011); the same is true in L2/3 of rodent auditory cortex for frequency tuning (Bandyopadhyay et al., 2010; Rothschild et al., 2010; reviewed in Kanold et al., 2014). A similar salt-and-pepper organization exists in mouse whisker S1, in which nearby L2/3 cells are tuned for different whiskers, intermixed within the same anatomic column (Kerr et al., 2007; Sato et al., 2007; Clancy et al., 2015). In each column, the most common tuning is for the anatomically matched whisker, such that somatotopy is correct, on average, but with very high local scatter. As a result, whisker deflection evokes spiking in a distributed set of L2/3 neurons, both within the anatomically corresponding column and in neighboring columns (Clancy et al., 2015) (Figure 1.3E). This topographic scatter may reflect cross-columnar projections in L2/3, and/or the routing of less-tuned paralemniscal input to columnar L2 in mice (Bureau et al., 2006). Whether similar scatter exists in other layers is not known. Notably, L2/3 remains capable of particularly robust plasticity in adulthood (reviewed in Feldman & Brecht, 2005), suggesting that its sparsely responsive and diversely tuned cells might provide a substrate for the formation of context-dependent subnetworks during associative learning (Yassin et al., 2010; Margolis et al., 2012; reviewed in Petersen & Crochet, 2013).

1.2.6. Response dynamics and multi-whisker integration

Topographic precision within the whisker map also varies with time from stimulus onset. On the population level, single-whisker deflection evokes initial spiking and subthreshold responses that are strongly peaked within the anatomically corresponding column, then spread to neighboring columns. For strong stimuli, subthreshold responses may spread over ~40 milliseconds to encompass the entire S1 whisker map and beyond. This has been observed for spiking and subthreshold responses in all cortical layers in anesthetized rats, using extracellular recordings (Frostig et al., 2008; cf. Ghazanfar & Nicolelis, 1999, Petersen & Diamond, 2000), and for subthreshold responses in L2/3 in both anesthetized rats and awake mice, using voltage-sensitive dye imaging (Petersen et al., 2003; Ferezou et al., 2006, 2007; Lustig et al., 2013). The spread of activation runs preferentially along column rows, matching the pattern of cross-columnar axonal projections (Petersen et al., 2003; Lustig et al., 2013). Additional spread beyond S1 borders is likely mediated by long-range projections, which run laterally for great distances in L2/3 and L5–6 (Frostig et al., 2008; Mohajerani et al., 2013; Stehberg et al., 2014).

Integration of multi-whisker responses in S1 remains poorly understood. Spiking responses within a whisker column to the anatomically matched whisker are typically inhibited by prior deflection of an adjacent whisker (e.g., Ego-Stengel et al., 2005; Boloori & Stanley, 2006;

Civillico & Contreras, 2006; Lustig et al., 2013). This likely reflects cortical and thalamic inhibition, though specific circuit mechanisms remain unclear. During moving wavefronts of whisker stimulation, this surround suppression enhances S1 responses to whiskers at the leading edge of the wavefront (Drew & Feldman, 2007). However, recent studies of more complex multi-whisker stimuli have discovered S1 neurons that are tuned to specific spatiotemporal patterns of multi-whisker deflection, including directions of moving wavefronts (Jacob et al., 2008), center-surround motion contrast and coherence (Estebanez et al., 2012, 2016), and specific 2- and 3-whisker combinations and sequences (Ramirez et al., 2014). Whether these multi-whisker stimulus preferences are organized systematically within the somatotopic map in S1 remains unknown.

1.2.7. Maps of whisker deflection direction and other parameters

In addition to the whisker somatotopic map, rodent S1 contains a map of whisker deflection direction, and may also contain maps of other features. The direction map is most evident in L2/3, and has a pinwheel-like organization within each column. Many individual neurons throughout the whisker system show a tuning preference for direction of whisker deflection (e.g., upward, downward, rostral, or caudal deflection of the single whisker from its resting position) (Lichtenstein et al., 1990; Minnery & Simons, 2003). Within VPM barreloids, a systematic map of direction tuning is present (Timofeeva et al., 2003). This map is less prominent and not statistically significant within cortical L4 barrels, but then re-emerges in columnar L2/3 (Andermann & Moore, 2006). In anesthetized rats, this subcolumnar map of direction tuning in L2/3 is organized systematically and aligned with the somatotopic map, such that neurons preferring caudal deflection are located in the quadrant of the barrel column nearest the column representing the next-caudal whisker (Andermann & Moore, 2006; Kremer et al., 2011) (Figure 1.3F). This suggests that cortical circuits help refine or shape the direction map. Puzzlingly, the spatial orientation of the direction map may be reversed in awake mice whisking on objects (Peron et al., 2015). The L2/3 direction map emerges only in adulthood, suggesting that it may be sculpted by experience (Kremer et al., 2011; cf. Wilson et al., 2010). One two-photon calcium imaging study in rats also suggests that L2/3 may contain a map of surface texture, which rats can discriminate using whisker sensation. L2/3 neurons were often best driven by sandpapers of specific roughness, with some indication that roughness tuning was organized on a rostro-medial to caudo-lateral gradient (Garion et al., 2014). As with primates, additional work remains to be done in whisker cortex to elucidate the mapping of somatosensory parameters beyond topography.

1.3. DETERMINANTS OF CORTICAL MAGNIFICATION IN SOMATOSENSORY MAPS

A common feature of the tactile, visual, and auditory systems is that sensory receptor neurons are not distributed with uniform density over the sensory epithelium (i.e., skin, retina, cochlea). Instead, the epithelium includes densely innervated regions that execute critical discriminative functions (e.g., the fovea in vision; regions of the cochlea representing speech frequencies in humans and echolocation frequencies in bats), and larger, more sparsely innervated regions

representing the bulk of the sensory surface. More highly innervated regions are typically magnified in central nervous system maps. Somatosensory examples include the digits of primates, and the whiskers of rats and mice. A dramatic example is the star-nosed mole, named for its 11 motile glabrous skin appendages (rays) around each nostril, which it uses to palpate its environment seeking small insects as prey. The star's representation is highly magnified in the principal trigeminal nucleus (Catania et al., 2011), and to an even greater degree in S1 and S2, where it occupies 52% of the somatotopic map (Catania & Kaas, 1995).

What determines the relative magnification of specialized sensory regions like the digits or the nose-star? In most sensory maps, magnification is proportional to the density of peripheral receptors: each receptor neuron in the periphery is represented by a constant number of cells in a given map, and because cell density across a given cortical area is largely invariant, richly innervated peripheral regions occupy larger areas of the map. This is true for the hand and body map in owl monkeys (Sur et al., 1980), and for the size of whisker-related barrel columns in rat and mouse S1, which varies with the innervation density of the matching whisker follicle (Lee & Woolsey, 1975; Welker & Van der Loos, 1986; Meyer et al., 2013; cf. Ma, 1991, in barrelettes). However, in some cases, central circuits increase the cortical area associated with each peripheral receptor in a given body region, making that region's representation larger than expected from the number of afferents. This "afferent magnification" (Catania & Kaas, 1997) is seen in the representation of the fovea in primate V1 (Azzopardi & Cowey, 1993), and in the representation of the 11th ray of the star-nosed mole. The 11th ray functions as a tactile fovea, used in detailed examination of objects after initial contact by the other rays. At successive levels in the ascending somatosensory pathway, the proportional representation of the 11th ray increases, until in S1 and S2 it claims over 25% of total map area—a four-fold greater allocation of cortical tissue per mechanoreceptor afferent compared to the other rays (Catania & Kaas, 1995, 1997; Catania & Remple, 2004). This strong afferent magnification is established at least in part by intrinsic mechanisms during embryonic development (Catania, 2001). Later, in adult life, the magnification of specific sensory inputs within maps can be adjusted based on patterns of sensory use (see section 1.4).

In addition to greater relative magnification, specialized sensory regions may receive a greater number of duplicate representations in cortex. The clearest example is the mole's nose-star, which in addition to its S1 and S2 representations is mapped in a third region with no obvious equivalent in most mammals (Catania & Kaas, 1995). In species that depend heavily on somatic sensation, S1 itself is enlarged relative to other primary sensory cortices. Thus, in naked mole-rats and manatees—which navigate their environment using teeth or tactile hairs, at the expense of vision and audition—S1 claims territory occupied by the primary visual and auditory cortices in related species (Catania & Remple, 2002; reviewed in Sarko et al., 2011).

1.4. PLASTICITY OF SOMATOSENSORY MAPS

1.4.1. Overview of map plasticity

Somatosensory maps are stable in adult animals when sensory input patterns remain constant (Chen et al., 2005). However, altered sensory use or peripheral or central lesions drive robust

plasticity of somatosensory maps at multiple levels of the nervous system (reviewed in Darian-Smith, 2008, and Xerri, 2012). Use- and lesion-dependent plasticity occur into adulthood, unlike other sensory systems, where plasticity is often restricted to early developmental critical periods. Plasticity does not involve changes in the number or location of cortical neurons, but instead reflects adjustments to their receptive fields. These adjustments involve changes in the efficacy of existing synapses (including long-term potentiation and depression), rapid synapse formation and removal, and slower structural modifications of axons or dendrites.

In most forms of somatosensory map plasticity, tactile regions that are overused, or behaviorally more salient, gain representation (Jenkins et al., 1990; Recanzone et al., 1992a; Xerri et al., 1994; Glazewski & Fox, 1996); regions that are deprived or deafferented lose representation (Merzenich et al., 1984; Pons et al., 1991; Glazewski & Fox, 1996); and regions that are synchronously active develop a merged representation (Clark et al., 1988; Allard et al., 1991; Diamond et al., 1993; Wang et al., 1995). Somatosensory maps thus actively reallocate cortical space to reflect behaviorally relevant sensory statistics in the environment. These changes are thought to alter perception to suit behavioral demands, and to compensate for injury. In this section, we summarize plasticity in primate and rodent somatosensory maps in cerebral cortex, and give a brief overview of the underlying mechanisms.

1.4.2. Somatosensory map plasticity in non-human primates

Sensory map plasticity in adult primates was first discovered in New World monkeys. Following median nerve section or finger amputation, the functional representation of the spared hand or fingers was shown to expand into the deafferented cortical region in areas 3b and 1 (Merzenich et al., 1983a, 1983b, 1984). The expansion began immediately, and its spatial extent (1–2 mm) matched the typical span of thalamo-cortical afferents. This immediate expansion is thought to represent, in part, unmasking of sensory responses that are normally suppressed via lateral inhibition (Merzenich et al., 1983b; Calford & Tweedale, 1988, 1991a–c; Silva et al., 1996; cf. Weiss et al., 2000, in a human patient). Sustained, large-scale peripheral deafferentation was subsequently found to elicit remapping on a larger spatial scale (Figure 1.4D). In macaques and owl monkeys, arm deafferentation by dorsal rhizotomy or dorsal column lesions triggers massive reorganization in areas 3b and 1, in which chin and lower jaw representations expand over months or years to fully occupy the adjacent, deafferented arm territory—a ~10–18 mm distance in macaques (Pons et al., 1991; Garraghty & Kaas, 1991; Jain et al., 1997, 2008; reviewed in Kaas et al., 2008). This functional remapping is mediated by spared dorsal column and trigeminal afferents, rather than other spinal pathways (Jain et al., 1997), and occurs without changes in the histologic patterning of finger modules in area 3b (Jain et al., 1998a). Similar large-scale functional remapping occurs in areas S2 and PV, but with a broader range of facial regions invading the deafferented arm representation (Tandon et al., 2009).

Map plasticity also occurs in adults in response to prolonged periods (weeks to months) of altered sensory use. When adult owl monkeys use specific fingertips to earn food rewards—by applying pressure to a textured disk, or by retrieving food pellets from small wells—the representation of these skin regions in area 3b expands (Jenkins et al., 1990; Xerri et al., 1999) (Figure 1.4A). During this plasticity, receptive fields contract, such that the normal inverse

relationship between magnification and receptive field size is maintained (cf. Figure 1.4B). By contrast, when monkeys discriminate vibratory stimuli applied to a small region on the finger, the representation of this skin region expands as expected—but in this case receptive fields are enlarged as well, perhaps reflecting the relative lack of competing input from adjacent skin locations (Recanzone et al., 1992a, 1992b). Robust reorganization of the hand representation in area 3b also occurs in monkeys following surgical fusion of two fingers (syndactyly) (Clark et al., 1988; Allard et al., 1991), monkeys that experience synchronous multi-finger tactile stimulation (Wang et al., 1995), and monkeys trained to perform repetitive movements to induce focal hand dystonia (Byl et al., 1996, 1997; Blake et al., 2002). In these experiments, finger representations within area 3b merge, and neurons acquire multi-finger receptive fields spanning the coactive fingers. This type of plasticity, driven by temporal correlations in tactile input, is a basic prediction of Hebbian synaptic plasticity (see section 1.4.5).

These findings show that the amount, behavioral salience, and temporal structure of tactile input all drive profound changes in cortical somatosensory maps. Map reorganization also occurs after lesions to central somatosensory areas. In New World monkeys, focal lesions in area 3b cause surrounding cortex to reorganize to re-establish the ablated representations. This reorganization occurs over weeks to months, and inputs that are overused during the recovery period are magnified (Jenkins & Merzenich, 1987; Xerri et al., 1998). Similar reorganization occurs in S2 after ablation of the S1 hand representations. In this case, the S2 hand area is initially silent, but over weeks develops responsiveness to the foot. This invasion of the foot representation, rather than nearby trunk or limb, may reflect the predominance of glabrous inputs in S2 (Pons et al., 1988).

1.4.3. Somatosensory map plasticity in humans

Human somatosensory cortex exhibits similar use-dependent plasticity to that seen in non-human primates, as shown in fMRI, MEG, EEG, and magnetic source imaging (MSI) studies (reviewed in Elbert & Rockstroh, 2004). Several hours of synchronous stimulation to multiple fingers causes their cortical representations to move closer together, whereas representations of asynchronously stimulated fingers become more discrete (Pilz et al., 2004; Stavrinou et al., 2007; Vidyasagar et al., 2014). Stringed instrument players and Braille readers develop magnified cortical representations of the preferentially used fingers (Elbert et al., 1995; Sterr et al., 1998a, 1998b; but see Burton et al., 2002), while Braille readers who use multiple fingers, and patients with focal hand dystonia, develop merged or disordered finger representations that may reflect experience with synchronous cross-digit input (Sterr et al., 1998a, 1998b; Elbert et al., 1998; Butterworth et al., 2003; Nelson et al., 2009). These forms of reorganization are directly parallel to the use-dependent changes in non-human primates summarized above. Importantly, patients with congenital syndactyly or focal hand dystonia who undergo corrective surgery or retraining develop more structured finger somatotopy, indicating that maps can renormalize when typical sensory input patterns are restored (Mogilner et al., 1993; Candia et al., 2003).

Cortical map reorganization after limb amputation has been hypothesized to be a contributing factor in phantom limb pain in human patients. Human arm amputees show an extensive expansion of the face representation into the deafferented arm region in

somatosensory cortex, as measured by MSI and MEG (Elbert et al., 1994; Yang et al., 1994). In the cortical model of phantom limb pain, activation of afferents from the face and arm stump drive spiking in the deafferented arm region, thus eliciting sensations localized perceptually to the missing limb (reviewed in Ramachandran et al., 1993, and Flor et al., 2006). Why these sensations are felt as painful is not clear; it has been suggested that the pain percept results from an incongruence between motor intentions and proprioceptive feedback, due to mismatched somatotopy at different levels of the sensorimotor pathway (Harris, 1999; McCabe et al., 2005). Supporting this model, patients' degree of phantom limb pain is correlated with the extent of reorganization in area 3b, as assessed by MSI (Flor et al., 1995; Grüsser et al., 2001; Karl et al., 2001). However, other studies suggest that phantom pain can occur in the absence of cortical reorganization, and vice versa (Elbert et al., 1994; Makin et al., 2013, 2015; reviewed in Jutzeler et al., 2015). Moreover, in some cases, phantom sensations may be generated peripherally (Birbaumer et al., 1997; Vaso et al., 2014). Thus, how phantom limb pain relates to map plasticity in somatosensory cortex remains an open question.

1.4.4. Somatosensory map plasticity in rodents

Use-dependent map plasticity has been studied extensively in rodent S1, where whisker input can be controlled by simply trimming or plucking a subset of whiskers ("deprivation") (reviewed in Feldman & Brecht, 2005, and Erzurumlu & Gaspar, 2012). Depriving a subset of whiskers drives two major, distinct changes in S1 whisker-evoked responses (Figure 1.4C). First, neurons in cortical columns associated with the deprived whiskers reduce their spiking responses to those whiskers (measured by calibrated deflections of the whisker stub). Second, neurons in both deprived and spared columns increase their spiking responses to spared whiskers (Glazewski & Fox, 1996; Barth et al., 2000). As a result, the S1 representation of deprived whiskers weakens and contracts, whereas that of spared whiskers strengthens and expands. These changes are analogous to the use-dependent reorganization of finger representations in primate somatosensory cortex (see sections 1.4.2, 1.4.3). Both weakening and strengthening are driven, in part, by competition between inputs (Glazewski & Fox, 1996; Glazewski et al., 1998; Allen et al., 2003); therefore, depriving whiskers in a "chessboard" spatial pattern elicits particularly robust plasticity (Fox & Wallace, 1999; Wallace et al., 2001). In deprivation protocols where only two whiskers neighboring each other are spared, neurons in the home column for each spared whisker increase responses to the spared neighbor; this increases overlap between the representations of the two whiskers, similar to the merged representations of coactivated fingers in primates (Diamond et al., 1993, 1994; Armstrong-James et al., 1994). As with use-dependent plasticity in primates, all these phenomena in rodent S1 are consistent with predictions of Hebbian plasticity (see section 1.4.5).

Use-dependent plasticity persists in rodent S1 throughout life, but with distinct properties depending on both cortical layer and animal age. In L4, experience can substantially reorganize receptive fields during a critical period in the first postnatal week (Fox, 1992), when thalamo-cortical synapses are developing and circuits in L4 have not yet matured. In L2/3, experience-dependent plasticity of receptive fields is greatest between postnatal days 10 and 15, when L4–L2/3 synapses are first maturing (Stern et al., 2001). After postnatal day 15 and through

adulthood, receptive field plasticity is modest in L4 but remains robust in L2/3 and L5 (Glazewski & Fox, 1996). In addition, weakening of deprived whisker responses is most prevalent in juveniles < 2 months of age, whereas strengthening of spared whisker responses is the dominant mechanism of plasticity in adults (Wallace et al., 2001).

Other features of sensory use, besides deprivation, also drive whisker map plasticity in S1. Environmental enrichment in adults accelerates plasticity (Rema et al., 2006), and shrinks whisker receptive fields and sharpens the whisker map in L2/3 (Polley et al., 1999, 2004) (Figure 1.4C). Prolonged, repetitive mechanical stimulation of a single whisker contracts its representation in S1 (Welker et al., 1992; Knott et al., 2002; cf. Polley et al., 1999). Pairing deflection of specific whiskers with aversive or appetitive stimuli (classical conditioning) potentiates cortical responses to the paired whiskers (Siucinska & Kossut, 1996, 2004). Outside the whisker system, environmental enrichment also sharpens receptive fields in the forepaw region of S1 (Coq & Xerri, 1998), and nursing behavior in lactating female rats causes a twofold enlargement of the S1 representation of the nipples and ventral thoracic skin with concomitant contraction of receptive fields (Xerri et al., 1994) (Figure 1.4B). Thus, rodent somatosensory maps are highly plastic throughout life in response to the statistics and behavioral relevance of tactile input.

As in primates, use-dependent plasticity in rodent S1 is mediated by functional changes in receptive fields; the anatomic position of neurons themselves is fixed. Anatomic barrels are structurally plastic only during the first postnatal week, and only in response to whisker afferent lesions, not changes in whisker sensory activity (e.g., trimming) (van der Loos & Woolsey, 1973; Weller & Johnson, 1975; Waite & Taylor, 1978). During this period, limb amputation disrupts development of the forepaw barrels in S1 (Dawson & Killackey, 1987; McCandlish et al., 1996; Pearson et al., 1999). Thus, anatomic clustering of L4 neurons is established in a brief postnatal window (reviewed in Li & Crair, 2011), after which sensory use alters receptive fields extensively, while macroscopic anatomy remains largely stable (but see Polley et al., 2004).

1.4.5. Mechanisms of somatosensory map plasticity

The cellular and synaptic mechanisms for use-dependent plasticity in somatosensory cortex have been best described in rodents. Use-dependent maturation of thalamo-cortical synapses during the early L4 critical period involves long-term potentiation (LTP), activation of silent glutamatergic synapses, and long-term depression (LTD) (reviewed in Feldman et al., 1999). Whisker trimming also induces structural plasticity including retraction of thalamo-cortical axons from VPM (Wimmer et al., 2010; Oberlaender et al., 2012) and remodeling of dendritic spines in L4 neurons (Chen et al., 2015; Miquelajauregui et al., 2015). This use-dependent cellular remodeling in L4 persists into adulthood, even as L4 receptive field plasticity becomes very limited.

The cellular and circuit mechanisms for plasticity in L2/3 and L5 have been extensively studied (reviewed in Margolis et al., 2014). Depression of deprived whisker responses and potentiation of spared whisker responses are standard predictions of Hebbian synaptic plasticity, in which firing rates and correlations drive strengthening and weakening of synapses in excitatory networks (Hebb, 1949; Stent, 1973). Consistent with this model, substantial evidence

suggests that depression of deprived whisker responses in L2/3 involves LTD at L4–L2/3 synapses (Celikel et al., 2004; Bender et al., 2006; Nevian & Sakmann, 2006; Li et al., 2009), as well as reduced L2/3–L2/3 excitatory connectivity (reviewed in Feldman, 2009). Likewise, potentiation of spared whisker responses involves LTP at excitatory synapses, including L4–L2/3 synapses (Clem & Barth, 2006; Wright et al., 2008; Dachtler et al., 2011; Jacob et al., 2012); potentiation can also result from non-Hebbian homeostatic synaptic scaling (Greenhill et al., 2015). In L5, distinct subclasses of pyramidal cells mediate the depression and potentiation components of plasticity, due to differential regulation of excitatory synaptic inputs onto these subclasses (Jacob et al., 2012). In addition to regulation of synapse strength, plasticity also clearly involves synapse removal, formation, and differential stabilization, which can be observed in dendritic spine dynamics (reviewed in Holtmaat & Svoboda, 2009; Wilbrecht et al., 2010). Finally, anatomic restructuring of horizontal axons contributes to map plasticity as well (De Paola et al., 2006; Broser et al., 2008; Marik et al., 2010). Thus, map reorganization in somatosensory cortex is implemented by diverse synaptic and cellular changes in excitatory circuits, and across layers and columns.

Map plasticity also involves changes in inhibitory circuits. Whisker deprivation weakens whisker-evoked inhibition in L2/3 pyramidal cells due to reduced activation of L2/3 parvalbumin-positive interneurons, which reflects weakened L4 excitation onto these cells (House et al., 2011; Li et al., 2014). Deprivation also reduces recurrent inhibition in L2/3 (Shao et al., 2013). Parvalbumin-positive interneuron circuits are increasingly recognized as a site of rapid plasticity in sensory cortex (Griffin & Maffei, 2014), which may serve both to homeostatically regulate cortical firing rate, and to provide rapid disinhibition that enables subsequent Hebbian plasticity in excitatory networks (Kuhlman et al., 2013, in mouse V1).

Less is known about mechanisms of peripheral lesion–induced reorganization. However, processes comparable to those in use-dependent plasticity are presumably involved. In one model, the initial unmasking of previously subthreshold horizontal excitation in deafferented cortical territory may subsequently enable Hebbian reorganization of excitatory inputs that adjusts cortical receptive fields (Garraghty & Kaas, 1991; Garraghty et al., 1996, 2006; Myers et al., 2000; Wellman et al., 2002). As cortical receptive fields and maps shift, there is large-scale reorganization of horizontal axons (Florence et al., 1998; cf. Marik et al., 2014, in primate V1). In addition, in both primates and rodents, some cortical reorganization after peripheral or spinal cord lesions is driven by remapping in brainstem and thalamic nuclei (reviewed in Wall et al., 2002, and Kaas et al., 2008; Jain et al., 2008; Li et al., 2013, 2014; Kambi et al., 2014; Liao et al., 2016).

1.4.6. Relevance to recovery of function after stroke or peripheral injury

It seems reasonable to presume that a fuller understanding of map plasticity will enable new therapeutic interventions to promote recovery of function after peripheral injury or stroke, by optimizing map reorganization (reviewed in Xerri, 2012, and Qi et al., 2014). So far, progress has been slow, and drugs that effectively promote plasticity and recovery of function are lacking. Some studies in rodents and primates have focused on chondroitinase ABC, an enzyme that disrupts the extracellular matrix; this may facilitate axonal growth from surviving afferents when

injected locally after spinal cord lesions (Bradbury et al., 2002; Bowes et al., 2012), or traumatic brain injury (Harris et al., 2013). A second potentially useful strategy involves promoting the rapid disinhibition that precedes, and may gate, some forms of map plasticity (Kuhlman et al., 2013); manipulations of inhibition may re-open critical periods for plasticity, enabling recovery of function in adults (Davis et al., 2015). A third approach is to identify behavioral strategies that maximize normative map reorganization. For example, in rodent and primate models, somatotopic reorganization after focal cortical ischemia or cervical spinal cord injury is markedly more precise when environmental enrichment is applied during recovery. This is also associated with improvements in behavioral recovery (Xerri & Zennou-Azogui, 2003; Martinez et al., 2009; Qi et al., 2014; cf. Xerri et al., 1998). In the visual system, some researchers are exploring a promising but opposite approach, in which brief periods of sensory deprivation are used to reactivate plasticity in adult visual cortex, which is then followed by visual experience in order to promote recovery of visual function in models of amblyopia (Eaton et al., 2016). Which recovery paradigms are most effective remains to be determined, but the findings may be of great importance for clinicians and patients.

1.5. CONCLUSION

Although the general somatosensory map layout described by Penfield and Woolsey remains roughly accurate, the past three decades have greatly deepened our knowledge of the topography, functional dynamics, and plasticity of somatosensory maps. Further studies will be needed to describe the spatial distribution of single-cell tuning in cortical layers beyond L2/3 and in species beyond rodents, and to understand how complex naturalistic stimuli are processed within somatosensory maps. In particular, the potential mapping of sub-modalities within primates and rodents remains under-studied. Much of our current knowledge derives from neurophysiologic measurements under anesthesia; to understand how tactile information is processed for perceptual classification and decision-making, we need to examine map function in awake behaving animals more extensively. Sophisticated genetic techniques are now available for functionally assessing specific classes of neurons, at least in rodents. These studies are likely to reveal the distinct roles of particular cell types in fine-scale map organization. Perhaps most importantly for clinical applications, much additional work is necessary to determine how recovery from injury might be aided by interventions based on specific plasticity mechanisms, and on the biological processes that regulate plasticity and critical periods.

1.6. FIGURES FOR CHAPTER 1

Figure 1.1: Somatosensory pathways and maps in primates.

Figure 1.2: Somatotopic maps in humans.

Figure 1.3: Somatosensory maps in rats and mice.

Figure 1.4: Map plasticity in primates and rodents.

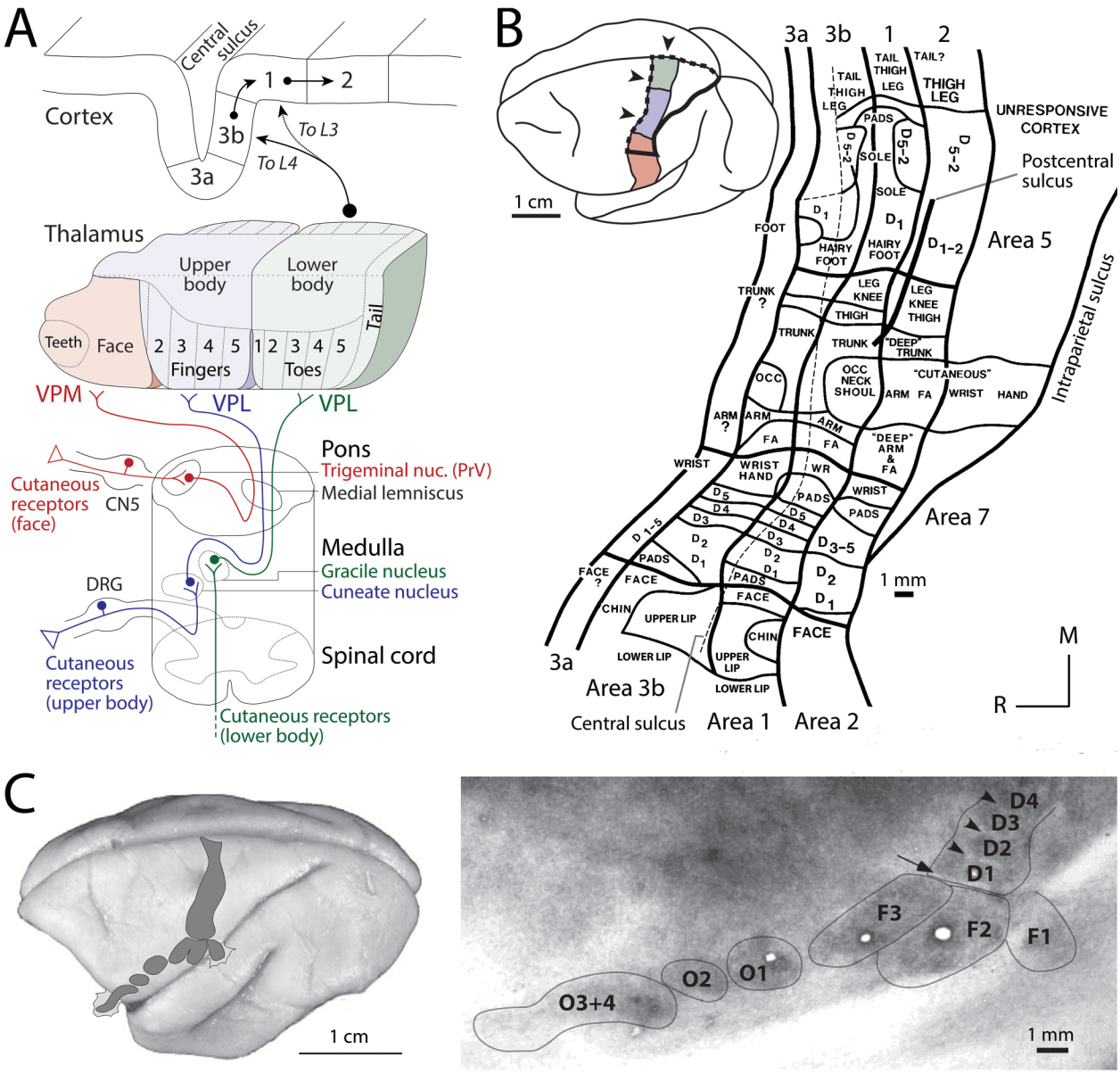

FIGURE 1.1: Somatosensory pathways and maps in primates.
Captions next page

FIGURE 1.1: Somatosensory pathways and maps in primates.

(A) Pathway for cutaneous input to anterior parietal cortex. DRG, dorsal root ganglia; CN5, trigeminal nerve; PrV, principal trigeminal nucleus; VPL, ventro-postero-lateral nucleus of the thalamus; VPM, ventro-postero-medial nucleus of the thalamus. The projection from dorsal column nuclei (gracile and cuneate) and trigeminal nuclei to thalamus is contralateral. The thalamo-cortical projection to layer (L) 4 of area 3b is a strong driving projection, whereas the projection to L3 of area 1 is lesser, and may be more modulatory. Diagram of the thalamus is based on its organization in squirrel monkeys (Kaas et al., 1984).

(B) Somatotopy of macaque anterior parietal cortex (areas 3a, 3b, 1, and 2), based on microelectrode recordings of cutaneous receptive fields under anesthesia. The map shows the postcentral gyrus, in addition to "unfolded" portions of the central sulcus (containing area 3a and most of 3b) and medial wall (the topmost portion of the figure, including the tail and portions of the thigh and leg). Note the magnification of the face, hand, and foot; mirror-reversal of representations in adjoining areas; and reduced precision of the area 2 map versus areas 3b and 1 (reproduced from Pons et al., 1985b).

Inset: outline of the regions of the macaque brain surface shown in the map. Arrowheads and dotted lines indicate the central sulcus and medial wall; lower body, upper body, and face representations colored as in panel A (adapted from Padberg et al., 2009). Note that the lower portion of the face and oral representation (red) is not included in the map (see Manger et al., 1996).

(C) Modular subdivisions of area 3b in the owl monkey.

Left: Location of major anatomical modules. The longest strip includes the body representation; smaller modules represent specific facial and oral features. Reproduced from Kaas et al., 2006.

Right: Myelin staining of flattened cortex showing myelin-rich modules separated by cell-poor septa. D1–4, modules for fingers 1 through 4. Arrowheads, septa between modules. F1, upper face. F2, upper lip. F3, lower lip. O1, contralateral teeth. O2, contralateral tongue. O3+O4, ipsilateral teeth and tongue. Holes in the tissue section are electrolytic marking lesions used to localize recordings during mapping (reproduced from Jain et al., 2001).

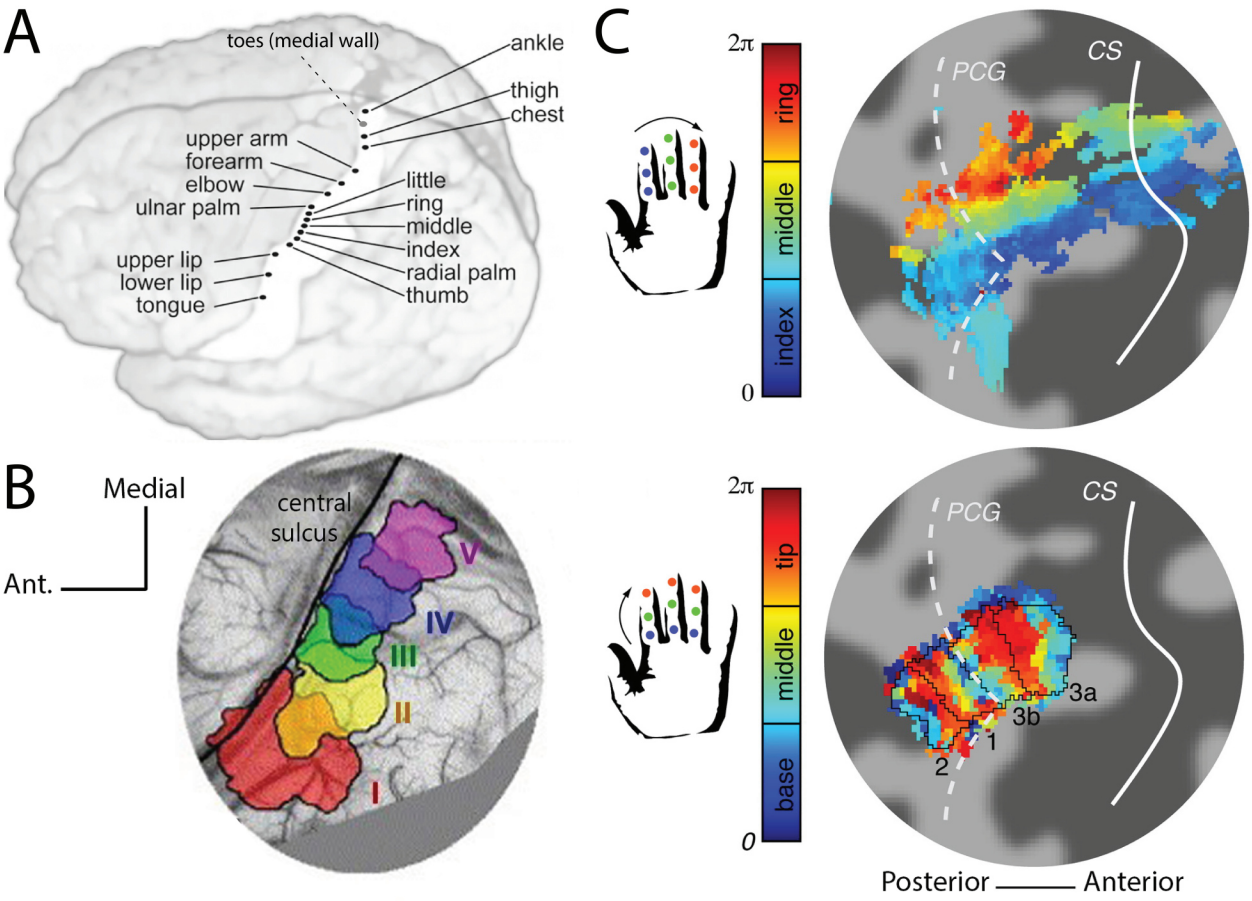

FIGURE 1.2: Somatotopic maps in humans.
Captions next page

FIGURE 1.2: Somatotopic maps in humans.

(A) Somatotopy in human area 3b, from magnetoencephalography (MEG) during tactile stimulation. Points show localization of different body parts (mean from five awake subjects) on the posterior bank of the central sulcus, based on sensory-evoked magnetic field components attributed to area 3b. The point localizing the toes refers to a position on the medial wall (reproduced from Kaas, 2012, based on Nakamura et al., 1998).

(B) Finger somatotopy in area 1 of an anesthetized patient during brain surgery, assessed by intrinsic signal optical imaging (ISOI) in response to electrical stimulation of the contralateral fingers. ISOI is an indirect measure of population neural activity (sub- and suprathreshold) based on modulations of red light reflectance by blood flow and oxygenation changes. Digits 1–5 (thumb through little finger) are represented from lateral to medial, with substantial overlap (reproduced from Sato et al., 2005).

(C) Finger somatotopy in areas 3a, 3b, 1, and 2, from 7-Tesla fMRI during vibrotactile stimulation of contralateral digits 2–4 (index, middle, and ring fingers) (reproduced from Sánchez-Panchuelo et al., 2014).

Top: Representation of digits 2–4, assessed by sequentially stimulating one finger at a time, with all three distal-to-proximal phalanges stimulated simultaneously. In this paradigm, digit identity corresponds to phase (0–2π) of the fMRI signal. A lateral-to-medial mapping of digits 2–4 is apparent.

Bottom: Somatotopic representation of the proximal-to-distal dimension along the fingers, assessed by sequentially stimulating proximal to distal phalanges, but across digits 2–4 simultaneously. Here, phase (0–2π) reflects proximal to distal position. Mirror reversals of finger representations are evident at the borders between adjacent areas.

CS: central sulcus; PCG: post-central gyrus. Boundaries of areas 3a, 3b, 1, and 2 are indicated. Cortical curvature has been flattened to a single depth.

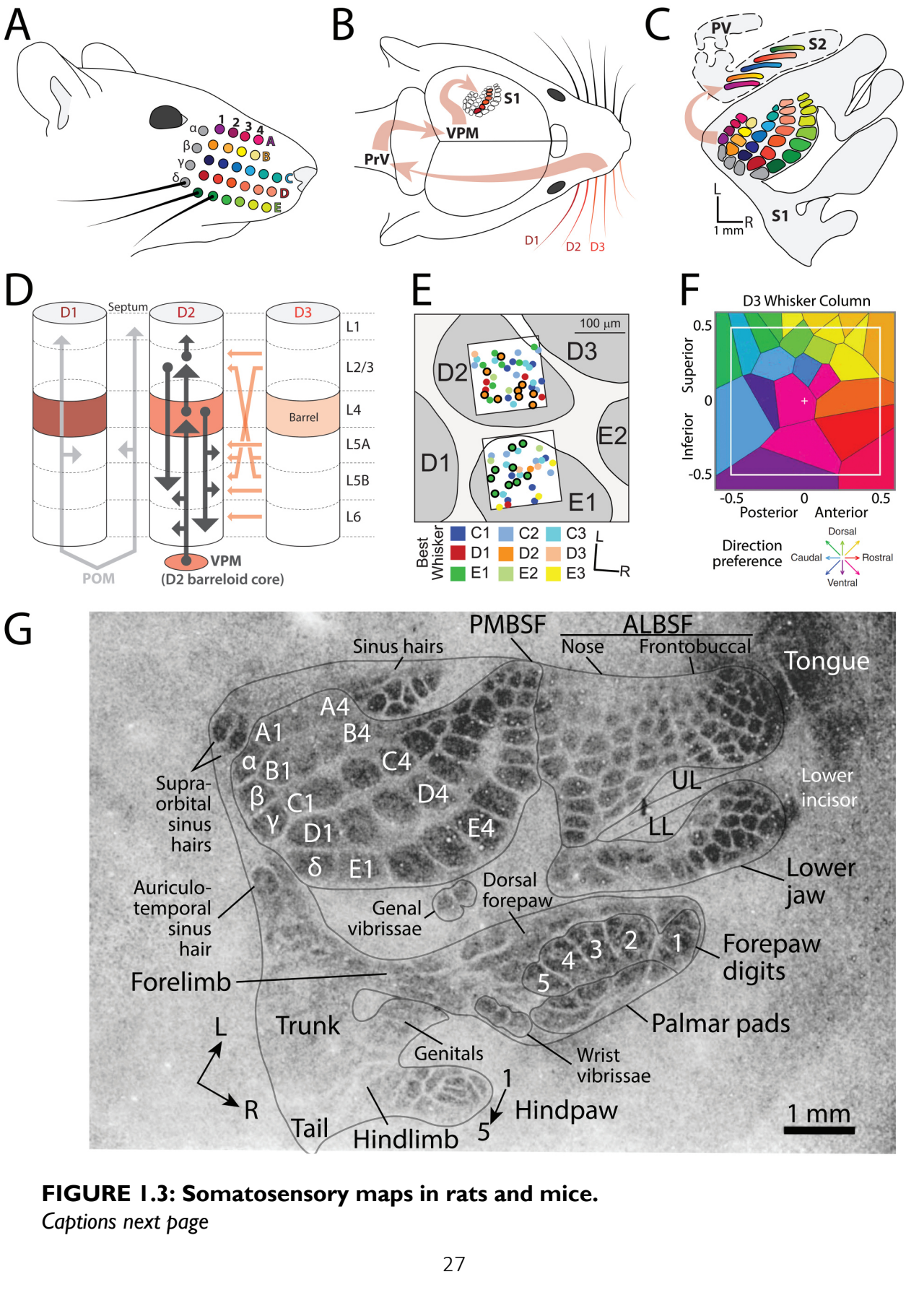

FIGURE 1.3: Somatosensory maps in rats and mice.
Captions next page

FIGURE 1.3: Somatosensory maps in rats and mice.

(A) The large facial whiskers (macrovibrissae) of rats and mice are identified by row (A–E) and arc (1–4+) coordinates, plus four straddler whiskers shown in grey (α, β, γ, δ).

(B) Tactile input to the whiskers is relayed via the principal trigeminal nucleus (PrV) and ventro-postero-medial nucleus of the thalamus (VPM) to the whisker barrels in layer 4 (L4) of primary somatosensory cortex (S1).

(C) Anatomical layout of whisker-related barrels in S1. Each barrel corresponds anatomically to one whisker, indicated by a color code shared with panel A. In secondary somatosensory cortex (S2), the whiskers in each row (A–E) are represented by a continuous band. A third body map exists in the parietal ventral area (PV). Note that the body representations are mirrored across the S1/S2 and S2/PV areal boundaries.

(D) Schematic of information flow within S1. Cylinders are cortical columns centered on each L4 barrel. The lemniscal pathway (dark grey) is oriented mainly vertically within columns, and largely preserves columnar segregation of whisker information. Surround whisker information also enters each column, especially outside of L4, via (a) horizontal connections between columns (shown from D3 to D2 columns; orange), and (b) the para-lemniscal pathway (light grey), which relays multi-whisker inputs via POm to L5A, L1, and (in the mouse) L2/3. In rats, septa between columns receive their major input from the para-lemniscal pathway.

(E) Micro-scale organization of somatotopic tuning within single whisker columns in L2 of mouse S1, as shown by two-photon calcium imaging. Each dot is a neuron, colored to indicate the whisker evoking the strongest response ("best whisker"). Two imaging fields are shown, superimposed on histologically confirmed L4 barrel outlines. In each column, neurons show intermixed, salt-and-pepper tuning for different whiskers, with a plurality of neurons tuned for the whisker anatomically corresponding to the column (dots with bold outlines) (adapted from Clancy et al., 2015).

(F) Map of direction preference in layers 2–4 of the D3 whisker column in rat S1, inferred from extracellular single-unit recordings. The white box indicates borders of the D3 column. Colors indicate regions of different direction preference for D3 whisker deflection, as defined in the legend (inset, below) (reproduced from Anderman & Moore, 2006).

(G) Somatotopic organization of rat S1, revealed by staining for the mitochondrial enzyme succinate dehydrogenase (SDH). The cortex has been flattened. PMBSF, posteromedial barrel subfield, containing whisker-related barrels (as in panel C). ALBSF, anterolateral barrel subfield, containing smaller barrels for the microvibrissae. UL, upper lip; LL, lower lip (histological image reproduced from Dawson & Killackey, 1987; localization of the genitals based on Lenschow et al., 2016).

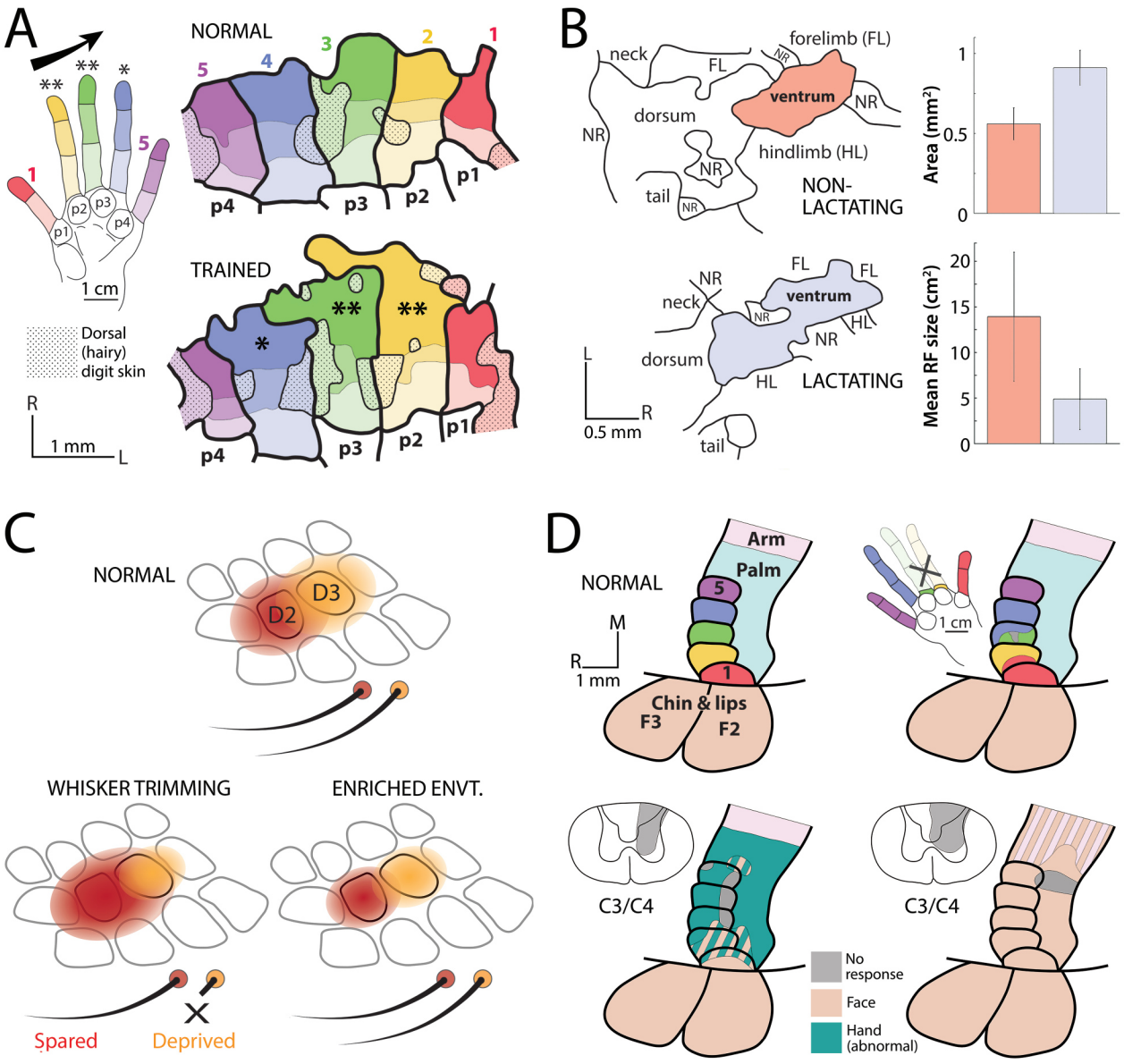

FIGURE 1.4: Map plasticity in primates and rodents.
Captions next page

FIGURE 1.4: Map plasticity in primates and rodents.

(A) Use-dependent plasticity of finger representations in area 3b of an adult owl monkey. Maps of the hand region were determined from extracellular recordings of cutaneous receptive fields (RFs) under anesthesia. After a few months of daily training on a task requiring application of regulated fingertip pressure to a revolving textured disk for food reward, representation of the fingertips most used in the task expanded (**; fingers 2 & 3), with lesser enlargement of a fingertip occasionally stimulated in the task (*; finger 4) (adapted from Jenkins et al., 1990).

(B) Use-dependent plasticity of the ventrum map in rat S1 associated with nursing in lactating females.

Left: example maps for one non-lactating (top) and one lactating (bottom) rat, measured by extracellular recording under anesthesia. NR, no cutaneous response.

Right: Cortical area representing the ventrum (top) and mean receptive field (RF) size (bottom), in non-lactating (red) and lactating (blue) rats. Error bars are SDs (adapted from Xerri et al., 1994).

(C) Schematic of use-dependent plasticity of the whisker representations in L2/3 of rat S1. Top: depiction of L2/3 representations of two whiskers, superimposed on L4 barrel outlines. Bottom left: trimming one whisker for several days to weeks causes depression and contraction of the trimmed whisker representation (response depression), and potentiation and expansion of the spared surrounding whisker representations (response potentiation). Bottom right: Environmental enrichment causes whisker representations to sharpen and contract.

(D) Lesion-induced reorganization in area 3b of adult owl monkeys. Top left: normal organization of the arm, hand, and face representations in area 3b. Top right: 8.5 months after amputation of fingers 2 and 3, the finger stumps are topographically represented, but large portions of the amputated finger territories are invaded by representations of the neighboring fingers (adapted from Merzenich et al., 1984). Bottom left: six months after partial dorsal column section at the level of spinal nerves C3/C4, the hand representation is partially invaded by the face representation, and otherwise shows abnormal hand responses (expanded representation of spared afferents from the palm and certain digits) (adapted from Jain et al., 1997, 1998b). Bottom right: eight months after complete dorsal column section at the C3/C4 level, the fully de-afferented hand region is invaded by the facial representation, and the arm representation displays mixed face and arm responses (adapted from Jain et al., 1997). Note the persistence of unresponsive "silent" zones (grey). Maps are based on multi-unit recordings under anesthesia.

CHAPTER 2:
SOMATOTOPIC PRECISION OF WHISKER TUNING IN LAYER 2/3 OF RAT BARREL CORTEX

INTRODUCTION

A consistent feature of mammalian primary visual (V1), auditory (A1), and somatosensory (S1) cortex is the representation of the sensory periphery by topographic maps across the cortical surface (Hubel & Wiesel, 1974; Schreiner & Winer, 2007; Chapter 1). Although each of these cortices maintains map topography at a coarse scale, the local tuning of single cells may be largely homogeneous (e.g., orientation tuning in cat V1), or may follow a heterogeneous "salt-and-pepper" organization in which nearby cells have diverse receptive fields (e.g., rodent V1 and A1; Ohki et al., 2005; Bandyopadhyay et al., 2010; Rothschild et al., 2010; Bonin et al., 2011; Kanold et al., 2014). Local topography can also vary by cortical layer, as thalamic inputs are sequentially processed to integrate mapped parameters and refine representations (e.g., Winkowski & Kanold, 2013). Here, we test the precision of the whisker map in the upper layers (2/3) of rat S1, for comparison to both the homogeneous tuning classically described in layer 4 and the salt-and-pepper tuning recently shown in mouse layer 2.

Rodent S1 contains a model somatotopic map, in which each of the large facial whiskers is represented by a cortical column centered on a distinct cluster ("barrel") of thalamorecipient cells in layer (L) 4 (Woolsey & van der Loos, 1970). The majority of cells in the L4 barrels are tuned to the whisker anatomically matched to their column (the columnar whisker, CW), with weaker responses to neighboring whiskers (surround whiskers, SW) (Simons, 1978; Brecht & Sakmann, 2002). Because whisker signals are processed mainly vertically within each column—canonically, from L4 $\rightarrow$ L2/3 $\rightarrow$ L5 and L6 (Feldmeyer, 2012)—it is often assumed that cells throughout each column retain the largely homogeneous CW tuning described in L4. However, more recent calcium imaging studies in mice have revealed salt-and-pepper tuning within columnar L2, with markedly different CW selectivity even among neighboring cells (Sato et al., 2007), and fewer than one third of cells best driven by the CW as compared with its eight surrounds (Clancy et al., 2015). It is unclear whether similarly heterogeneous tuning is seen in mouse L3, or in rat L2/3; both layer and species differences are plausible. In mouse, L3 and L2 receive distinct inputs—from the mono-whisker lemniscal pathway and multi-whisker paralemniscal pathway, respectively (Bureau et al., 2006). By contrast, in rats, columnar L2/3 appears to be driven throughout by lemniscal input from L4 (Shepherd & Svoboda, 2005), with lesser input from L5 to upper L2/3 (Staiger et al., 2014). Rat S1 remains a powerful model system for map plasticity and sensory coding (Feldmeyer et al., 2013), and an accurate model of map precision in rat L2/3 is therefore of considerable value.

Whisker tuning in rat L2/3 cells has been directly examined in a limited number of studies, using extracellular recordings in anesthetized animals. Classical extracellular recording studies found that within rat whisker columns, the group of whiskers that best drive spiking includes the CW in 80–90% of cells in both L2/3 and L4 (Simons, 1978; Armstrong-James & Fox, 1987). Subsequent studies have found that 10% of columnar L2/3 cells were better tuned to a single tested surround whisker than to the CW, suggesting that for a high proportion of cells the absolute best whisker may be a surround whisker if all SWs were tested (Glazewski & Fox, 1996;

Glazewski et al., 1999, 2000). More recently, it was reported that only 26% of L2/3 regular-spiking cells displayed significant responses to CW stimulation in both rostral and caudal directions, in contrast with more stable tuning in L4 and among fast-spiking cells (Le Cam et al., 2011); thus, somatotopy in L2/3 may be direction-dependent, with CW tuning in single cells less robust across diverse stimuli than is often assumed. The picture of L2/3 somatotopy emerging from this work is unclear and somewhat conflicting, and to our knowledge no recent studies have aimed to comprehensively describe single-whisker tuning in rat L2/3.

The present experiments examine the precision of the rat L2/3 whisker map, by describing the tuning of neurons to the CW and its eight SWs under single-whisker stimulation. Using extracellular recordings in L2/3 whisker columns, we investigated what fraction of regular-spiking (RS) cells had the CW or an SW as their absolute best whisker (BW), or among a statistically equivalent group of best whiskers (equal best whiskers, eBWs). Relatedly, we assessed the sharpness of the tuning curve in CW-and SW-tuned cells, and examined whether response latencies in these subgroups varied as consistent with distinct intracortical pathways. We further studied whether these tuning properties differed among cells from different depths or radial positions within the L2/3 column. Finally, we asked whether fast-spiking (FS) cells follow a similar tuning distribution to that seen for our RS units.

2.1. MATERIALS AND METHODS

All procedures were approved by the University of California, Berkeley Animal Care and Use Committee, and followed NIH guidelines. Subjects were male Long-Evans rats (mean, s.d.: 285 ± 60 g, 53 ± 11 postnatal days, n = 14).

2.1.1. Surgery, anesthesia, and whisker mapping

Rats were anesthetized with urethane (1.4 g/kg, 20% in sterile saline, i.p.). A craniotomy was made over left S1 (5.5 mm lateral, 2.5 mm caudal to bregma) and a durotomy completed to allow electrophysiological recording. Throughout each experiment, anesthesia was maintained with 5–10% supplemental urethane as needed, body temperature was held at 37°C, and the brain was kept moist with sterile saline.

Initial mapping of whisker columns was assessed based on L4 multi-unit activity (650–900 µm subpial) recorded with tungsten electrodes (FHC). We used search stimuli including both the biphasic waveform used for our main analyses and caudo-rostral ramp-hold-return deflections (4 ms risetime, 400 ms plateau), all presented to multiple single whiskers at multiple amplitudes. We considered a penetration to lie within a given whisker column if the anatomically matched whisker (columnar whisker, CW), as compared to its eight immediate surround whiskers (SWs), elicited multi-unit responses with the shortest latency and largest number of evoked spikes in a 100-ms window after stimulus onset, according to online analysis routines in IgorPro (Wavemetrics).

2.1.2. Whisker stimuli

Stimuli were delivered to the putative CW and to its eight immediate SWs using a custom-built 3×3 array of independent, computer-controlled piezoelectric benders (Noliac CMBP05), each extended by a carbon fiber bar. Whiskers were glued, 5 mm from the face, to lightweight plastic tubes attached to the carbon fiber bars. Stimuli were delivered in pseudorandom interleaved order, with a period of 1.4–1.8 ms. The stimulus was a naturalistic, 50-ms, roughly biphasic waveform along the rostro-caudal axis (Estebanez et al., 2012, "common filter 2"), applied with peak amplitudes of 0.5° and 1° in the rostral and in the caudal direction (i.e., 4 amplitude/direction combinations × 9 whiskers = 36 total stimuli). Each stimulus (i.e., each amplitude/direction combination) was presented to each whisker 200–300 times (100 times in one experiment, 20150820; n = 2 FS units). Stimulus delivery was controlled and recorded using custom routines in IgorPro (Wavemetrics). Piezoelectric benders were calibrated using a laser displacement sensor (Micro-Epsilon optoNCDT 1700-2). Ringing of the piezo benders was measured at 4–5.7% of stimulus amplitude; fractional bleed-through to the central piezo from simultaneous motion of the eight surround piezos was measured at 7–7.5% of stimulus amplitude.

In seven experiments (20150824, 20150827, 20160128, 20160519, 20160830, 20160901, 20160906), 1.5° stimuli were also applied. In one experiment (20150820), rostral stimuli were not applied; in two experiments (20150824; 20150827), rostral stimuli were applied only at 1°. Analyses comparing rostral versus caudal stimuli (Figures 2.3 and 2.4A) were performed only for those stimulus amplitudes presented in both directions in a recording.

2.1.3. Extracellular recording

Extracellular activity was recorded using 16- or 32-channel silicon polytrodes (NeuroNexus, A1x16-Poly2-5mm-50s-177 or A1x32-Poly2-5mm-50s-177; electrode size 177 μm^2). Signals were acquired in discrete sweeps (500–1000 ms) including ≥ 200 ms pre-stimulus and ≥ 300 ms post–stimulus onset. Signals were preamplified (20×, Plexon Instruments HST/16V-G20 or HST/32V-G20), further amplified (50×, Plexon Instruments PBX2/16sp-G50), bandpass filtered (0.3–8 kHz), and digitized at 31.25 kHz. L2/3 recordings were made at 150–650 µm subpial depth.

2.1.4. Histology

DiI markings (DiCarlo et al., 1996) were placed in the whisker cortex at the end of each recording, to allow histological verification of MUA-based targeting of whisker columns and analysis of recordings by their normalized location in the column. Markings were placed at the site of recording, using a polytrode with the same geometry as that used for recording. Rats were then anesthetized with isoflurane before decapitation, the brain was removed and fixed with 4% paraformaldehyde, and the cortex was subsequently isolated and flattened. 100-µm tangential sections were prepared and stained for cytochrome oxidase (CO) to visualize the L4 whisker barrels.

To locate penetrations in a normalized whisker-column with polar coordinates, a line was fit to the centroids of the DiI-marked whisker barrel and its two neighbors in the same barrel row (ImageJ, National Institutes of Health). The parallel line through the centroid of the marked

barrel, and pointing toward the barrel one arc behind (CW arc − 1) in the same row, was taken as the polar axis. The penetration location was then recorded as the polar coordinates of the centroid of the DiI marking, with angle given relative to the polar axis and radius given by the fractional distance to the edge of the CO-stained barrel (edge = 1).

2.1.5. Spike sorting

Spike waveforms were detected, aligned, and hierarchically clustered offline using UltraMegaSort 2000 (Hill et al., 2011; detection threshold 3.5 s.d. above noise; 1.5 ms waveform window; 0.5 ms censoring shadow), with reduction of the noise floor across electrodes by common-average referencing (Ludwig et al., 2009). Clusters were manually refined to identify single units, based on waveform shape, separability (in principle component space and by the Fisher linear discriminant), and interspike-interval distributions. Units were excluded from analysis if they displayed > 1% refractory period violations (interspike interval < 1.4 ms) or > 30% missing spikes (based on comparison of the Gaussian-fitted distribution of spike amplitudes on each unit's best tetrode channel with the 3.5 s.d. spike-detection threshold).

Single units of acceptable quality were obtained from "upper" L2/3 (here defined as 150–399 µm) in all 14 animals, and from "lower" L2/3 (400–650 µm) in 13 of these. Units were identified as **regular-spiking** (**RS**) or **fast-spiking** (**FS**) based on the trough-to-peak time of the mean spike waveform on each unit's best tetrode channel (i.e., the channel capturing the largest negative amplitude for the unit). We identified two distinct clusters, with FS units having trough-to-peak time < 0.5 ms, and RS > 0.5 ms.

2.1.6. Data analysis

Analysis of single-unit and population data was performed in MATLAB (MathWorks). The single-whisker stimuli applied during recording were analyzed pooled by amplitude (0.5° or 1°; 200–300 presentations of each stimulus to each whisker), pooled by direction (rostral or caudal; 200–300 presentations), and pooled by both amplitude and direction (400–600 presentations), with comparison between whiskers in each case. Baseline and post-stimulus spike count distributions were calculated for 100-ms windows before and after stimulus onset, respectively; net-evoked spike count distributions were calculated by subtracting the baseline counts from the post-stimulus counts.

For all analyses, the **onset latency** of single- or multi-unit responses to each stimulus, as applied to a given whisker, was calculated by a binless algorithm using a Poisson cumulative distribution function to identify the first timepoint at which the total cumulative spikes after stimulus onset had probability < 0.05 of being generated under the mean baseline firing rate (Victor, 2002; Chase & Young, 2007). The response to a stimulus to a given whisker was considered significant if its latency was within the 100-ms response window after stimulus onset. For each stimulus, the **significant whiskers** were defined as those eliciting latencies within the response window. The **best whisker** (BW) was the significant whisker eliciting the highest mean net-evoked spike count, with ties going to the whisker with a shorter latency. The group of statistically equivalent best whiskers (**equal best whiskers**, eBWs) were identified as those whiskers eliciting mean net-evoked spike counts not significantly different from that of the best

whisker, based on the bootstrapped confidence interval for each mean difference (1000 iterations, alpha = 0.05; controlling for false-discovery rate per Benjamini & Hochberg, 1995). The **eBW70** was defined as the group of eBWs eliciting mean net-evoked spike counts > 70% that elicited by the BW.

For comparison of responses to caudal and rostral stimuli, the **within-row center of mass** (**WRCM**) was calculated as the mean net-evoked spikes (S) for the rostral row-mate whisker ("CW + 1"), minus the mean net-evoked spikes for the caudal row-mate whisker ("CW − 1"), all divided by the sum of the mean net-evoked spikes for the CW and both row-mates:

$$[S_{(CW+1)} - S_{(CW-1)}] / [S_{(CW+1)} + S_{CW} + S_{(CW-1)}]$$

To measure the sharpness of tuning about the BW, we calculated a **BW tuning score** by dividing the mean BW net-evoked spike count by the grand mean net-evoked spike count for the BW's tested surround whiskers. The **CW tuning score** was calculated by dividing the mean CW net-evoked spike count by the grand mean net-evoked spike count for the CW's eight surrounds.

2.2. RESULTS

We recorded and analyzed single units within rat L2/3 whisker columns, at 150–650 µm subpial depths (n = 14 rats, 16 penetrations; Figure 2.1D). Whisker columns were targeted during recording based on multi-unit activity, and targeting was later confirmed by recovery of DiI markings from cytochrome oxidase–stained tangential sections through the L4 barrel field (Figure 2.1B–C). The columnar whisker (CW) for the targeted column and its eight surrounds were stimulated one at a time, in pseudorandom order, using a deflection waveform previously shown to capture a majority of the variance among optimal stimuli derived for single units in layers 4–6 by reverse correlation (Estebanez et al., 2012; Figure 2.1A). To test for variations in tuning based on stimulus direction (e.g., Le Cam et al., 2011), we delivered our stimuli with the peak amplitude in the rostral direction, and also with the peak in the caudal direction.

Whisker tuning curves derived using overly strong stimuli may yield underestimates of receptive field sharpness, for multiple reasons. First, such stimuli may saturate responses to multiple whiskers. In addition, single spikes are identified in extracellular recording data when the signal crosses a detection threshold, and a censoring window is then applied to avoid multiple detections of the same event; therefore, if multiple cells generate spikes closely time-locked to strong stimulation of a shared best whisker, these spikes may be preferentially lost to censoring. To address these concerns, we applied stimuli with low peak amplitudes (0.5°, 1°, and 1.5°) at or below the plateau of multi-unit responses to the CW. The best whisker distribution and population nine-whisker tuning curves obtained for regular-spiking units by analyzing only 0.5° stimuli (Supplemental Figure 1) closely match those obtained from our main analyses pooling stimuli across all amplitudes and directions (cf. Figures 2.4, 2.5). Thus, the amplitude range used here does not appear to distort tuning by eliciting maximal responses or censoring.

Our recordings yielded 128 units, isolated via automated clustering and manual refinement according to strict quality metrics (Figure 2.2A–B; see Materials and Methods). These

comprised 104 regular-spiking (RS) units and 24 fast-spiking (FS) units (18.75%), distinguished based on the trough-to-peak interval of each unit's waveform (Figure 2.2C–D; Table 2.1). Only two RS units and one FS unit displayed no significant response to any stimulus tested; these three units were excluded from subsequent analysis. In analyzing the tuning properties of each unit, we first calculated the response onset latency to stimuli applied to each whisker, using a binless algorithm that detects the first significant deviation of the spike rate from the baseline distribution under Poisson assumptions (Chase & Young, 2007). We considered a unit's significant whiskers under a given stimulus to be those eliciting latencies within 100 ms of stimulus onset; the significant whisker eliciting the largest number of net-evoked spikes in this time window was identified as the best whisker (BW).

2.2.1. Tuning does not differ systematically under caudal and rostral stimuli (Figure 2.3)

We initially asked whether the whisker tuning of L2/3 cells differed under caudal versus rostral applications of our stimulus. The best whisker as assessed under caudal and rostral stimuli was indeed different for many units; only 59% of RS units (61/103), and 62% of FS units (13/21), had the same BW for both stimulus directions. We therefore tested whether these direction-dependent changes in the tuning of individual units followed systematic patterns, such that our RS and FS cell populations might display different tuning distributions under caudal and rostral stimuli.

First, we considered that stimulus direction may modulate the strength of cells' responses. To test this possibility we calculated, for each unit, the ratio of evoked spike counts under rostral versus caudal stimuli (grand mean across all nine whiskers; Figure 2.3A); the ratio of mean BW-evoked spike counts under rostral versus caudal stimuli (Figure 2.3B); and the difference between the BW response onset latencies under caudal versus rostral stimuli (Figure 2.3C). Among RS and among FS units, all three values were distributed normally with means close to zero. Thus, although individual units were more responsive to caudal or to rostral stimuli, there was no consistent bias in favor of either stimulus direction at the population level.

Second, we considered that stimulus direction might modulate the shape of cells' whisker tuning curves about the CW—such that, for example, caudal stimuli promote increased responsiveness to rostral surround whiskers (Andermann & Moore, 2006). To obtain a quantitative measure of the effect of stimulus direction on tuning, we calculated the within-row center of mass (WRCM): the center of mass of evoked responses to the CW and to its two SWs in the same whisker row (which drive spikes in the home column more effectively than SWs from different rows; see, e.g., Figure 2.4C–D). Under both caudal and rostral stimuli, we found many individual units with a WRCM displaced from the CW. However, the mean WRCM for the RS and the FS populations was centered on the CW under both stimulus directions (Figure 2.3D). To test whether individual cells' WRCM values changed systematically between caudal and rostral stimuli, we calculated the difference between caudal and rostral WRCMs for each unit. For both RS and FS units, the change in WRCM was distributed normally about zero (Figure 2.3E). Thus, as with the measures of responsiveness detailed above, there was no consistent effect of stimulus direction on whisker tuning within the CW row.

It is possible that more notable direction effects would be found using strictly caudal and rostral stimuli (rather than the multi-phasic waveform we applied), or by using older animals (in which direction mapping may have developed more fully; Kremer et al., 2011). For the present analysis, we pooled caudal and rostral stimuli together on the basis that their effect on tuning at the population level appears to be neutral.

2.2.2. The columnar whisker is usually among the best whiskers for regular-spiking units, but often not the absolute best (Figure 2.4)

Analyzing responses to all stimuli pooled together (i.e., across directions and amplitudes), we found that the CW was the best whisker in 59% of RS units (60/102; Figure 2.4A). Because identifying a unit's best whisker based simply on evoked spike counts may draw a statistically arbitrary distinction between whiskers evoking slightly different response rates, we also determined the group of statistically equivalent best whiskers for each unit (equal best whiskers, eBWs). We identified the eBWs using bootstrapped confidence intervals for the difference in mean evoked counts between the BW and each other significant whisker. We found that RS units had on average 6.58 ± 2.49 (s.d.) equal best whiskers (Figure 2.4B, x = 0 data point). The CW was among the eBWs in nearly all RS units (100/102), but was the sole eBW in only 4% (4/102).

The high number of equal best whiskers identified for most cells here is at odds with the relatively sharp tuning documented in L2/3 by prior studies (e.g., de Kock et al., 2007; Clancy et al., 2015), suggesting the possibility that under-sampling in our data rendered some whiskers statistically indistinguishable from the BW despite their driving many fewer spikes. To test this, we determined how many of the eBWs for each unit yielded a mean evoked spike count exceeding various fractions of the best whisker's mean evoked count (Figure 2.4B). As suspected, a unit's eBWs on average included some whiskers driving as few as 20% as many spikes as the BW, demonstrating that the eBW metric on its own offered an over-inclusive picture of whisker tuning. We therefore selected the subset of eBWs eliciting at least 70% as many spikes as the BW as a reasonable compromise between simplistic identification of a single best whisker and an overly broad equivalence between many responsive whiskers. This subset of eBWs, the "eBW70", is used in several subsequent analyses, and comprised 2.79 ± 2.17 whiskers on average. The CW was among the eBW70 in 88% of RS units (90/102; Figure 2.4A), and was the sole eBW70 member in 31% of RS units, spread throughout L2/3 (32/102; mean depth 419.5 ± 147.5 µm, range 175–650).

Taken together, these data indicate that although the CW is *among* the group of comparably significant "best" whiskers in as many as 90% of L2/3 RS cells, it is likely the *absolute* best whisker in < 60%, and is uniquely predominant (e.g., the sole eBW70) in only a minority. This bias toward CW tuning among single RS cells is sufficient to produce clear CW tuning in the multi-unit activity (e.g., Figure 2.5A), which we observed at all columnar recording sites. It exceeds the prevalence of CW tuning reported in mouse L2 cells with calcium imaging (Clancy et al., 2015; see discussion of tuning as a function of depth, section 2.2.4), while falling short of the strict CW tuning canonically described in L4.

Among the 41% of RS units (42/102) for which the CW was not the best whisker, the BW was most often the CW's immediately rostral or caudal row-mate (in 16% and 12% of RS units, respectively), and rarely lay in the superior or inferior row (Figure 2.4C). Similarly, the row-mate whiskers were each members of the eBW70 for 40% of units (41/102), with whiskers from the superior or inferior row included less frequently (12%–29%; Figure 2.4D). These results are consistent with the preferential horizontal connectivity along column rows rather than arcs in S1 (Hoeflinger et al., 1995, Petersen et al., 2003).

When we analyzed RS units based on their responses to caudal or to rostral stimuli separately (n = 103), a slightly lower fraction of units had the CW as the best whisker (50.5% and 51.5%, respectively), or among the eBW70 (82.5% and 80.6%) or eBW (92.2% and 93.2%) (Figure 2.4A). This results from a subset of units in which CW-evoked responses were exceeded by an SW in one direction, or by different SWs in each direction, but nonetheless predominated when the two directions were pooled together. Indeed, only 35.9% of RS units (37/103) had the CW as the best whisker under both caudal and rostral stimuli, while 71.8% (74/103) had the CW among the eBW70 under both conditions (90.3% for the eBW). Although lower than the values obtained by pooling caudal and rostral stimuli together, these fractions are still much higher than the mere 26% of L2/3 RS units previously found to be *responsive* to the CW under stimuli in both directions (Le Cam et al., 2011, using similar stimulus amplitudes and anesthesia). This may result from our use of a stimulus with bidirectional components.

2.2.3. Whisker tuning curves reveal regular-spiking units sharply tuned to the columnar whisker or to surround whiskers (Figures 2.5 & 2.6)

We next examined whether CW- and SW-tuned RS units differed in how sharply they were tuned. In particular, we considered the possibility that units best driven by a surround whisker might represent a population more broadly responsive than the CW-tuned majority. To test whether tuning sharpness varied with best whisker identity across the cell population, we divided RS units into three tuning groups (Table 2.1): units with the CW as best whisker ("**CW-units**", n = 60/102), units with an SW as best whisker and the CW among the eBW70 ("**SW/CW-units**", n = 30/102), and units with an SW as best whisker and the CW not among the eBW70 ("**SW-units**", n = 12/102). SW/CW- and SW-units together comprise "**non-CW-units**". As expected, SW-units had BW-evoked spike counts significantly different from their CW-evoked counts ($p = 0.00094$, two-tailed paired *t*-test). There was no significant effect of tuning group on units' baseline firing rates (Welch's ANOVA, $p = 0.54$; means ± s.d.: 0.64 ± 0.89, 0.97 ± 1.46, and 0.76 ± 1.28, respectively; Figure 2.5E), or on units' BW-evoked spike count (Welch's ANOVA, $p = 0.67$; means 0.22 ± 0.28, 0.18 ± 0.20, 0.21 ± 0.16; Supplemental Figure 2). Thus, the apparent tuning differences between these groups do not reflect major differences in baseline activity, and are not an artifact of insufficient sampling in poorly responsive units.

To compare the three tuning groups using a quantitative measure of tuning sharpness about the best whisker, we calculated a BW tuning score by dividing the mean BW-evoked spikes by the grand mean of spikes evoked by the adjacent whiskers (for those units with data available for at least five adjacent whiskers: 60 CW-units, 24 SW/CW-units, 10 SW-units). Lower scores indicate broader tuning. There was a significant ($p < 0.05$) effect of tuning group on BW tuning

score (Welch's ANOVA, p = 0.0001), and CW-units had BW tuning scores (5.0 ± 3.7) significantly different from the lower scores of SW/CW-units (2.4 ± 1.4). However, the BW tuning scores of SW-units (3.6 ± 1.6) did not differ significantly from those of the other two groups (Games-Howell *post hoc* test). Thus, a subset of RS units were tuned to an SW with sharpness comparable to that of the CW-tuned population. A single recording site often included units tuned clearly to the CW or to a specific BW, in addition to other units with less selective tuning, as demonstrated by their nine-whisker tuning curves and peristimulus time histograms (PSTHs) (Figure 2.5A).

This result is supported by visual examination of the BW-centered nine-whisker tuning curves for the full RS unit population and for the units in each tuning group (i.e., CW-units, SW/CW-units, and SW-units). The curve for all RS units demonstrated clear BW tuning, with non-best whiskers eliciting fewer than half as many spikes per stimulus (mean non-best/BW spike count fraction 0.34, range 0.21–0.49; Figure 2.5B). The population curves for the 60 CW-units (mean fraction 0.29, range 0.19–0.48) and the 12 SW-units (0.31, 0.15–0.52) were similar to the curve for the full RS population; the curve for the 30 SW/CW units was somewhat broader (0.53, 0.31–0.72; Figures 2.5C–E, top panels). BW-evoked PSTHs for all three groups demonstrated a clear stimulus-locked response (Figures 2.5C–E, bottom panels). Tuning curves for each unit in all three tuning groups are shown in Figure 2.6 (A–C).

2.2.4. CW- and non-CW regular-spiking units: comparison of whisker latencies, depth, and location within the column (Figures 2.7 & 2.8; Supplemental Figure 3)

It is plausible that CW-units and non-CW-units might receive inputs from their driving whiskers via distinct intracortical pathways. For example, CW-units might be preferentially located in lower L2/3 and receive stronger lemniscal input from L4 (or directly from thalamus; Oberlaender et al., 2012); non-CW-units might receive initial CW-dominated input, from co-columnar L4, that is subsequently exceeded by SW signals via horizontal inputs, perhaps targeting particular depths or radial locations within the column. We tested for such differences indirectly, by comparing RS units in different tuning groups in terms of their response onset latencies, depth within the whisker column, or radial distance from the column center.

We first compared best whisker latencies in CW-units (n = 60) and in non-CW-units (n = 42, including 30 SW/CW-units, and 12 SW-units). Best whisker latencies were shorter for the CW-units (25.1 ± 8.5 ms, vs. 29.8 ± 15.9 ms), and this difference approached significance (p = 0.06, two-sample *t*-test). (The mean BW latency for the 12 SW-units was 27.9 ± 16.4 ms). In addition, whereas the CW yielded the shortest onset latency in 72% (43/60) of CW-units, the preferred SW yielded the shortest onset latency in only 45% (19/42) of non-CW-units (including 7/12 SW-units). These trends are consistent with a less direct pathway for SW inputs.

We therefore considered that CW stimuli might evoke the fastest responses even in units where an SW evoked more spikes. However, among non-CW-units, the mean BW and CW onset latencies were almost identical (BW, 29.8 ± 15.9 ms; CW, 30.1 ± 14.2 ms; p = 0.22, two-tailed paired *t*-test, n = 40; two SW units were excluded from this analysis because they lacked a significant CW response) (Figure 2.7B). In addition, the distribution of differences between the CW and BW onset latency for these units was roughly normal, with a mean close to zero (1.74

ms; Figure 2.7C). Therefore, CW latencies are not preferentially shorter than BW latencies in non-CW-units. This may result from a less direct CW input pathway to these units that allows an SW to predominate, although it is possible that in some of these units the longer CW latency, and weaker CW responses, result from censoring.

Next, we asked whether the prevalence of CW- and non-CW-units in L2/3 varies according to depth within the column. We found that the BW and eBW70 distributions reported above for all L2/3 RS units were similar to those for RS units limited to upper or lower L2/3 (150–399 and 400–650 µm, respectively; Supplemental Figure 3). Among upper L2/3 RS units, 59% had the CW as BW (29/49), and 86% had the CW among the eBW70 (42/49); in lower L2/3, these proportions were 58% (31/53) and 91% (48/53). Preferential representation of CW row-mates over neighboring-row whiskers was nearly identical in both groups to the population as a whole. There was also no significant ($p < 0.05$) main effect of CW tuning group on unit depth (Welch's ANOVA, $p = 0.30$). However, our small sample of SW-units (i.e., those with the CW not in the eBW70; $n = 12$) were on average more superficial (mean depth for RS units where CW was BW, 418 ± 134 µm; for SW-tuned RS units with CW among eBW70, 411 ± 160 µm; for SW-tuned RS units with CW not among eBW70, 344 ± 144 µm; Table 2.1, Supplemental Figure 3). Thus, CW- and non-CW-units appear to be spread evenly throughout columnar L2/3, with the most strictly SW-tuned units possibly more common in the upper portion.

Finally, it is possible that CW tuning of RS neurons varies according to radial position within a column. The normalized distance of a recording site from the column center did not predict the fraction of RS units at that site best tuned to the CW, nor the fraction of cells with the CW among the eBW70 ($R^2 = 0.0039$ and 0.0021 respectively, simple linear regression; Figure 2.8A). This is consistent with the observation of SW-tuned cells throughout L2 of mouse whisker columns, not just at the column edge (Clancy et al., 2015). Notably, we did not observe increased SW tuning toward column edges, or systematic variation in the direction preference of RS units by their location in the whisker column, as reported by prior studies (Armstrong-James et al., 1992; Andermann & Moore, 2006). This may result in part from our exclusion of recording sites not clearly within the column borders defined by L4 barrels; it is also possible that our histological localization of recording sites within the column includes some error arising in the application of DiI stain using a separate probe after recording completion. In addition, the young adult rats (53 ± 11 PND; 285 ± 60 g) used in our recordings may not yet have fully developed the L2/3 direction map, which has been observed specifically in slightly older animals (81–112 PND; ~350–400 g; Andermann & Moore, 2006; Kremer et al., 2011). What does seem clear is that both CW- and non-CW-units are distributed across the vertical and horizontal dimensions of columnar L2/3, without domains of strictly homogeneous CW tuning.

2.2.5. Fast-spiking units are more frequently tuned to the columnar whisker (Figure 2.9)

In contrast with the RS units, the majority (18/23) of our FS units were recorded in lower L2/3 (i.e., 400–650 µm). However, because RS units exhibited similar tuning properties in lower and upper L2/3 (Supplemental Figure 3), any differences in FS tuning properties are not explained by this bias toward sampling from deeper sites. We found that the CW was the best whisker in 78% of FS units (18/23), in contrast to 59% of RS units (Figures 2.9A, 2.9C); this difference approached

significance (p = 0.10, Fisher's exact test). The CW was the sole eBW in 13% of FS units (3/23), and the sole eBW70 in 39% (9/23; mean depth 483 µm, range 200–625), both values higher than the equivalents for RS units (4% and 31%). Similarly, a slightly higher proportion of FS than RS units had the CW among the eBW70 (96% vs. 88%; p = 0.46). Thus, L2/3 FS units as a group appear to be tuned to the CW more reliably than RS units, as seen in some prior studies of S1 (Le Cam et al., 2011). FS units' mean onset latencies for their best whiskers were also notably shorter than those for RS units (18.0 ms vs. 27.0 ms; Figure 2.9G), similar to the shorter latencies observed in FS and parvalbumin-positive (PV) cells in A1 and S1 (Atencio & Schreiner 2008; Moore & Wehr, 2013; Sachidhanandam, 2016). This shorter latency of FS units is consistent with their uniquely robust glutamatergic synaptic input (Mateo et al., 2011; Avermann et al., 2012).

The more prevalent CW tuning of FS units in our data could be observed if FS cells are in general more sharply tuned to their best whiskers, such that CW-tuned FS cells are less likely than their RS counterparts to by chance fire more spikes to a surround whisker during recording. However, tuning about the BW among all FS units was similar to that for the RS population (mean SW/BW spike count fraction 0.32, range 0.21–0.51; Figure 2.9E; cf. Figure 2.5B). FS and RS units had similar BW tuning scores (FS, 4.0 ± 2.4; RS, 4.2 ± 3.3), as did the subset of each group with the CW as best whisker (n = 18 FS, 60 RS units: FS, 4.4 ± 2.5; RS, 5.0 ± 3.7). Relatedly, the eBW and eBW70 for FS units were of similar size as in RS units (mean FS unit eBWs 6.4 ± 2.7 whiskers; mean eBW70 3.2 ± 2.6 whiskers; Figure 2.9B). Therefore, although FS cells are tuned to the CW more often than RS cells, they do not appear to be tuned with greater specificity. As with RS units, CW row-mate whiskers were typically more effective than other surround whiskers at driving FS units (Figure 2.9D; cf. Figure 2.4D).

2.3. DISCUSSION

We characterized tuning to single-whisker stimuli in regular-spiking (RS) and fast-spiking (RS) units recorded in L2/3 of rat S1 whisker columns. We find that only a narrow majority of RS cells in columnar L2/3 respond best to the anatomically matched whisker (CW), demonstrating less prevalent CW tuning than is canonically described in L4. However, the tuning observed is more homogeneous than that reported in mouse L2, and appears consistent throughout L2/3, suggesting differences in the fine-scale somatotopy of the whisker maps of these two model species. Relative to RS units, FS units displayed markedly more prevalent CW tuning and shorter latencies, consistent with input from an indiscriminate sampling of local excitatory cells.

2.3.1. Laminar and species differences in local tuning heterogeneity of regular-spiking cells

Nearly 60% of RS units in L2/3 columns had the CW as their best whisker; defining the *group* of best whiskers as the eBW70, 31% of L2/3 RS units had the CW as their unique best whisker, whereas 88% had the CW among their group of best whiskers. By contrast, in mouse, as few as 25% of L2 cells have the CW as their best whisker (Clancy et al., 2015). Our larger fraction of cells with the CW as best whisker may result in part from several methodological differences. First, extracellular recording is biased toward more responsive units, in contrast to the sampling of a complete local population achieved with calcium imaging. Second, our RS population likely

includes a small number of non-FS inhibitory neurons, in contrast to the exclusion of all interneurons by GAD67-GFP labelling in the mouse L2 study. Finally, the choice of stimuli for assessing tuning can be critical (Le Cam et al., 2011), and our use of a multi-phasic, low-amplitude stimulus was specifically designed to minimize response saturation as well as spike censoring, thus reducing the chance of a CW-tuned unit being misclassified. With these caveats in mind, the nearly doubled proportion of CW-tuned cells in our rat L2/3 data relative to mouse L2 does suggest that tuning is less heterogeneous in the rat.

This result is consistent with known differences in laminar specialization between the two species. The supragranular layers of rodent S1 process both mono-whisker lemniscal signals relayed via L4, and multi-whisker paralemniscal signals relayed via L5 (Bosman et al., 2011; Deschênes & Urbain, 2016). Whereas these two information streams are partially segregated into columnar and septal pathways in the rat, in the smaller cortex of the mouse—which lacks well-developed septa—they are routed to columnar L3 and L2, respectively (Shepherd & Svoboda, 2005; Bureau et al., 2006). The greater prevalence of CW tuning in the rat, and its consistency across depth, may in part reflect this predominance of L4 lemniscal input throughout the rat upper layers. However, rat upper L2/3 does also receive driving input from L5, in addition to more extensive horizontal connections than lower L2/3 (Staiger et al., 2014). It is possible that this is evidenced by the slightly shallower average depth of our SW-tuned units for which the CW is not among the eBW70 (n = 12); a larger data set would be required to explore this possibility.

Although our results indicate more robust CW tuning in rat L2/3 than in mouse L2, the 50–60% of cells best tuned to the CW still falls short of the CW dominance expected in L4. Moreover, SW-tuned RS cells in rat L2/3 columns appear to be present at various horizontal distances from the column center, rather than being strictly confined to the column edge where horizontal SW inputs might be expected to predominate (although sampling of sites at the column edge in our data is not sufficient to rule out the possibility of increased SW tuning with distance from the center; cf. Armstrong-James et al., 1992; Andermann & Moore, 2006). This echoes the finding that SW-tuned cells are present throughout the column in mouse L2 (Clancy et al., 2015). Thus, diversity of tuning appears to be a defining feature of L2/3 across S1, V1, and A1 in rats and mice (cf. Ohki et al., 2005; Bandyopadhyay et al., 2010; Rothschild et al., 2010; Bonin et al., 2011; Winkoswki & Kanold, 2013). Subpopulations of broadly tuned and SW-tuned RS cells in the S1 upper layers may reflect the emergence of complex and integrated representations of whisker stimuli, including direction and texture parameters (Andermann & Moore, 2006; Kremer et al., 2011; Garion et al., 2014).

It should be noted that our L4 data from the present experiments suggested *less* prevalent CW-tuning than we observed in L2/3. These analyses were not presented here, as it appears highly likely that this result is an artifact of spike censoring associated with the higher evoked firing rates of L4 cells (and evidenced in our data by depression of tuning curve centers with larger-amplitude stimuli, not seen in L2/3). Nonetheless, although CW tuning is clearly predominant in L4 (de Kock et al., 2007; Le Cam et al., 2011), SW-tuned cells may be more common in this layer than is often assumed. Classical studies reporting CW tuning in 80–90% of L4 cells refer to units for which the CW was the sole whisker *or among the group of whiskers* driving evoked spike counts in the upper range for the unit (Armstrong-James & Fox, 1987), and another study found that 10% of cells in both L2/3 and L4 were better tuned to a single tested

surround whisker than to the CW (Glazewski & Fox, 1996). A standardized comparison of tuning in rat L4 alongside L2/3, as we set out to include here, is essential to a full characterization of the laminar transformation of whisker tuning. This might be accomplished using cell-attached recordings to avoid the challenges of sampling bias and censoring intrinsic to extracellular data.

2.3.2. Homogeneous columnar whisker tuning among fast-spiking cells

We also found that FS cells were tuned more homogeneously than their RS neighbors, with the CW more often their best whisker. This is predictable from the fact that, in contrast with the nonrandom connections of pyramidal cells in primary sensory cortex, FS (or parvalbumin-positive) inhibitory interneurons sample inputs from excitatory cells broadly and unselectively, and therefore display responses approximating the average tuning of the local pyramidal population (Kerlin et al., 2010; Bock et al., 2011; Hofer et al., 2011; Harris & Mrsic-Flogel, 2013). Since a narrow majority of our (putatively pyramidal) RS units responded best to the CW, and ~90% included the CW among the eBW70, FS units—like the field multi-unit activity—would thus be expected to show the reliable and specific CW tuning we observe.

Studies in mouse and cat V1, and mouse A1, have reported similarly homogeneous responses among FS or parvalbumin-positive (PV+) cells. However, the shape of FS/PV+ tuning curves varies. In mouse A1 and cat V1—which feature clear tonotopy and orientation columns, respectively—FS/PV+ cells are tuned with sharpness comparable to their excitatory neighbors (Cardin et al., 2007; Moore & Wehr, 2013). In mouse V1—which lacks orientation columns—broader tuning is seen (Kerlin et al., 2010; Kuhlman et al., 2011; Zariwala et al., 2011). The relatively sharp CW tuning of our FS population is consistent with the finding that over half of L2/3 RS cells are CW-tuned, with many more effectively driven by the CW. It would be of interest to determine whether the more markedly heterogeneous whisker mapping in mouse L2/3 yields broader FS tuning curves than we observe here in the rat.

2.3.3. Conclusion and future questions

The data presented here support two broad conclusions about the receptive fields of L2/3 neurons in rat whisker columns. First, regular-spiking cells in rat L2/3 are tuned to the columnar whisker less reliably than cells in rat L4, but more faithfully than cells in mouse L2. Second, and in contrast, fast-spiking cells in rat L2/3 are reliably tuned to the columnar whisker. Further work would be needed to determine whether single-whisker tuning differs in rat L2/3 among subtypes of excitatory cells and non-fast-spiking inhibitory cells (Feldmeyer, 2012; Crochet & Petersen, 2013), or among cells with different projection targets (e.g., Sato & Svoboda, 2010; Clancy et al., 2015). We also did not characterize tuning among cells in the rat's intercolumn septa, which would be valuable for comparison to mouse L2 as respective sites for the processing of paralemniscal inputs encoding multi-whisker kinematics (Alloway, 2008; Bosman et al., 2011). Similarly, in the mouse, whisker tuning has not been fully characterized in L3, or among fast-spiking (or parvalbumin-positive) cells. It therefore remains to be seen whether mouse L3 cells are tuned to their columnar whisker more frequently than L2 cells (in keeping with their stronger lemniscal input), and whether L2/3 fast-spiking cells are more broadly tuned in the mouse than in the rat (as might be predicted from the mouse's more heterogeneous local somatotopy).

Finally, our data were collected from anesthetized rats, and with stimulation of only one whisker at a time. Critical questions remain about how differences in fine-scale somatotopy between the rat and mouse affect the representation of multi-whisker stimuli across cortical layers (e.g., Estebanez et al., 2012, 2016), and about the implications of such differences for behavioral repertoires and for cortical plasticity.

2.4. FIGURES & TABLES FOR CHAPTER 2

Figure 2.1: Whisker stimuli and recording from verified whisker columns.

Figure 2.2: Single-unit sorting and identification of regular- and fast-spiking units.

Figure 2.3: Whisker tuning and onset latency under rostral versus caudal stimuli.

Figure 2.4: Best whisker identity in regular-spiking units.

Figure 2.5: Nine-whisker tuning curves of regular-spiking units.

Figure 2.6: Tuning curves for all regular-spiking units.

Figure 2.7: CW vs. BW onset latencies in regular-spiking units.

Figure 2.8: Regular-spiking unit tuning properties by location within the whisker-column.

Figure 2.9: Fast-spiking units are tuned to the CW more frequently than regular-spiking units.

Table 2.1: Tuning properties and recording parameters for all analyzed units, by tuning group.

Supplemental Figure 1: Tuning properties of regular-spiking units under minimal-amplitude (0.5°) stimuli only.

Supplemental Figure 2: BW and CW tuning scores for regular-spiking units as a function of mean BW-evoked spikes per stimulus.

Supplemental Figure 3: Tuning properties of regular-spiking units from upper L2/3 and from lower L2/3.

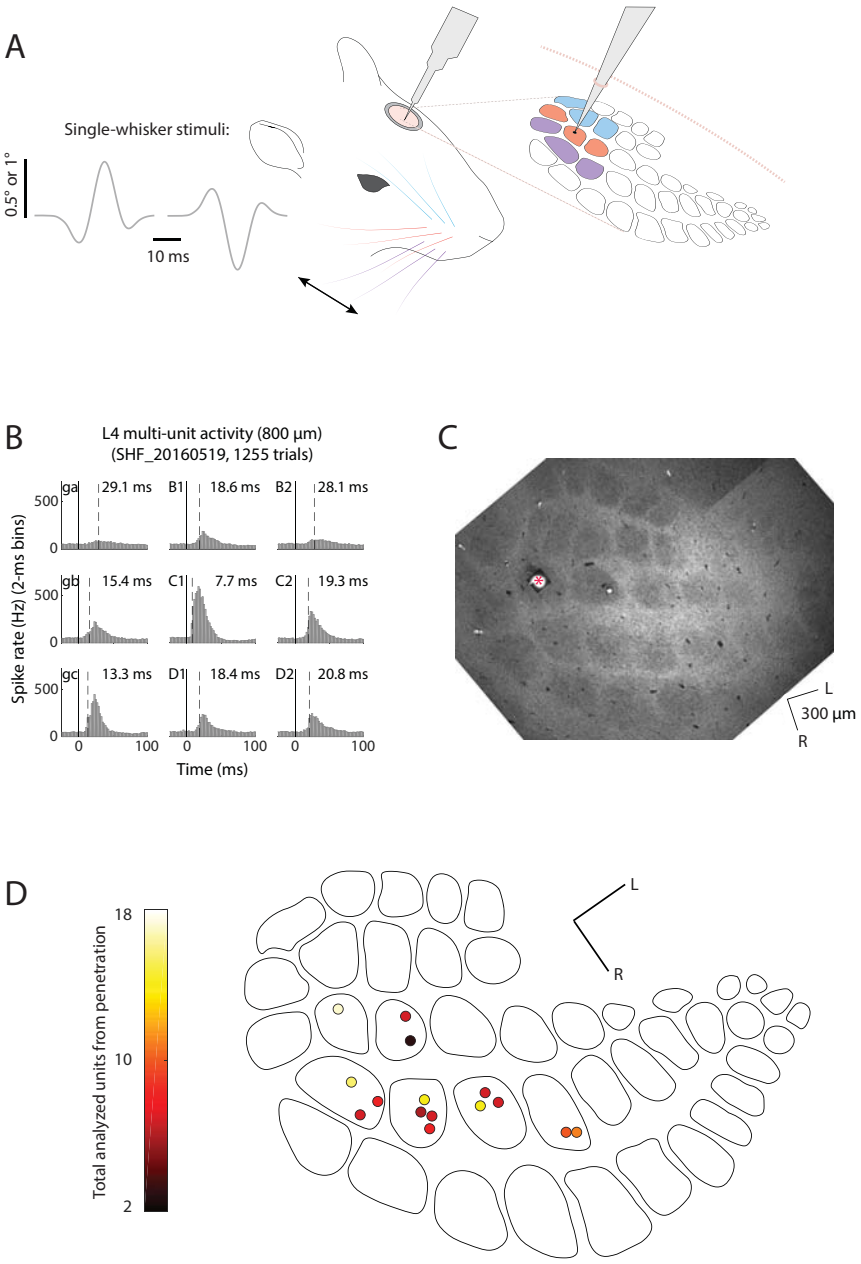

FIGURE 2.1: Whisker stimuli and recording from verified whisker columns.
Captions next page

FIGURE 2.1: Whisker stimuli and recording from verified whisker columns.

(A) Polytrode recording from L2/3 (150–650 µm) of a whisker column during stimulation of the anatomically matched whisker (columnar whisker, CW) and the eight surround whiskers. Stimuli were applied to one whisker at a time, in rostral or caudal direction.

(B) Example L4 (800 µm) multi-unit PSTHs for stimuli to whisker C1 and its eight surrounds, used to target a polytrode penetration to the C1 column. Solid line: stimulus onset. Dashed lines: onset latency of the multi-unit response.

(C) Cytochrome oxidase–stained tangential section from L4 of the rat recorded in panel B, showing a DiI marking lesion in the C1 barrel below the recorded L2/3 sites.

(D) Histologically determined localization of each penetration within L2/3 whisker columns, relative to the borders of the L4 barrels. Color code indicates the total analyzed units recovered from each penetration (125 units, 15 penetrations, 14 rats).

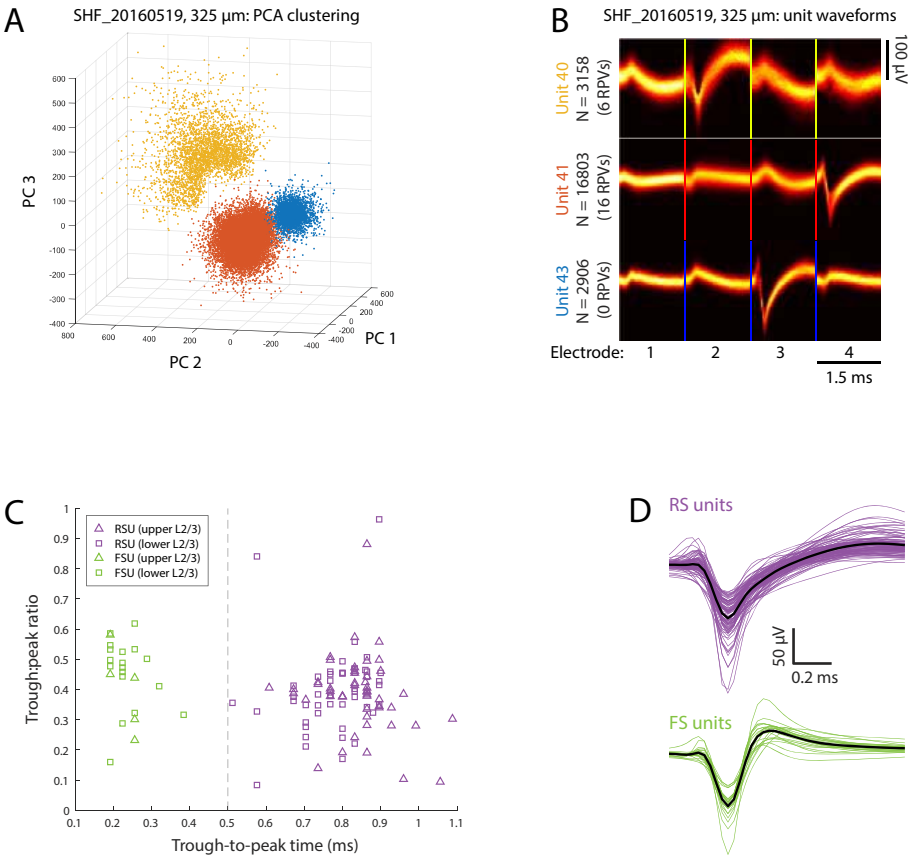

FIGURE 2.2: Single-unit sorting and identification of regular- and fast-spiking units.
Captions next page

FIGURE 2.2: Single-unit sorting and identification of regular- and fast-spiking units.

(A) Clustering of units isolated from one tetrode site (four electrodes, centered at 325 µm) from the example recording shown in Figures 2.1B and 2.1C, by principal components analysis (PCA).

(B) Density plots of the spike waveforms for the three units shown in (A). N: total spikes for each unit. RPVs: refractory period violations.

(C) Classification of all analyzed units as regular-spiking units (RS units) or fast-spiking units (FS units), based on the interval between the waveform trough and peak. Units with trough-to-peak interval > 0.5 ms were classified as RS units. Squares: units from lower L2/3 (400–650 µm). Triangles: units from upper L2/3 sites (150–399 µm).

(D) Top, mean waveforms for each RS unit (purple; n = 102) and for the RS unit population (black). Bottom, for FS units (n = 23).

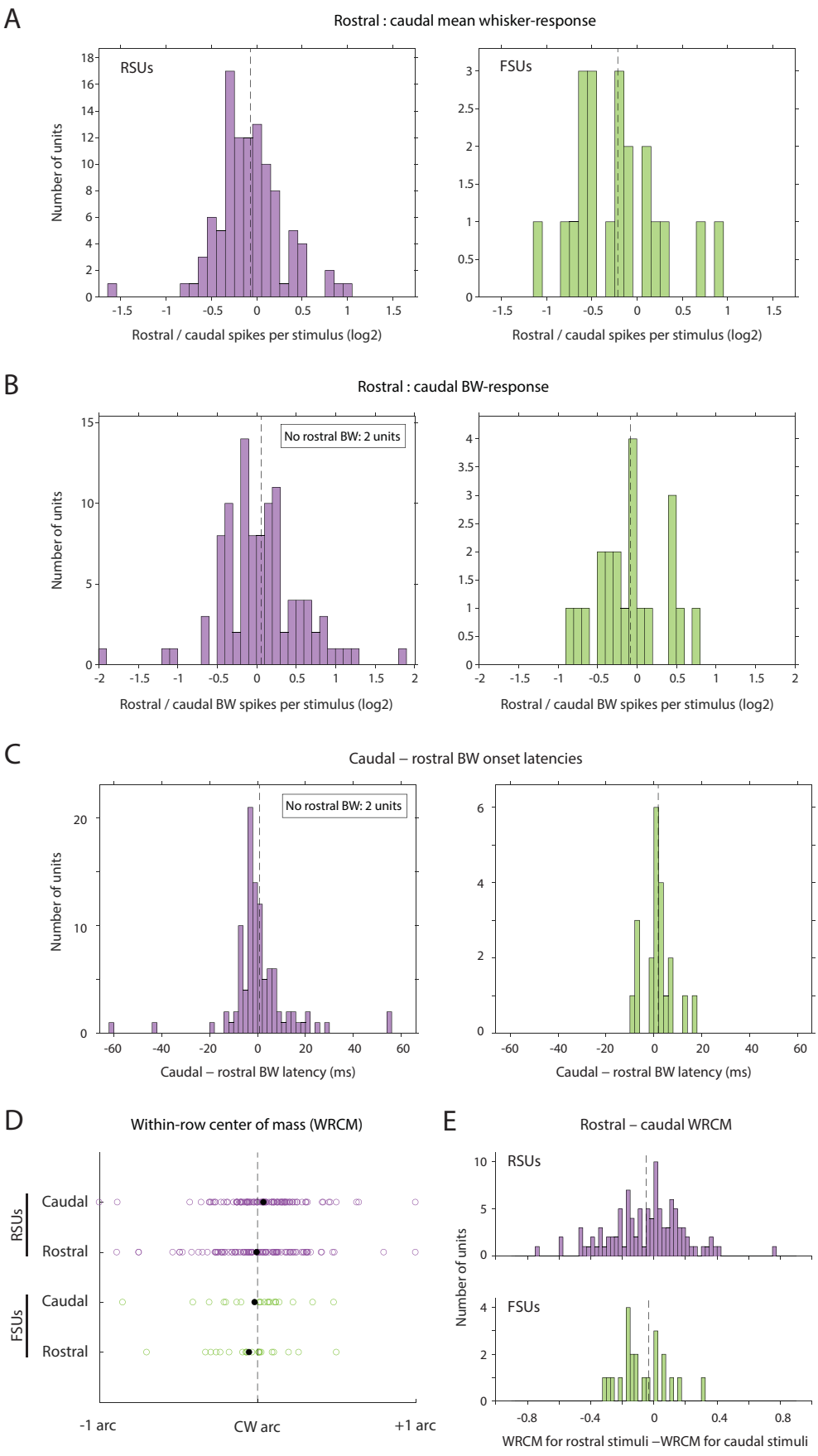

FIGURE 2.3: Whisker tuning and onset latency under rostral versus caudal stimuli.

Captions next page

FIGURE 2.3: Whisker tuning and onset latency under rostral versus caudal stimuli.

(A) Distribution of the ratio [mean spikes per rostral stimulus to any whisker] : [mean spikes per caudal stimulus to any whisker], across all RS units (left; n = 102) and all FS units (right = 23). Dashed lines: mean ratios for each population (RS units, −0.07 ± 0.36; FS units, −0.21 ± 0.49).

(B) Distribution of the ratio [mean spikes per rostral stimulus to each unit's rostral best whisker (BW)] : [mean spikes per caudal stimulus to the unit's caudal BW], for RS units and FS units. Dashed lines: mean ratios for each population (RS units, 0.06 ± 0.52; FS units, −0.08 ± 0.43). Two excluded RS units displayed a significant caudal response but no response to any whisker with rostral stimuli.

(C) Distribution of the difference between onset latency to the caudal BW and to the rostral BW, for RS units and FS units. Dashed lines: mean latency differences for each population (RS units, 0.79 ± 13.24 ms; FS units, 1.81 ± 6.30 ms). Two RS units excluded, as in panel B.

(D) Tuning center of mass within the CW row (within-row center of mass, WRCM), under caudal and under rostral stimuli, for all RS units (top) and all FS units (bottom). WRCM for each unit is calculated as mean spikes per stimulus to the CW's rostral row-mate (i.e., +1 arc) minus mean spikes per stimulus to the CW's caudal row-mate (i.e., −1 arc), divided by the sum of mean spikes per stimulus to all three stimulated whiskers in the row (+1 arc, CW, −1 arc). Black dots: mean values (RS units: 0.04 ± 0.26 for caudal stimuli, 0 ± 0.29 for rostral. FS units: −0.02 ± 0.28 caudal, −0.05 ±0.24 rostral).

(E) Distribution of the difference in each unit's WRCM under rostral versus caudal stimuli, for RS units and FS units. Dashed lines: mean differences (RS units, −0.05 ± 0.24 arcs; FS units, −0.03 ± 0.25 arcs).

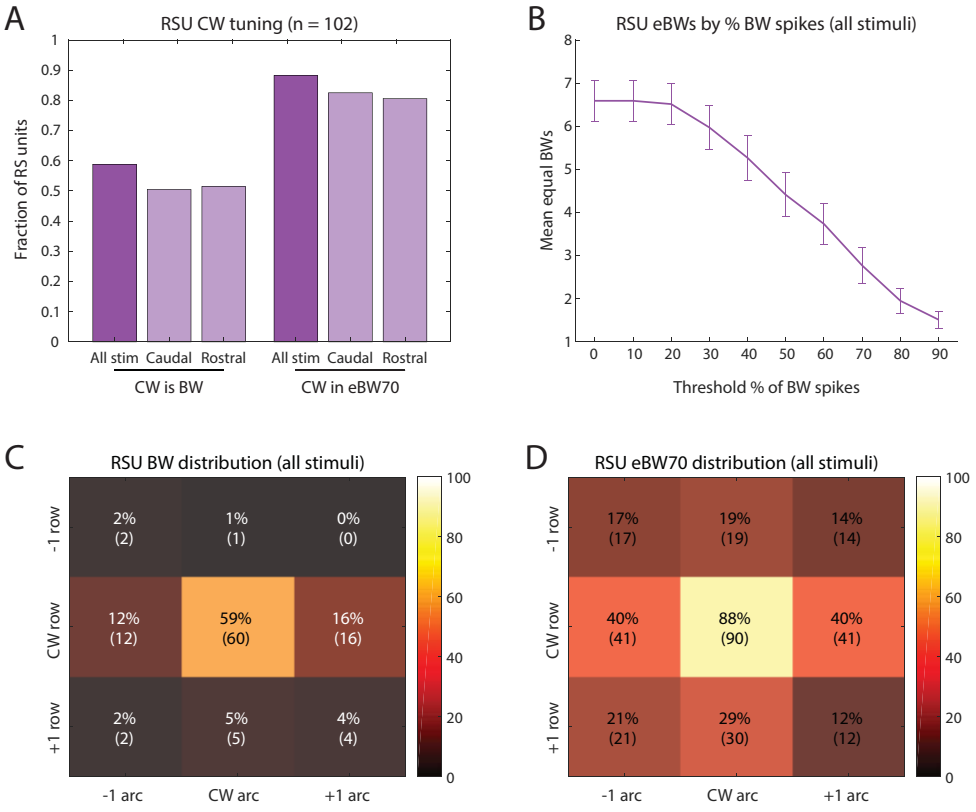

FIGURE 2.4: Best whisker identity in regular-spiking units.
Captions next page

FIGURE 2.4: Best whisker identity in regular-spiking units.

(A) Fraction of RS units for which the columnar whisker (CW) is the best whisker (BW), or is among the eBW70 (as defined in panel B). Data are shown with BW assessed across all stimuli, and for rostral and caudal stimuli separately.

(B) Mean number of statistically equivalent ("equal") BWs (eBWs) with mean evoked spikes above threshold fractions (10%–90%) of the BW's mean evoked spikes. Bars: 95% CI. With no threshold applied (0%), the eBWs comprise on average 6.58 ± 2.49 whiskers. At 70% threshold, the group (eBW70) comprises on average 2.79 ± 2.17 whiskers.

(C) Percentages of RS units (n = 102) best driven by the CW and by each of its eight surrounds.

(D) Prevalence of eBW70 membership for the CW and its eight surrounds, across all RS units (n = 102).

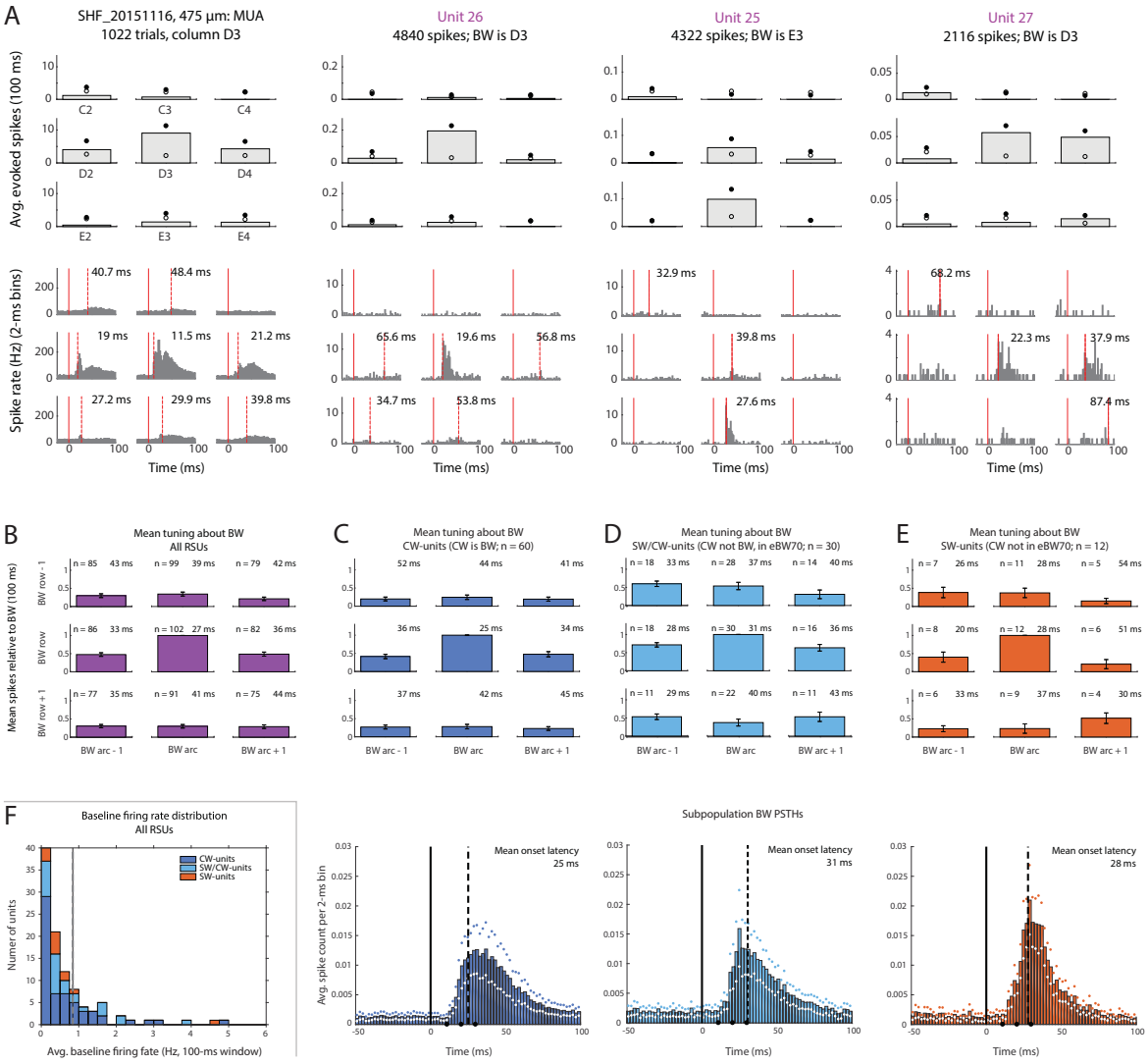

FIGURE 2.5: Nine-whisker tuning curves of regular-spiking units.
Captions next page

FIGURE 2.5: Nine-whisker tuning curves of regular-spiking units.

(A) Nine-whisker tuning curve (top) and PSTH (bottom) for multi-unit activity, and for three example units, from a single recording site (475 µm; D3 column). Tuning curves: filled circles, post-stimulus spike count; open circles, baseline spike count. PSTHs: solid red lines, stimulus onset; dashed red lines, response onset latency.

(B) Average RS unit tuning curve, with responses centered around each unit's BW and normalized to the BW mean evoked spikes (n = 102 RS units). Bars: 95% CI.

(C) Top, average tuning curve for RS units where the CW is the best whisker ("CW-units"; n = 60/102 RS units). Bars: 95% CI. Bottom, population PSTH with 95% CI for the BW response of these units. X-axis dots indicate timepoints of the local extrema in the stimulus waveform.

(D) Top, Average tuning curve for RS units where an SW is the best whisker, but the CW is among the eBW70 ("SW/CW-units", n = 30/102 RS units). Bars: 95% CI. Bottom, population PSTH with 95% CI for the BW response of these units.

(E) Top, Average tuning curve for RS units where an SW is the best whisker, and the CW is not among the eBW70 ("SW-units"; n = 12/102 RS units). Bars: 95% CI. Bottom, population PSTH with 95% CI for the BW response of these units.

(F) Distribution of RS unit baseline firing rates in a 100-ms pre-stimulus window. Dashed line: mean baseline FR (0.75 ± 1.14 Hz).

FIGURE 2.6A: Tuning curves for CW-units (RS units where CW is BW) (see legend under 2.6C)

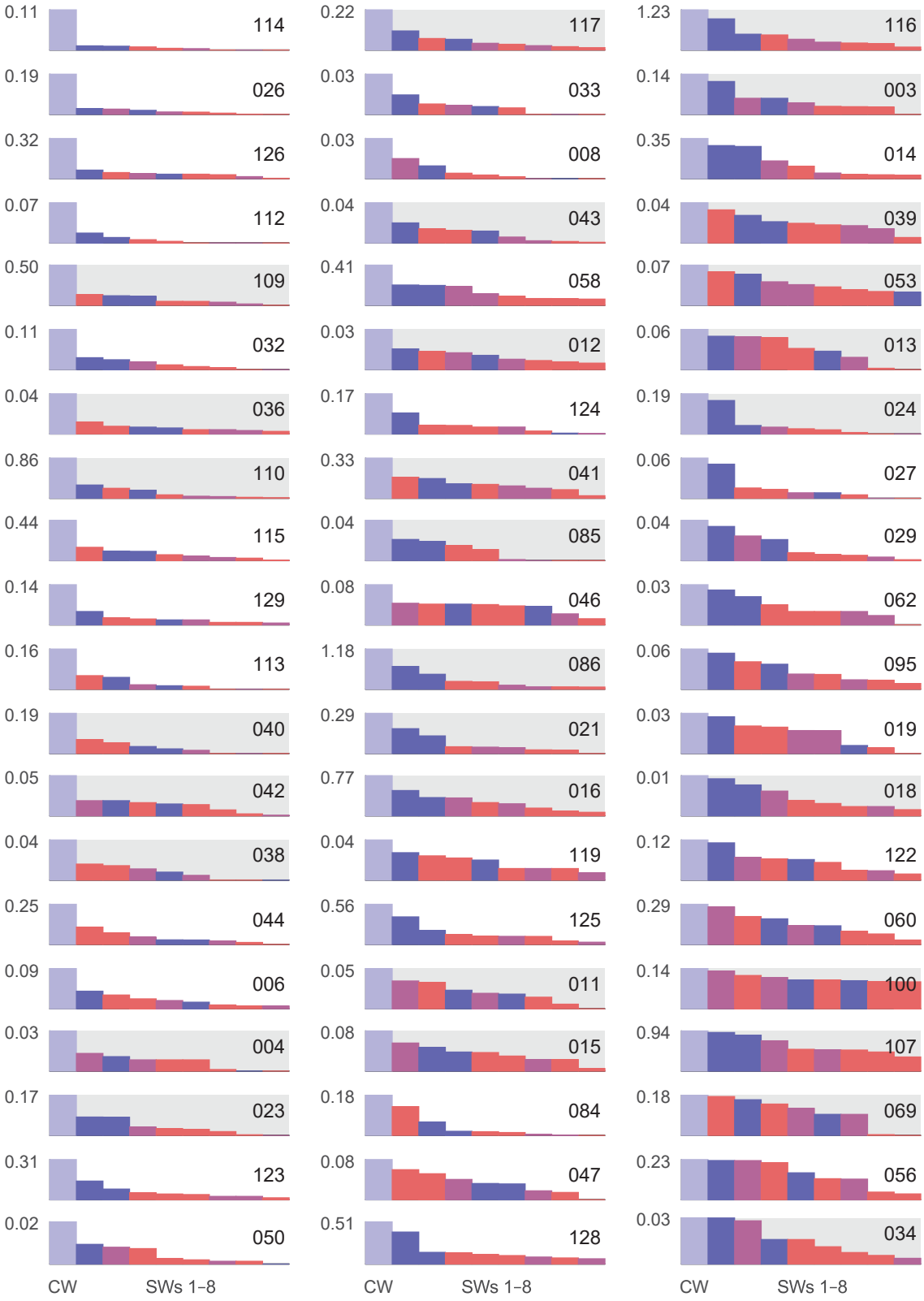

FIGURE 2.6B: Tuning curves for SW/CW-units (RS units where CW is in eBW70, but not BW)

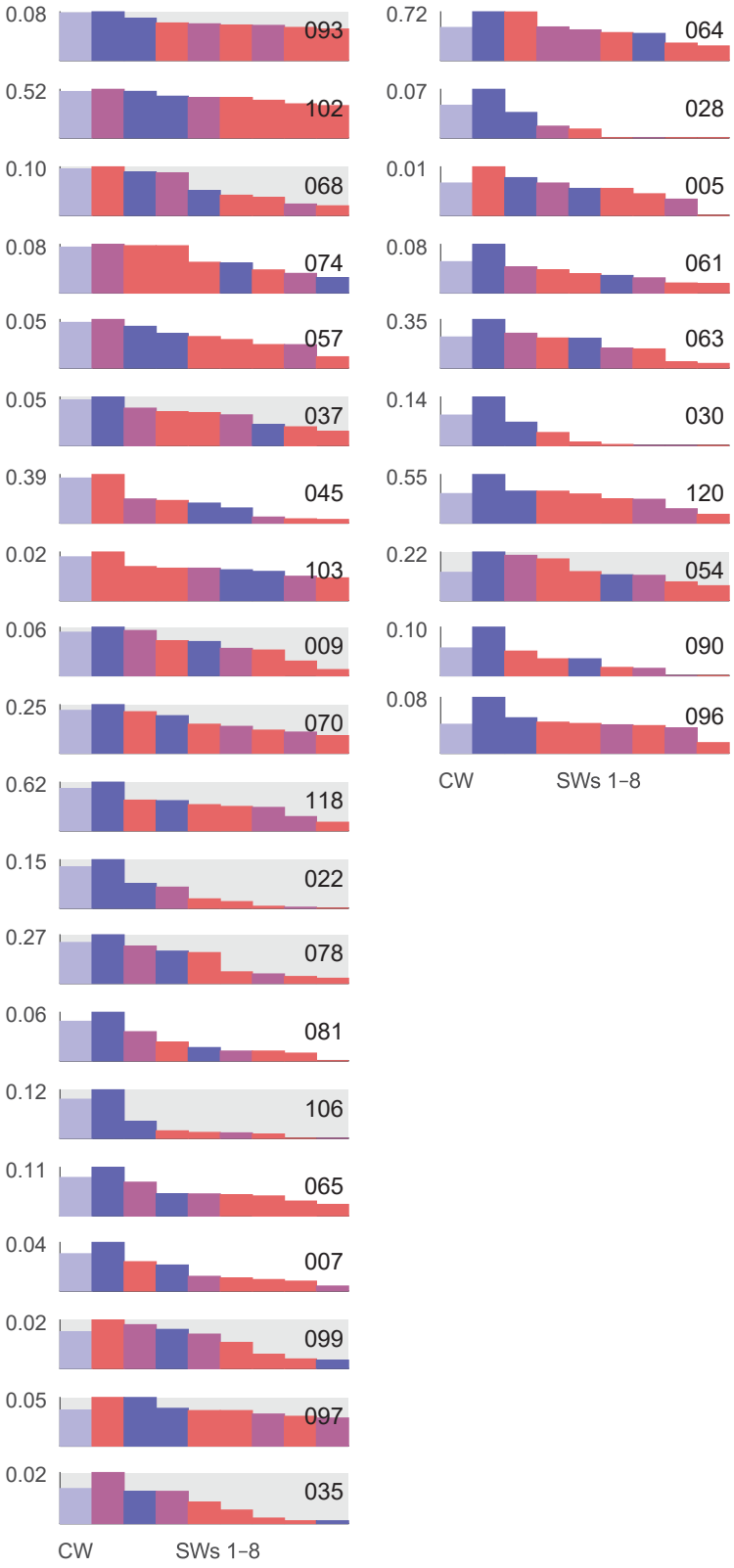

FIGURE 2.6C: Tuning curves for SW-units (RS units where CW is not in eBW70)

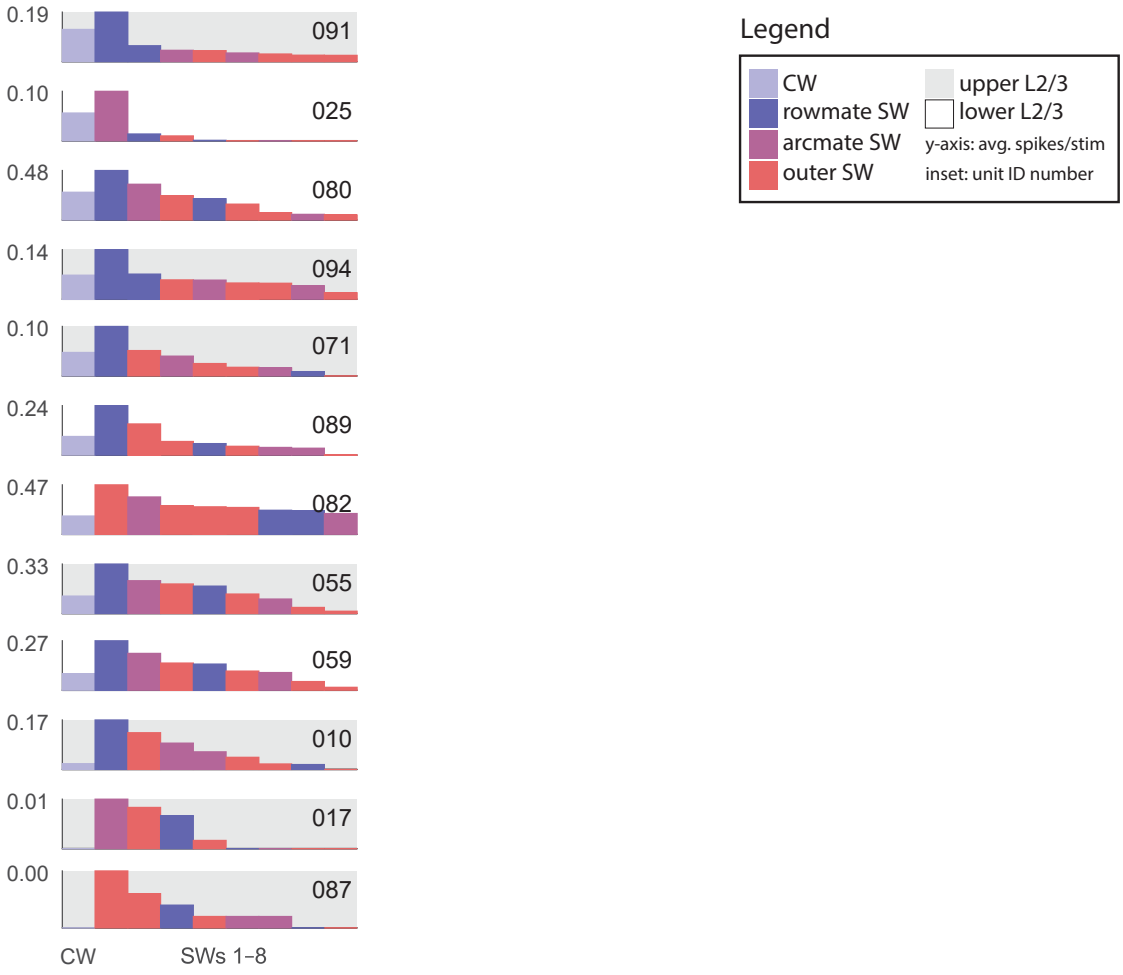

FIGURE 2.6: Tuning curves for all regular-spiking units.
Captions next page

FIGURE 2.6: Tuning curves for all regular-spiking units.

(A) CW-units (i.e., RS units where CW is BW; n = 60).

(B) SW/CW-units (i.e., RS units where CW is not BW, but is in eBW70; n = 30).

(C) SW-units (i.e., RS units where CW is not in eBW70; n = 12).

Units within each graph are ordered, top-to-bottom, from the highest to lowest ratio [CW-evoked spikes] : [best-SW-evoked spikes]. Grey background: upper L2/3 (150–399 μm). White background: lower L2/3 (400–650 μm).

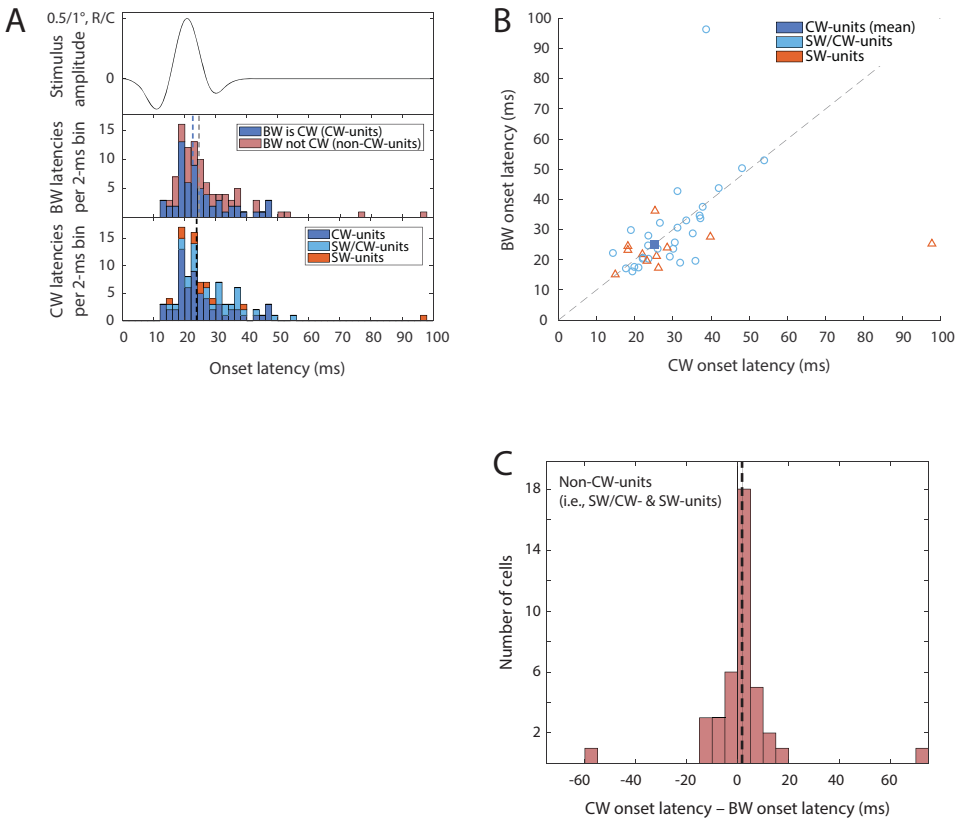

FIGURE 2.7: CW vs. BW onset latencies in regular-spiking units.
Captions next page

FIGURE 2.7: CW vs. BW onset latencies in regular-spiking units.

(A) Distribution of RS unit response onset latencies. Top: stimulus waveform. Middle: BW latencies (dashed lines are medians—22.6 ms for CW-units; 24.5 ms for non-CW-units). Bottom: CW latencies (dashed line, median for all units: 23.8 ms). Units with different tuning properties are stacked within bars (see legends, inset).

(B) BW vs. CW response onset latencies, for non-CW-units (i.e., 30 SW/CW- and 10 SW-units; two excluded RS units had no CW response). Mean BW latency, 29.76 ± 15.85 ms; mean CW latency, 30.13 ± 14.16 ms. Mean BW and CW latencies for these units are not significantly different ($p = 0.22$, two-tailed paired *t*-test). Blue square: mean latency for all CW-units (25.11 ± 8.5 ms; $n = 60$).

(C) Distribution of the difference between mean response onset latency to the CW and to the BW, for non-CW-units (30 SW/CW- and 10 SW-units). Dashed line: mean (1.74 ms).

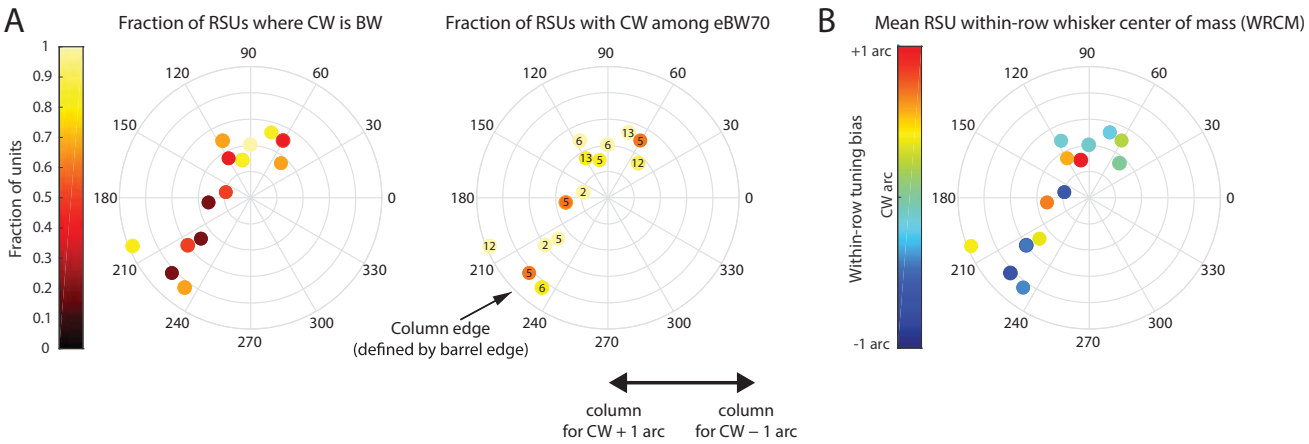

FIGURE 2.8: Regular-spiking unit tuning properties by location within the whisker-column.

Captions next page

FIGURE 2.8: Regular-spiking unit tuning properties by location within the whisker-column.

(A) Fraction of RS units in each penetration for which the CW is the BW (i.e., CW-units; left), and for which the CW is among the eBW70 (i.e., CW- and SW/CW-units; right), with penetrations plotted at their normalized coordinates in a circular column defined by L4 barrel boundaries. The number of analyzed RS units from each penetration is indicated in the eBW70 plot.

(B) Mean within-row center of mass (WRCM) of RS units in each penetration (calculated as in Figure 2.3D).

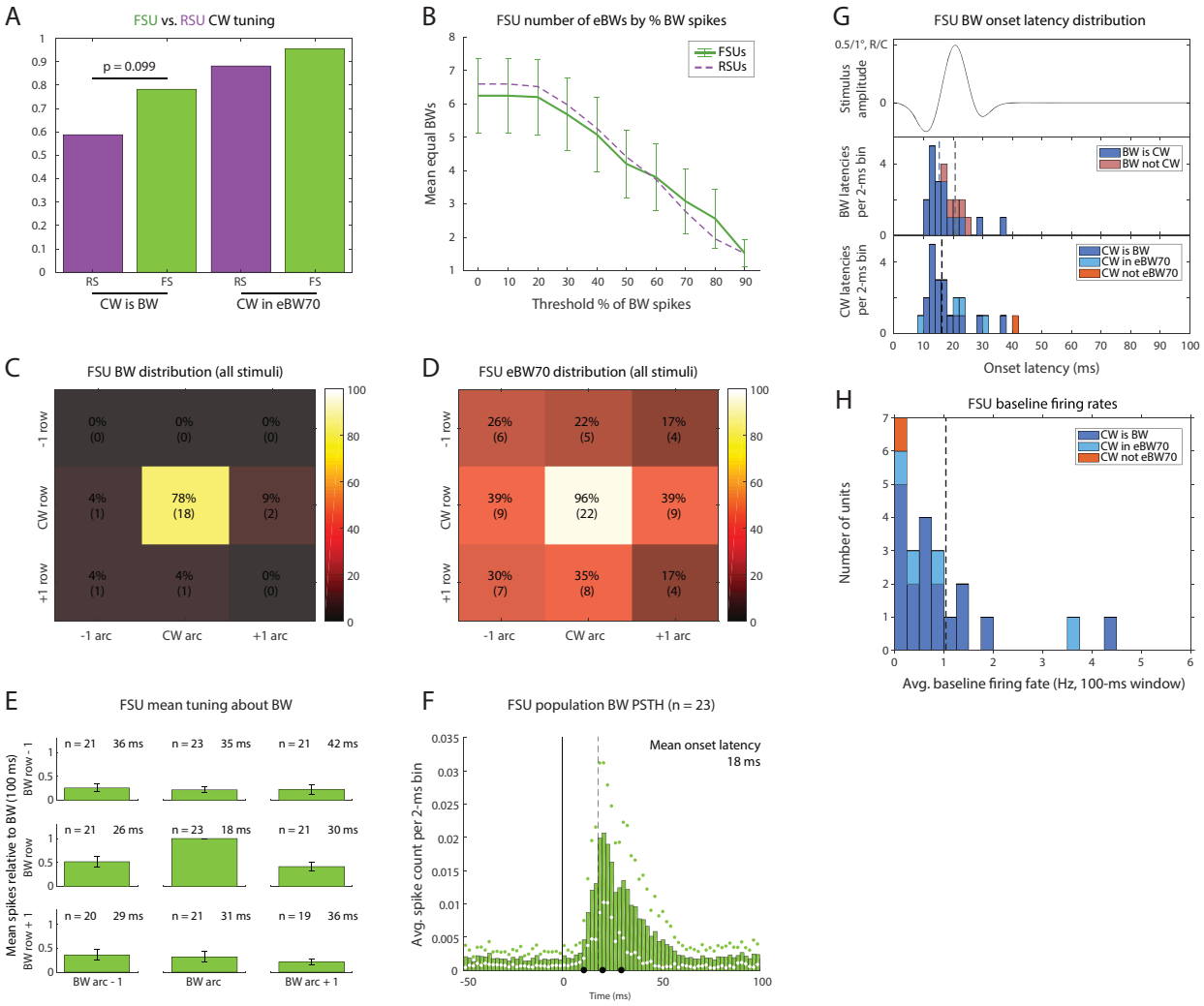

FIGURE 2.9: Fast-spiking units are tuned to the CW more frequently than regular-spiking units.

Captions next page

FIGURE 2.9: Fast-spiking units are tuned to the CW more frequently than regular-spiking units.

(A) Fraction of FS units (green; n = 23) versus RS units (purple; n = 102) for which the columnar whisker (CW) is the best whisker (BW) (p = 0.0985, Fisher's exact test), or is among the eBW70 (p = 0.4593).

(B) FS unit eBWs with mean evoked spikes above threshold fractions (10%–90%) of the BW response. Dashed line: RS units, for comparison. Bars: 95% CI. Mean eBWs 6.4 ± 2.7 whiskers; mean eBW70 3.2 ± 2.6 whiskers.

(C) Percentages of FS units (n = 23) best driven by the CW and by each of its eight surrounds.

(D) Prevalence of eBW70 membership for the CW and eight surrounds, across all FS units (n = 23).

(E) Average FS unit tuning curve, centered on and normalized to the BW (n = 23). Bars: 95% CI.

(F) PSTH for the BW response of FS units (n = 23). Dots: 95% CI.

(G) Distribution of FS unit response onset latencies. Top: stimulus waveform. Middle: latencies for the BW (dashed lines are medians—15.3 ms for FS units where CW is BW; 20.7 ms where CW is not BW). Bottom: latencies for the CW (median: 16.2 ms). Units with different tuning properties are stacked within bars (see legends, inset).

(H) Distribution of FS unit baseline firing rates in a 100-ms pre-stimulus window. Dashed line: mean baseline FR (0.91 ± 1.09 Hz).

	n	eBW70 size	% BW sole eBW70	% BW shortest latency	BW evoked spikes	BW tuning score	CW tuning score	BW latency (ms)	CW latency (ms)	depth (µm)	baseline firing rate (Hz)	RPVs %	missing spikes %	animal weight (g)
All RS units	102	2.8 ± 2.2	38	56	0.21 ± 0.24	4.2 ± 3.3	3.6 ± 3.3	27 ± 12	27 ± 11	406 ± 144	0.75 ± 1.13	0.13 ± 0.18	9.3 ± 8.3	295 ± 58
CW-units	60	2.1 ± 1.7	31	72	0.22 ± 0.28	5.0 ± 3.7	5.0 ± 3.7	25 ± 9	25 ± 9	416 ± 134	0.64 ± 0.89	0.15 ± 0.21	9.3 ± 8.3	303 ± 66
SW/CW-units	30	4.5 ± 2.1	--	40	0.18 ± 0.20	2.4 ± 1.4	1.7 ± 0.6	31 ± 16	30 ± 9	411 ± 160	0.97 ± 1.46	0.11 ± 0.15	9.8 ± 8.9	284 ± 46
SW-units	12	1.9 ± 2.0	58	58	0.21 ± 0.16	3.6 ± 1.6	1.1 ± 1.0	28 ± 16	31 ± 24	344 ± 144	0.76 ± 1.28	0.13 ± 0.12	7.7 ± 7.3	287 ± 40
non-CW-units (SW/CW & SW)	42	3.8 ± 2.4	17	45	0.19 ± 0.18	2.8 ± 1.5	1.5 ± 0.8	30 ± 16	30 ± 14	392 ± 157	0.91 ± 1.40	0.12 ± 0.14	9.2 ± 8.5	285 ± 44
All FS units	23	3.2 ± 2.6	39	70	0.20 ± 0.25	4.0 ± 2.4	3.8 ± 2.5	18 ± 6	19 ± 9	493 ± 157	0.95 ± 1.11	0.26 ± 0.27	9.7 ± 7.4	311 ± 50

TABLE 2.1: Tuning properties and recording parameters for all analyzed units, by tuning group.

BW: best whisker.

CW: columnar whisker.

RPVs: refractory period violations.

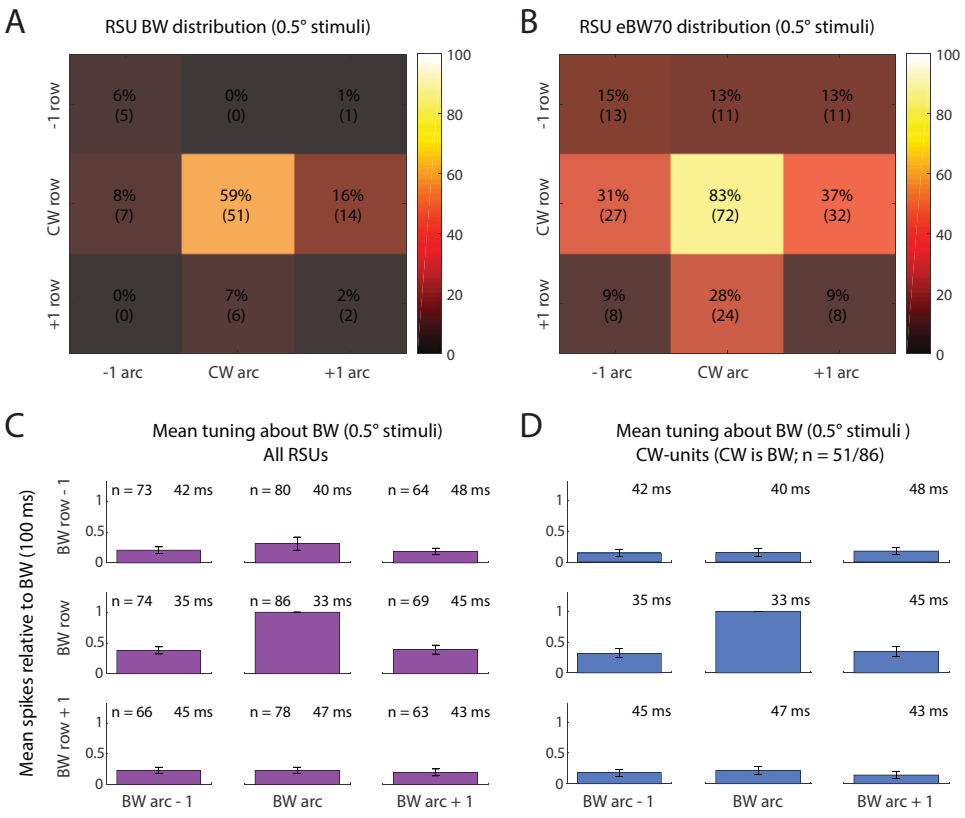

SUPPLEMENTAL FIGURE 1: Tuning properties of regular-spiking units under minimal-amplitude (0.5°) stimuli only.
Captions below

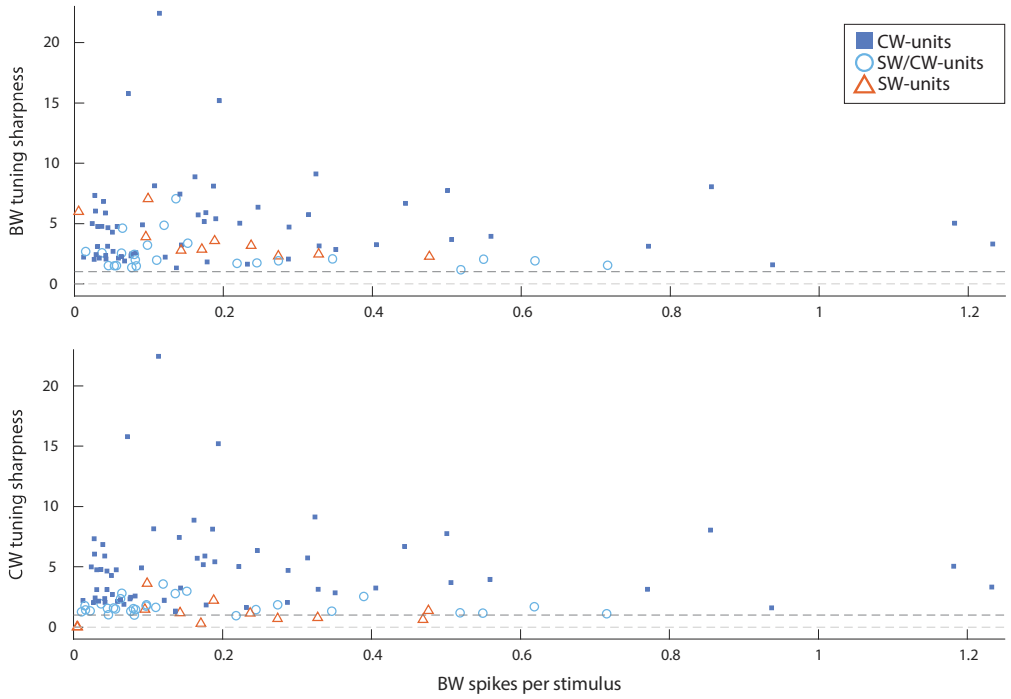

SUPPLEMENTAL FIGURE 2: BW and CW tuning scores for regular-spiking units as a function of mean BW-evoked spikes per stimulus.
Captions below

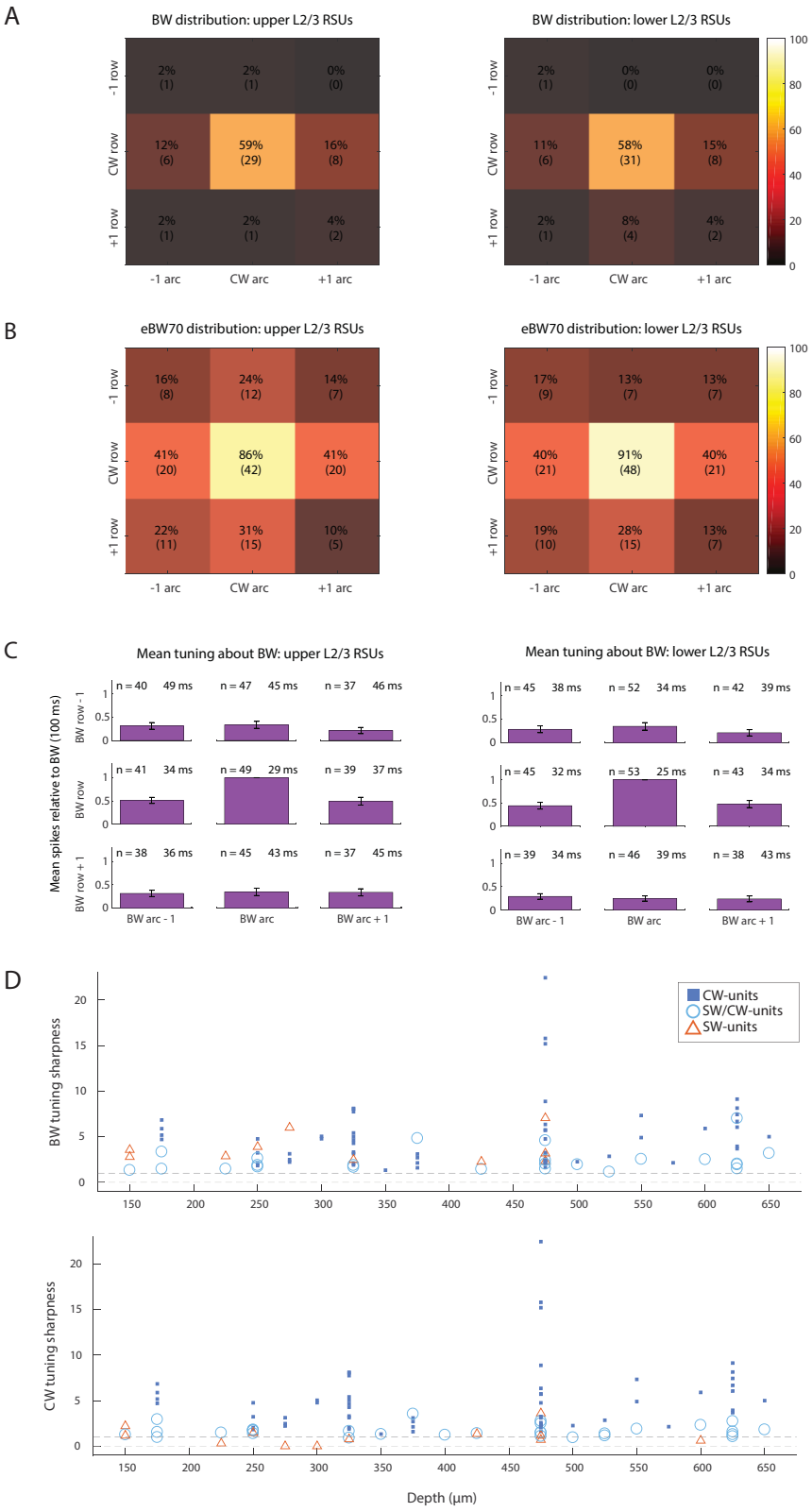

SUPPLEMENTAL FIGURE 3: Tuning properties of regular-spiking units from upper L2/3 and from lower L2/3.

Captions next page

SUPPLEMENTAL FIGURE 1: Tuning properties of regular-spiking units under minimal-amplitude (0.5°) stimuli only.

(A) Percentages of RS units (n = 86) best driven by the CW and by each of its eight surrounds.

(B) Prevalence of eBW70 membership for the CW and eight surrounds, across all RS units.

(C) Average RS unit tuning curve, with responses centered around each cell's BW and normalized to the BW mean evoked spikes. Bars: 95% CI.

(D) Average tuning curve for RS units where the CW is the best whisker ("CW-units"; n = 51/86 RS units). Bars: 95% CI.

SUPPLEMENTAL FIGURE 2: BW and CW tuning scores for regular-spiking units as a function of mean BW-evoked spikes per stimulus.

SUPPLEMENTAL FIGURE 3: Tuning properties of regular-spiking units from upper L2/3 and from lower L2/3.

Upper L2/3: 150–399 µm; n = 49 units.
Lower L2/3: 400–650 µm; n = 53 units.

(A) Percentages of RS units best driven by the CW and by each of its eight surrounds, in upper (left) and in lower (right) L2/3.

(B) Prevalence of eBW70 membership for the CW and eight surrounds, across RS units from upper (left) and lower (right) L2/3.

(C) Average BW-centered tuning curve for RS units from upper (left) and lower (right) L2/3. Bars: 95% CI.

(D) BW and CW tuning scores for all RS units as a function of recording depth. (CW tuning scores: n = 60 CW-units, 30 SW/CW-units, 12 SW-units. BW tuning scores are shown only for those units with data available for at least five adjacent whiskers; n = 60 CW-units, 24 SW/CW-units, 10 SW-units.)

REFERENCES

CHAPTER 1

Abraira VE & Ginty DD (2013). The sensory neurons of touch. Neuron 79(4): 618–639.

Adesnik H & Scanziani M (2010). Lateral competition for cortical space by layer-specific horizontal circuits. Nature 464(7292): 1155–1160.

Adrian ED (1941). Afferent discharges to the cerebral cortex from peripheral sense organs. J Physiol 100(2): 159–191.

Ahissar E, Sosnik R, Bagdasarian K, et al. (2001). Temporal frequency of whisker movement. II. Laminar organization of cortical representations. J Neurophysiol 86(1): 354–367.

Allard T, Clark SA, Jenkins WM, et al. (1991). Reorganization of somatosensory area 3b representations in adult owl monkeys after digital syndactyly. J Neurophysiol 66(3): 1048–1058.

Allen CB, Celikel T & Feldman DE (2003). Long-term depression induced by sensory deprivation during cortical map plasticity in vivo. Nat Neurosci 6(3): 291–299.

Alloway KD & Burton H (1991). Differential effects of GABA and bicuculline on rapidly- and slowly-adapting neurons in primary somatosensory cortex of primates. Exp Brain Res 85(3): 598–610.

Andermann ML & Moore CI (2006). A somatotopic map of vibrissa motion direction within a barrel column. Nat Neurosci 9(4): 543–551.

Armstrong-James M & Fox K (1987). Spatiotemporal convergence and divergence in the rat S1 "barrel" cortex. J Comp Neurol 263(2): 265–281.

Armstrong-James M, Diamond ME & Ebner FF (1994). An innocuous bias in whisker use in adult rats modifies receptive fields of barrel cortex neurons. J Neurosci 14(11 Pt 2): 6978–6991.

Arnold PB, Li CX & Waters RS (2001). Thalamocortical arbors extend beyond single cortical barrels: an in vivo intracellular tracing study in rat. Exp Brain Res 136(2): 152–168.

Ashaber M, Pálfi E, Friedman RM, et al. (2014). Connectivity of somatosensory cortical area 1 forms an anatomical substrate for the emergence of multifinger receptive fields and complex feature selectivity in the squirrel monkey (*Saimiri sciureus*). J Comp Neurol 522(8): 1769–1785.

Azzopardi P & Cowey A (1993). Preferential representation of the fovea in the primary visual cortex. Nature 361(6414): 719–721.

Bandyopadhyay S, Shamma SA & Kanold PO (2010). Dichotomy of functional organization in the mouse auditory cortex. Nat Neurosci 13(3): 361–368.

Barth AL & Poulet JFA (2012). Experimental evidence for sparse firing in the neocortex. Trends Neurosci 35(6): 345–355.

Barth AL, McKenna M, Glazewski S, et al. (2000). Upregulation of cAMP response element-mediated gene expression during experience-dependent plasticity in adult neocortex. J Neurosci 20(11): 4206–4216.

Bednar JA & Wilson SP (2016). Cortical maps. Neurosci 22(6): 604–617.

Bender VA, Bender KJ, Brasier DJ, et al. (2006). Two coincidence detectors for spike timing-dependent plasticity in somatosensory cortex. J Neurosci 26(16): 4166–4177.

Benison AM, Rector DM & Barth DS (2007). Hemispheric mapping of secondary somatosensory cortex in the rat. J Neurophysiol 97(1): 200–207.

Besle J, Sánchez-Panchuelo R-M, Bowtell R, et al. (2013). Single-subject fMRI mapping at 7 T of the representation of fingertips in S1: a comparison of event-related and phase-encoding designs. J Neurophysiol 109(9): 2293–2305.

Besle J, Sánchez-Panchuelo R-M, Bowtell R, et al. (2014). Event-related fMRI at 7T reveals overlapping cortical representations for adjacent fingertips in S1 of individual subjects. Hum Brain Mapp 35(5): 2027–2043.

Birbaumer N, Lutzenberger W, Montoya P, et al. (1997). Effects of regional anesthesia on phantom limb pain are mirrored in changes in cortical reorganization. J Neurosci 17(14): 5503–5508.

Blake DT, Byl NN, Cheung S, et al. (2002). Sensory representation abnormalities that parallel focal hand dystonia in a primate model. Somatosens Mot Res 19(4): 347–357.

Blankenburg F, Ruben J, Meyer R, et al. (2003). Evidence for a rostral-to-caudal somatotopic organization in human primary somatosensory cortex with mirror-reversal in areas 3b and 1. Cereb Cortex 13(9): 987–993.

Boloori A-R & Stanley GB (2006). The dynamics of spatiotemporal response integration in the somatosensory cortex of the vibrissa system. J Neurosci 26(14): 3767–3782.

Bonin V, Histed MH, Yurgenson S, et al. (2011). Local diversity and fine-scale organization of receptive fields in mouse visual cortex. J Neurosci 31(50): 18506–18521.

Bosman LWJ, Houweling AR, Owens CB, et al. (2011). Anatomical pathways involved in generating and sensing rhythmic whisker movements. Front Integr Neurosci 5: 53.

Bowes C, Massey JM, Burish M, et al. (2012). Chondroitinase ABC promotes selective reactivation of somatosensory cortex in squirrel monkeys after a cervical dorsal column lesion. Proc Natl Acad Sci USA 109(7): 2595–2600.

Bradbury EJ, Moon LDF, Popat RJ, et al. (2002). Chondroitinase ABC promotes functional recovery after spinal cord injury. Nature 416(6881): 636–640.

Brecht M & Sakmann B (2002). Dynamic representation of whisker deflection by synaptic potentials in spiny stellate and pyramidal cells in the barrels and septa of layer 4 rat somatosensory cortex. J Physiol 543(Pt 1): 49–70.

Brecht M, Preilowski B & Merzenich MM (1997). Functional architecture of the mystacial vibrissae. Behav Brain Res 84(1-2): 81–97.

Brecht M, Roth A & Sakmann B (2003). Dynamic receptive fields of reconstructed pyramidal cells in layers 3 and 2 of rat somatosensory barrel cortex. J Physiol 553(Pt 1): 243–265.

Broser P, Grinevich V, Osten P, et al. (2008). Critical period plasticity of axonal arbors of layer 2/3 pyramidal neurons in rat somatosensory cortex: layer-specific reduction of projections into deprived cortical columns. Cereb Cortex 18(7): 1588–1603.

Bureau I, von Saint Paul F & Svoboda K (2006). Interdigitated paralemniscal and lemniscal pathways in the mouse barrel cortex. PLoS Biol 4(12): e382.

Burton H, Sathian K & Shao DH (1990). Altered responses to cutaneous stimuli in the second somatosensory cortex following lesions of the postcentral gyrus in infant and juvenile macaques. J Comp Neurol 291(3): 395–414.

Burton H, Fabri M & Alloway K (1995). Cortical areas within the lateral sulcus connected to cutaneous representations in areas 3b and 1: a revised interpretation of the second somatosensory area in macaque monkeys. J Comp Neurol 355(4): 539–562.

Burton H, Snyder AZ, Conturo TE, et al. (2002). Adaptive changes in early and late blind: a fMRI study of Braille reading. J Neurophysiol 87(1): 589–607.

Butterworth S, Francis S, Kelly E, et al. (2003). Abnormal cortical sensory activation in dystonia: an fMRI study. Mov Disord 18(6): 673–682.

Byl NN, Merzenich MM & Jenkins WM (1996). A primate genesis model of focal dystonia and repetitive strain injury: I. Learning-induced dedifferentiation of the representation of the hand in the primary somatosensory cortex in adult monkeys. Neurology 47(2): 508–520.

Byl NN, Merzenich MM, Cheung S, et al. (1997). A primate model for studying focal dystonia and repetitive strain injury: effects on the primary somatosensory cortex. Phys Ther 77(3): 269–284.

Calford MB & Tweedale R (1988). Immediate and chronic changes in responses of somatosensory cortex in adult flying-fox after digit amputation. Nature 332(6163): 446–448.

Calford MB & Tweedale R (1991a). Immediate expansion of receptive fields of neurons in area 3b of macaque monkeys after digit denervation. Somatosens Mot Res 8(3): 249–260.

Calford MB & Tweedale R (1991b). Acute changes in cutaneous receptive fields in primary somatosensory cortex after digit denervation in adult flying fox. J Neurophysiol 65(2): 178–187.

Calford MB & Tweedale R (1991c). C-fibres provide a source of masking inhibition to primary somatosensory cortex. Proc Biol Sci 243(1308): 269–275.

Candia V, Wienbruch C, Elbert T, et al. (2003). Effective behavioral treatment of focal hand dystonia in musicians alters somatosensory cortical organization. Proc Natl Acad Sci USA 100(13): 7942–7946.

Carlson M, Huerta MF, Cusick CG, et al. (1986). Studies on the evolution of multiple somatosensory representations in primates: the organization of anterior parietal cortex in the New World Callitrichid, *Saguinus*. J Comp Neurol 246(3): 409–426.

Catania KC (2001). Early development of a somatosensory fovea: a head start in the cortical space race? Nat Neurosci 4(4): 353–354.

Catania KC (2011). The sense of touch in the star-nosed mole: from mechanoreceptors to the brain. Philos Trans R Soc Lond B Biol Sci 366(1581): 3016–3025.

Catania KC & Kaas JH (1995). Organization of the somatosensory cortex of the star-nosed mole. J Comp Neurol 351(4): 549–567.

Catania KC & Kaas JH (1997). Somatosensory fovea in the star-nosed mole: behavioral use of the star in relation to innervation patterns and cortical representation. J Comp Neurol 387(2): 215–233.

Catania KC & Remple MS (2002). Somatosensory cortex dominated by the representation of teeth in the naked mole-rat brain. Proc Natl Acad Sci USA 99(8): 5692–5697.

Catania KC & Remple FE (2004). Tactile foveation in the star-nosed mole. Brain Behav Evol 63(1): 1–12.

Catania KC, Leitch DB & Gauthier D (2011). A star in the brainstem reveals the first step of cortical magnification. PLoS One 6(7): e22406.

Cazala F, Vienney N & Stoléru S (2015). The cortical sensory representation of genitalia in women and men: a systematic review. Socioaffective Neurosci Psychol 5: 26428.

Celikel T, Szostak VA & Feldman DE (2004). Modulation of spike timing by sensory deprivation during induction of cortical map plasticity. Nat Neurosci 7(5): 534–541.

Chapin JK & Lin CS (1984). Mapping the body representation in the SI cortex of anesthetized and awake rats. J Comp Neurol 229(2): 199–213.

Charcot J (1887). *Leçons du mardi à la Salpêtrière [Tuesday Lectures at the Salpêtrière]*. Paris: Delahaye & Lecrosnier.

Chen C-C, Bajnath A & Brumberg JC (2015). The impact of development and sensory deprivation on dendritic protrusions in the mouse barrel cortex. Cereb Cortex 25(6): 1638–1653.

Chen LM, Friedman RM, Ramsden BM, et al. (2001). Fine-scale organization of SI (area 3b) in the squirrel monkey revealed with intrinsic optical imaging. J Neurophysiol 86(6): 3011–3029.

Chen LM, Friedman RM & Roe AW (2003). Optical imaging of a tactile illusion in area 3b of the primary somatosensory cortex. Science 302(5646): 881–885.

Chen LM, Friedman RM & Roe AW (2005). Optical imaging of SI topography in anesthetized and awake squirrel monkeys. J Neurosci 25(33): 7648–7659.

Chen LM, Friedman RM & Roe AW (2009). Optical imaging of digit topography in individual awake and anesthetized squirrel monkeys. Exp Brain Res 196(3): 393–401.

Chklovskii DB & Koulakov AA (2004). Maps in the brain: what can we learn from them? Annu Rev Neurosci 27: 369–392.

Civillico EF & Contreras D (2006). Integration of evoked responses in supragranular cortex studied with optical recordings in vivo. J Neurophysiol 96(1): 336–351.

Clancy KB, Schnepel P, Rao AT, et al. (2015). Structure of a single whisker representation in layer 2 of mouse somatosensory cortex. J Neurosci 35(9): 3946–3958.

Clark SA, Allard T, Jenkins WM, et al. (1988). Receptive fields in the body-surface map in adult cortex defined by temporally correlated inputs. Nature 332(6163): 444–445.

Clem RL & Barth A (2006). Pathway-specific trafficking of native AMPARs by in vivo experience. Neuron 49(5): 663–670.

Constantinople CM & Bruno RM (2013). Deep cortical layers are activated directly by thalamus. Science 340(6140): 1591–1594.

Coq JO & Xerri C (1998). Environmental enrichment alters organizational features of the forepaw representation in the primary somatosensory cortex of adult rats. Exp Brain Res 121(2): 191–204.

Cushing H (1909). A note upon the faradic stimulation of the postcentral gyrus in conscious patients. Brain (Oxford) 32(1): 44–53.

Cusick CG, Wall JT & Kaas JH (1986). Representations of the face, teeth and oral cavity in areas 3b and 1 of somatosensory cortex in squirrel monkeys. Brain Res 370(2): 359–364.

Cusick CG, Wall JT, Felleman DJ, et al. (1989). Somatotopic organization of the lateral sulcus of owl monkeys: area 3b, S-II, and a ventral somatosensory area. J Comp Neurol 282(2): 169–190.

Dachtler J, Hardingham NR, Glazewski S, et al. (2011). Experience-dependent plasticity acts via GluR1 and a novel neuronal nitric oxide synthase-dependent synaptic mechanism in adult cortex. J Neurosci 31(31): 11220–11230.

Darian-Smith C (2008). Plasticity of somatosensory function during learning, disease and injury. In: Basbaum A, et al. (eds.), *The Senses: A Comprehensive Reference*, v. 6, pp. 259–297 (6.13).

Dawson DR & Killackey HP (1987). The organization and mutability of the forepaw and hindpaw representations in the somatosensory cortex of the neonatal rat. J Comp Neurol 256(2): 246–256.

de Kock CPJ, Bruno RM, Spors H, et al. (2007). Layer- and cell-type-specific suprathreshold stimulus representation in rat primary somatosensory cortex. J Physiol 581(Pt 1): 139–154.

de Kock CPJ & Sakmann B (2009). Spiking in primary somatosensory cortex during natural whisking in awake head-restrained rats is cell-type specific. Proc Natl Acad Sci USA 106(38): 16446–16450.

De Paola V, Holtmaat A, Knott G, et al. (2006). Cell type-specific structural plasticity of axonal branches and boutons in the adult neocortex. Neuron 49(6): 861–875.

DeFelipe J, Conley M & Jones EG (1986). Long-range focal collateralization of axons arising from corticocortical cells in monkey sensory-motor cortex. J Neurosci 6(12): 3749–3766.

Deschênes M & Urbain N (2016). Vibrissal afferents from trigeminus to cortices. In: Prescott TJ, Ahissar E, Izhikevich E (eds.), *Scholarpedia of Touch*. Atlantis Press, Paris, pp. 657–672.

Diamond ME, Armstrong-James M & Ebner FF (1993). Experience-dependent plasticity in adult rat barrel cortex. Proc Natl Acad Sci USA 90(5): 2082–2086.

Diamond ME, Huang W & Ebner FF (1994). Laminar comparison of somatosensory cortical plasticity. Science 265(5180): 1885–1888.

Diamond ME, von Heimendahl M, Knutsen PM, et al. (2008). "Where" and "what" in the whisker sensorimotor system. Nat Rev Neurosci 9(8): 601–612.

DiCarlo JJ & Johnson KO (2002). Receptive field structure in cortical area 3b of the alert monkey. Behav Brain Res 135(1-2): 167–178.

Disbrow E, Roberts T & Krubitzer L (2000). Somatotopic organization of cortical fields in the lateral sulcus of Homo sapiens: evidence for SII and PV. J Comp Neurol 418(1): 1–21.

Disbrow E, Roberts T, Poeppel D, et al. (2001). Evidence for interhemispheric processing of inputs from the hands in human S2 and PV. J Neurophysiol 85(5): 2236–2244.

Disbrow E, Litinas E, Recanzone GH, et al. (2003). Cortical connections of the second somatosensory area and the parietal ventral area in macaque monkeys. J Comp Neurol 462(4): 382–399.

Douglas RJ & Martin KAC (2004). Neuronal circuits of the neocortex. Annu Rev Neurosci 27: 419–451.

Drew PJ & Feldman DE (2007). Representation of moving wavefronts of whisker deflection in rat somatosensory cortex. J Neurophysiol 98(3): 1566–1580.

Dreyer DA, Loe PR, Metz CB, et al. (1975). Representation of head and face in postcentral gyrus of the macaque. J Neurophysiol 38(3): 714–733.

Eaton NC, Sheehan HM & Quinlan EM (2016). Optimization of visual training for full recovery from severe amblyopia in adults. Learn Mem 23(2): 99–103.

Egger V, Nevian T & Bruno RM (2008). Subcolumnar dendritic and axonal organization of spiny stellate and star pyramid neurons within a barrel in rat somatosensory cortex. Cereb Cortex 18(4): 876–889.

Ego-Stengel V, Mello e Souza T, Jacob V, et al. (2005). Spatiotemporal characteristics of neuronal sensory integration in the barrel cortex of the rat. J Neurophysiol 93(3): 1450–1467.

Elbert T & Rockstroh B (2004). Reorganization of human cerebral cortex: the range of changes following use and injury. Neuroscientist 10(2): 129–141.

Elbert T, Flor H, Birbaumer N, et al. (1994). Extensive reorganization of the somatosensory cortex in adult humans after nervous system injury. Neuroreport 5(18): 2593–2597.

Elbert T, Pantev C, Wienbruch C, et al. (1995). Increased cortical representation of the fingers of the left hand in string players. Science 270(5234): 305–307.

Elbert T, Candia V, Altenmüller E, et al. (1998). Alteration of digital representations in somatosensory cortex in focal hand dystonia. Neuroreport 9(16): 3571–3575.

Erzurumlu RS & Gaspar P (2012). Development and critical period plasticity of the barrel cortex. Eur J Neurosci 35(10): 1540–1553.

Eskenasy AC & Clarke S (2000). Hierarchy within human SI: supporting data from cytochrome oxidase, acetylcholinesterase and NADPH-diaphorase staining patterns. Somatosens Mot Res 17(2): 123–132.

Estebanez L, El Boustani S, Destexhe A, et al. (2012). Correlated input reveals coexisting coding schemes in a sensory cortex. Nat Neurosci 15(12): 1691–1699.

Estebanez L, Bertherat J, Shulz DE, et al. (2016). A radial map of multi-whisker correlation selectivity in the rat barrel cortex. Nat Commun 7: 13528.

Fabri M & Burton H (1991). Ipsilateral cortical connections of primary somatic sensory cortex in rats. J Comp Neurol 311(3): 405–424.

Fang P-C, Jain N & Kaas JH (2002). Few intrinsic connections cross the hand-face border of area 3b of New World monkeys. J Comp Neurol 454(3): 310–319.

Feldman DE (2009). Synaptic mechanisms for plasticity in neocortex. Annu Rev Neurosci 32: 33–55.

Feldman DE & Brecht M (2005). Map plasticity in somatosensory cortex. Science 310(5749): 810–815.

Feldman DE, Nicoll RA & Malenka RC (1999). Synaptic plasticity at thalamocortical synapses in developing rat somatosensory cortex: LTP, LTD, and silent synapses. J Neurobiol 41(1): 92–101.

Feldmeyer D (2012). Excitatory neuronal connectivity in the barrel cortex. Front Neuroanat 6: 24.

Feldmeyer D, Egger V, Lubke J, et al. (1999). Reliable synaptic connections between pairs of excitatory layer 4 neurones within a single "barrel" of developing rat somatosensory cortex. J Physiol 521 Pt 1: 169–190.

Feldmeyer D, Brecht M, Helmchen F, et al. (2013). Barrel cortex function. Prog Neurobiol 103: 3–27.

Felleman DJ, Nelson RJ, Sur M, et al. (1983). Representations of the body surface in areas 3b and 1 of postcentral parietal cortex of Cebus monkeys. Brain Res 268(1): 15–26.

Ferezou I, Bolea S & Petersen CCH (2006). Visualizing the cortical representation of whisker touch: voltage-sensitive dye imaging in freely moving mice. Neuron 50(4): 617–629.

Ferezou I, Haiss F, Gentet LJ, et al. (2007). Spatiotemporal dynamics of cortical sensorimotor integration in behaving mice. Neuron 56(5): 907–923.

Fitzgerald PJ, Lane JW, Thakur PH, et al. (2006). Receptive field (RF) properties of the macaque second somatosensory cortex: RF size, shape, and somatotopic organization. J Neurosci 26(24): 6485–6495.

Flor H, Elbert T, Knecht S, et al. (1995). Phantom-limb pain as a perceptual correlate of cortical reorganization following arm amputation. Nature 375(6531): 482–484.

Flor H, Nikolajsen L & Staehelin Jensen T (2006). Phantom limb pain: a case of maladaptive CNS plasticity? Nat Rev Neurosci 7(11): 873–881.

Florence SL, Wall JT & Kaas JH (1991). Central projections from the skin of the hand in squirrel monkeys. J Comp Neurol 311(4): 563–578.

Florence SL, Taub HB & Kaas JH (1998). Large-scale sprouting of cortical connections after peripheral injury in adult macaque monkeys. Science 282(5391): 1117–1121.

Fox K (1992). A critical period for experience-dependent synaptic plasticity in rat barrel cortex. J Neurosci 12(5): 1826–1838.

Fox K (2008). Barrel Cortex. Cambridge University Press, Cambridge.

Friedman RM, Chen LM & Roe AW (2004). Modality maps within primate somatosensory cortex. Proc Natl Acad Sci USA 101(34): 12724–12729.

Friedman RM, Chen LM & Roe AW (2008). Responses of areas 3b and 1 in anesthetized squirrel monkeys to single- and dual-site stimulation of the digits. J Neurophysiol 100(6): 3185–3196.

Frostig RD, Xiong Y, Chen-Bee CH, et al. (2008). Large-scale organization of rat sensorimotor cortex based on a motif of large activation spreads. J Neurosci 28(49): 13274–13284.

Furuta T, Kaneko T & Deschênes M (2009). Septal neurons in barrel cortex derive their receptive field input from the lemniscal pathway. J Neurosci 29(13): 4089–4095.

Furuta T, Deschênes M & Kaneko T (2011). Anisotropic distribution of thalamocortical boutons in barrels. J Neurosci 31(17): 6432–6439.

Gardner EP & Costanzo RM (1980). Spatial integration of multiple-point stimuli in primary somatosensory cortical receptive fields of alert monkeys. J Neurophysiol 43(2): 420–443.

Garion L, Dubin U, Rubin Y, et al. (2014). Texture coarseness responsive neurons and their mapping in layer 2-3 of the rat barrel cortex in vivo. Elife 3: e03405.

Garraghty PE & Kaas JH (1991). Large-scale functional reorganization in adult monkey cortex after peripheral nerve injury. Proc Natl Acad Sci USA 88(16): 6976–6980.

Garraghty PE & Muja N (1996). NMDA receptors and plasticity in adult primate somatosensory cortex. J Comp Neurol 367(2): 319–326.

Garraghty PE & Sur M (1990). Morphology of single intracellularly stained axons terminating in area 3b of macaque monkeys. J Comp Neurol 294(4): 583–593.

Garraghty PE, Pons TP, Sur M, et al. (1989). The arbors of axons terminating in middle cortical layers of somatosensory area 3b in owl monkeys. Somatosens Mot Res 6(4): 401–411.

Garraghty PE, Florence SL & Kaas JH (1990a). Ablations of areas 3a and 3b of monkey somatosensory cortex abolish cutaneous responsivity in area 1. Brain Res 528(1): 165–169.

Garraghty PE, Pons TP & Kaas JH (1990b). Ablations of areas 3b (SI proper) and 3a of somatosensory cortex in marmosets deactivate the second and parietal ventral somatosensory areas. Somatosens Mot Res 7(2): 125–135.

Garraghty PE, Arnold LL, Wellman CL, et al. (2006). Receptor autoradiographic correlates of deafferentation-induced reorganization in adult primate somatosensory cortex. J Comp Neurol 497(4): 636–645.

Gentet LJ (2012). Functional diversity of supragranular GABAergic neurons in the barrel cortex. Front Neural Circuits 6: 52.

Georgiadis JR, Kortekaas R, Kuipers R, et al. (2006). Regional cerebral blood flow changes associated with clitorally induced orgasm in healthy women. Eur J Neurosci 24(11): 3305–3316.

Georgiadis JR, Reinders AATS, Paans AMJ, et al. (2009). Men versus women on sexual brain function: prominent differences during tactile genital stimulation, but not during orgasm. Hum Brain Mapp 30(10): 3089–3101.

Georgiadis JR, Farrell MJ, Boessen R, et al. (2010). Dynamic subcortical blood flow during male sexual activity with ecological validity: a perfusion fMRI study. Neuroimage 50(1): 208–216.

Ghazanfar AA & Nicolelis MA (1999). Spatiotemporal properties of layer V neurons of the rat primary somatosensory cortex. Cereb Cortex 9(4): 348–361.

Ghazanfar AA & Nicolelis MA (2001). Feature article: the structure and function of dynamic cortical and thalamic receptive fields. Cereb Cortex 11(3): 183–193.

Glazewski S & Fox K (1996). Time course of experience-dependent synaptic potentiation and depression in barrel cortex of adolescent rats. J Neurophysiol 75(4): 1714–1729.

Glazewski S, McKenna M, Jacquin M, et al. (1998). Experience-dependent depression of vibrissae responses in adolescent rat barrel cortex. Eur J Neurosci 10(6): 2107–2116.

Greenhill SD, Ranson A & Fox K (2015). Hebbian and homeostatic plasticity mechanisms in regular spiking and intrinsic bursting cells of cortical layer 5. Neuron 88(3): 539–552.

Griffen TC & Maffei A (2014). GABAergic synapses: their plasticity and role in sensory cortex. Front Cell Neurosci 8: 91.

Grüsser SM, Winter C, Mühlnickel W, et al. (2001). The relationship of perceptual phenomena and cortical reorganization in upper extremity amputees. Neuroscience 102(2): 263–272.

Guillery RW & Sherman SM (2011). Branched thalamic afferents: what are the messages that they relay to the cortex? Brain Res Rev 66(1-2): 205–219.

Haidarliu S & Ahissar E (2001). Size gradients of barreloids in the rat thalamus. J Comp Neurol 429(3): 372–387.

Haidarliu S, Yu C, Rubin N, et al. (2008). Lemniscal and extralemniscal compartments in the VPM of the rat. Front Neuroanat 2: 4.

Harris AJ (1999). Cortical origin of pathological pain. Lancet (London, England) 354(9188): 1464–1466.

Harris NG, Nogueira MSM, Verley DR, et al. (2013). Chondroitinase enhances cortical map plasticity and increases functionally active sprouting axons after brain injury. J Neurotrauma 30(14): 1257–1269.

Hebb DO (1949). The Organization of Behavior. Wiley & Sons, New York.

Hoeflinger BF, Bennett-Clarke CA, Chiaia NL, et al. (1995). Patterning of local intracortical projections within the vibrissae representation of rat primary somatosensory cortex. J Comp Neurol 354(4): 551–563.

Hoffer ZS, Hoover JE & Alloway KD (2003). Sensorimotor corticocortical projections from rat barrel cortex have an anisotropic organization that facilitates integration of inputs from whiskers in the same row. J Comp Neurol 466(4): 525–544.

Holtmaat A & Svoboda K (2009). Experience-dependent structural synaptic plasticity in the mammalian brain. Nat Rev Neurosci 10(9): 647–658.

Horton JC & Adams DL (2005). The cortical column: a structure without a function. Philos Trans R Soc Lond B Biol Sci 360(1456): 837–862.

House DRC, Elstrott J, Koh E, et al. (2011). Parallel regulation of feedforward inhibition and excitation during whisker map plasticity. Neuron 72(5): 819–831.

Hughlings Jackson J (1873). On the anatomical and physiological localisation of movements in the brain. Lancet, Oxford University Press 101(2577): 84–85.

Isaacson JS & Scanziani M (2011). How inhibition shapes cortical activity. Neuron 72(2): 231–243.

Iwamura Y, Tanaka M, Sakamoto M, et al. (1983a). Functional subdivisions representing different finger regions in area 3 of the first somatosensory cortex of the conscious monkey. Exp Brain Res, Springer-Verlag 51(3): 315–326.

Iwamura Y, Tanaka M, Sakamoto M, et al. (1983b). Converging patterns of finger representation and complex response properties of neurons in area 1 of the first somatosensory cortex of the conscious monkey. Exp Brain Res 51(3): 327–337.

Iyengar S, Qi H-X, Jain N, et al. (2007). Cortical and thalamic connections of the representations of the teeth and tongue in somatosensory cortex of new world monkeys. J Comp Neurol 501(1): 95–120.

Jacob V, Le Cam J, Ego-Stengel V, et al. (2008). Emergent properties of tactile scenes selectively activate barrel cortex neurons. Neuron 60(6): 1112–1125.

Jacob V, Petreanu L, Wright N, et al. (2012). Regular spiking and intrinsic bursting pyramidal cells show orthogonal forms of experience-dependent plasticity in layer V of barrel cortex. Neuron 73(2): 391–404.

Jain N, Catania KC & Kaas JH (1997). Deactivation and reactivation of somatosensory cortex after dorsal spinal cord injury. Nature 386(6624): 495–498.

Jain N, Catania KC & Kaas JH (1998a). A histologically visible representation of the fingers and palm in primate area 3b and its immutability following long-term deafferentations. Cereb Cortex 8(3): 227–236.

Jain N, Florence SL & Kaas JH (1998b). Reorganization of somatosensory cortex after nerve and spinal cord injury. News Physiol Sci 13: 143–149.

Jain N, Qi HX, Catania KC, et al. (2001). Anatomic correlates of the face and oral cavity representations in the somatosensory cortical area 3b of monkeys. J Comp Neurol 429(3): 455–468.

Jain N, Qi H-X, Collins CE, et al. (2008). Large-scale reorganization in the somatosensory cortex and thalamus after sensory loss in macaque monkeys. J Neurosci 28(43): 11042–11060.

Jenkins WM & Merzenich MM (1987). Reorganization of neocortical representations after brain injury: a neurophysiological model of the bases of recovery from stroke. Prog Brain Res 71: 249–266.

Jenkins WM, Merzenich MM, Ochs MT, et al. (1990). Functional reorganization of primary somatosensory cortex in adult owl monkeys after behaviorally controlled tactile stimulation. J Neurophysiol 63(1): 82–104.

Jensen KF & Killackey HP (1987). Terminal arbors of axons projecting to the somatosensory cortex of the adult rat. I. The normal morphology of specific thalamocortical afferents. J Neurosci 7(11): 3529–3543.

Jones EG (1975). Lamination and differential distribution of thalamic afferents within the sensory-motor cortex of the squirrel monkey. J Comp Neurol 160(2): 167–203.

Jones EG & Friedman DP (1982). Projection pattern of functional components of thalamic ventrobasal complex on monkey somatosensory cortex. J Neurophysiol 48(2): 521–544.

Jones EG, Schwark HD & Callahan PA (1986). Extent of the ipsilateral representation in the ventral posterior medial nucleus of the monkey thalamus. Exp Brain Res 63(2): 310–320.

Jutzeler CR, Curt A & Kramer JLK (2015). Relationship between chronic pain and brain reorganization after deafferentation: A systematic review of functional MRI findings. NeuroImage Clin 9: 599–606.

Kaas JH (1983). What, if anything, is SI? Organization of first somatosensory area of cortex. Physiol Rev 63(1): 206–231.

Kaas JH (1997). Topographic maps are fundamental to sensory processing. Brain Res Bull 44(2): 107–112.

Kaas JH (2008). The somatosensory thalamus and associated pathways. In: Basbaum A, et al. (eds.), *The Senses: A Comprehensive Reference*, v. 6, pp. 117–141 (6.07).

Kaas JH, Nelson RJ, Sur M, et al. (1979). Multiple representations of the body within the primary somatosensory cortex of primates. Science 204(4392): 521–523.

Kaas JH, Nelson RJ, Sur M, et al. (1984). The somatotopic organization of the ventroposterior thalamus of the squirrel monkey, Saimiri sciureus. J Comp Neurol 226(1): 111–140.

Kaas JH, Qi H-X & Iyengar S (2006). Cortical network for representing the teeth and tongue in primates. Anat Rec A Discov Mol Cell Evol Biol 288(2): 182–190.

Kaas JH, Qi H-X, Burish MJ, et al. (2008). Cortical and subcortical plasticity in the brains of humans, primates, and rats after damage to sensory afferents in the dorsal columns of the spinal cord. Exp Neurol 209(2): 407–416.

Kambi N, Halder P, Rajan R, et al. (2014). Large-scale reorganization of the somatosensory cortex following spinal cord injuries is due to brainstem plasticity. Nat Commun 5: 3602.

Kanold PO, Nelken I & Polley DB (2014). Local versus global scales of organization in auditory cortex. Trends Neurosci 37(9): 502–510.

Karl A, Birbaumer N, Lutzenberger W, et al. (2001). Reorganization of motor and somatosensory cortex in upper extremity amputees with phantom limb pain. J Neurosci 21(10): 3609–3618.

Kell CA, von Kriegstein K, Rösler A, et al. (2005). The sensory cortical representation of the human penis: revisiting somatotopy in the male homunculus. J Neurosci 25(25): 5984–5987.

Kerr JND, de Kock CPJ, Greenberg DS, et al. (2007). Spatial organization of neuronal population responses in layer 2/3 of rat barrel cortex. J Neurosci 27(48): 13316–13328.

Kichula EA & Huntley GW (2008). Developmental and comparative aspects of posterior medial thalamocortical innervation of the barrel cortex in mice and rats. J Comp Neurol 509(3): 239–258.

Kim U & Ebner FF (1999). Barrels and septa: separate circuits in rat barrels field cortex. J Comp Neurol 408(4): 489–505.

Knott GW, Quairiaux C, Genoud C, et al. (2002). Formation of dendritic spines with GABAergic synapses induced by whisker stimulation in adult mice. Neuron 34(2): 265–273.

Kolasinski J, Makin TR, Jbabdi S, et al. (2016). Investigating the stability of fine-grain digit somatotopy in individual human participants. J Neurosci 36(4): 1113–1127.

Krause T, Kurth R, Ruben J, et al. (2001). Representational overlap of adjacent fingers in multiple areas of human primary somatosensory cortex depends on electrical stimulus intensity: an fMRI study. Brain Res 899(1-2): 36–46.

Kremer Y, Léger J-F, Goodman D, et al. (2011). Late emergence of the vibrissa direction selectivity map in the rat barrel cortex. J Neurosci 31(29): 10689–10700.

Krubitzer LA & Kaas JH (1987). Thalamic connections of three representations of the body surface in somatosensory cortex of gray squirrels. J Comp Neurol 265(4): 549–580.

Krubitzer LA & Kaas JH (1990). The organization and connections of somatosensory cortex in marmosets. J Neurosci 10(3): 952–974.

Krubitzer L, Clarey J, Tweedale R, et al. (1995). A redefinition of somatosensory areas in the lateral sulcus of macaque monkeys. J Neurosci 15(5 Pt 2): 3821–3839.

Krubitzer L, Huffman KJ, Disbrow E, et al. (2004). Organization of area 3a in macaque monkeys: contributions to the cortical phenotype. J Comp Neurol 471(1): 97–111.

Krubitzer L, Campi KL & Cooke DF (2011). All rodents are not the same: a modern synthesis of cortical organization. Brain Behav Evol 78(1): 51–93.

Kuhlman SJ, Olivas ND, Tring E, et al. (2013). A disinhibitory microcircuit initiates critical-period plasticity in the visual cortex. Nature 501(7468): 543–546.

Kurth R, Villringer K, Curio G, et al. (2000). fMRI shows multiple somatotopic digit representations in human primary somatosensory cortex. Neuroreport 11(7): 1487–1491.

Land PW & Simons DJ (1985). Cytochrome oxidase staining in the rat SmI barrel cortex. J Comp Neurol 238(2): 225–235.

Land PW & Erickson SL (2005). Subbarrel domains in rat somatosensory (S1) cortex. J Comp Neurol 490(4): 414–426.

Land PW, Buffer SA & Yaskosky JD (1995). Barreloids in adult rat thalamus: three-dimensional architecture and relationship to somatosensory cortical barrels. J Comp Neurol 355(4): 573–588.

Larsen DD & Callaway EM (2006). Development of layer-specific axonal arborizations in mouse primary somatosensory cortex. J Comp Neurol 494(3): 398–414.

Le Cam J, Estebanez L, Jacob V, et al. (2011). Spatial structure of multiwhisker receptive fields in the barrel cortex is stimulus dependent. J Neurophysiol 106(2): 986–998.

Lee KJ & Woolsey TA (1975). A proportional relationship between peripheral innervation density and cortical neuron number in the somatosensory system of the mouse. Brain Res 99(2): 349–353.

Lenschow C, Copley S, Gardiner JM, et al. (2016). Sexually monomorphic maps and dimorphic responses in rat genital cortex. Curr Biol 26(1): 106–113.

Leyton ASF & Sherrington CS (1917). Observations on the excitable cortex of the chimpanzee, orang-utan, and gorilla. Q J Exp Physiol 11(2): 135–222.

Li CX, Yang Q, Vemulapalli S, et al. (2013). Forelimb amputation-induced reorganization in the cuneate nucleus (CN) is not reflected in large-scale reorganization in rat forepaw barrel subfield cortex (FBS). Brain Res 1526: 26–43.

Li CX, Chappell TD, Ramshur JT, et al. (2014). Forelimb amputation-induced reorganization in the ventral posterior lateral nucleus (VPL) provides a substrate for large-scale cortical reorganization in rat forepaw barrel subfield (FBS). Brain Res 1583: 89–108.

Li H & Crair MC (2011). How do barrels form in somatosensory cortex? Ann N Y Acad Sci 1225: 119–129.

Li L, Bender KJ, Drew PJ, et al. (2009). Endocannabinoid signaling is required for development and critical period plasticity of the whisker map in somatosensory cortex. Neuron 64(4): 537–549.

Li L, Gainey MA, Goldbeck JE, et al. (2014). Rapid homeostasis by disinhibition during whisker map plasticity. Proc Natl Acad Sci USA 111(4): 1616–1621.

Liao C-C, Gharbawie OA, Qi H, et al. (2013). Cortical connections to single digit representations in area 3b of somatosensory cortex in squirrel monkeys and prosimian galagos. J Comp Neurol 521(16): 3768–3790.

Liao C-C, Reed JL, Kaas JH, et al. (2016). Intracortical connections are altered after long-standing deprivation of dorsal column inputs in the hand region of area 3b in squirrel monkeys. J Comp Neurol 524(7): 1494–1526.

Lichtenstein SH, Carvell GE & Simons DJ (1990). Responses of rat trigeminal ganglion neurons to movements of vibrissae in different directions. Somatosens Mot Res 7(1): 47–65.

Lipton ML, Liszewski MC, O'Connell MN, et al. (2010). Interactions within the hand representation in primary somatosensory cortex of primates. J Neurosci 30(47): 15895–15903.

Lu SM & Lin RC (1993). Thalamic afferents of the rat barrel cortex: a light- and electron-microscopic study using Phaseolus vulgaris leucoagglutinin as an anterograde tracer. Somatosens Mot Res 10(1): 1–16.

Lübke J, Egger V, Sakmann B, et al. (2000). Columnar organization of dendrites and axons of single and synaptically coupled excitatory spiny neurons in layer 4 of the rat barrel cortex. J Neurosci 20(14): 5300–5311.

Lübke J, Roth A, Feldmeyer D, et al. (2003). Morphometric analysis of the columnar innervation domain of neurons connecting layer 4 and layer 2/3 of juvenile rat barrel cortex. Cereb Cortex 13(10): 1051–1063.

Lustig BR, Friedman RM, Winberry JE, et al. (2013). Voltage-sensitive dye imaging reveals shifting spatiotemporal spread of whisker-induced activity in rat barrel cortex. J Neurophysiol 109(9): 2382–2392.

Ma PM (1991). The barrelettes—architectonic vibrissal representations in the brainstem trigeminal complex of the mouse. I. Normal structural organization. J Comp Neurol 309(2): 161–199.

Ma PM & Woolsey TA (1984). Cytoarchitectonic correlates of the vibrissae in the medullary trigeminal complex of the mouse. Brain Res 306(1-2): 374–379.

Makin TR, Scholz J, Filippini N, et al. (2013). Phantom pain is associated with preserved structure and function in the former hand area. Nat Commun 4: 1570.

Makin TR, Scholz J, Henderson Slater D, et al. (2015). Reassessing cortical reorganization in the primary sensorimotor cortex following arm amputation. Brain 138(Pt 8): 2140–2146.

Manger PR, Woods TM & Jones EG (1995). Representation of the face and intraoral structures in area 3b of the squirrel monkey (*Saimiri sciureus*) somatosensory cortex, with special reference to the ipsilateral representation. J Comp Neurol 362(4): 597–607.

Manger PR, Woods TM & Jones EG (1996). Representation of face and intra-oral structures in area 3b of macaque monkey somatosensory cortex. J Comp Neurol 371(4): 513–521.

Manger PR, Woods TM, Muñoz A, et al. (1997). Hand/face border as a limiting boundary in the body representation in monkey somatosensory cortex. J Neurosci 17(16): 6338–6351.

Manns ID, Sakmann B & Brecht M (2004). Sub- and suprathreshold receptive field properties of pyramidal neurones in layers 5A and 5B of rat somatosensory barrel cortex. J Physiol 556(Pt 2): 601–622.

Margolis DJ, Lütcke H, Schulz K, et al. (2012). Reorganization of cortical population activity imaged throughout long-term sensory deprivation. Nat Neurosci 15(11): 1539–1546.

Margolis DJ, Lütcke H & Helmchen F (2014). Microcircuit dynamics of map plasticity in barrel cortex. Curr Opin Neurobiol 24(1): 76–81.

Marik SA, Yamahachi H, McManus JNJ, et al. (2010). Axonal dynamics of excitatory and inhibitory neurons in somatosensory cortex. PLoS Biol 8(6): e1000395.

Marik SA, Yamahachi H, Meyer zum Alten Borgloh S, et al. (2014). Large-scale axonal reorganization of inhibitory neurons following retinal lesions. J Neurosci 34(5): 1625–1632.

Marshall WH, Woolsey CN & Bard P (1937). Cortical representation of tactile sensibility as indicated by cortical potentials. Science 85(2207): 388–390.

Marshall WH, Woolsey CN & Bard P (1941). Observations on cortical somatic sensory mechanisms of cat and monkey. J Neurophysiol 4(1): 1–24.

Martinez M, Brezun J-M, Zennou-Azogui Y, et al. (2009). Sensorimotor training promotes functional recovery and somatosensory cortical map reactivation following cervical spinal cord injury. Eur J Neurosci 30(12): 2356–2367.

Martuzzi R, van der Zwaag W, Farthouat J, et al. (2014). Human finger somatotopy in areas 3b, 1, and 2: a 7T fMRI study using a natural stimulus. Hum Brain Mapp 35(1): 213–226.

Mauguiere F & Courjon J (1978). Somatosensory epilepsy: a review of 127 cases. Brain 101(2): 307–332.

McCabe CS, Haigh RC, Halligan PW, et al. (2005). Simulating sensory-motor incongruence in healthy volunteers: implications for a cortical model of pain. Rheumatology (Oxford) 44(4): 509–516.

McCandlish CA, Li CX, Waters RS, et al. (1996). Digit removal leads to discrepancies between the structural and functional organization of the forepaw barrel subfield in layer IV of rat primary somatosensory cortex. Exp Brain Res 108(3): 417–426.

Merzenich MM, Kaas JH, Sur M, et al. (1978). Double representation of the body surface within cytoarchitectonic areas 3b and 1 in "SI" in the owl monkey (*Aotus trivirgatus*). J Comp Neurol 181(1): 41–73.

Merzenich MM, Kaas JH, Wall J, et al. (1983a). Topographic reorganization of somatosensory cortical areas 3b and 1 in adult monkeys following restricted deafferentation. Neuroscience 8(1): 33–55.

Merzenich MM, Kaas JH, Wall JT, et al. (1983b). Progression of change following median nerve section in the cortical representation of the hand in areas 3b and 1 in adult owl and squirrel monkeys. Neuroscience 10(3): 639–665.

Merzenich MM, Nelson RJ, Stryker MP, et al. (1984). Somatosensory cortical map changes following digit amputation in adult monkeys. J Comp Neurol 224(4): 591–605.

Meyer HS, Egger R, Guest JM, et al. (2013). Cellular organization of cortical barrel columns is whisker-specific. Proc Natl Acad Sci USA 110(47): 19113–19118.

Michels L, Mehnert U, Boy S, et al. (2010). The somatosensory representation of the human clitoris: an fMRI study. Neuroimage 49(1): 177–184.

Minnery BS & Simons DJ (2003). Response properties of whisker-associated trigeminothalamic neurons in rat nucleus principalis. J Neurophysiol 89(1): 40–56.

Minnery BS, Bruno RM & Simons DJ (2003). Response transformation and receptive-field synthesis in the lemniscal trigeminothalamic circuit. J Neurophysiol 90(3): 1556–1570.

Miquelajauregui A, Kribakaran S, Mostany R, et al. (2015). Layer 4 pyramidal neurons exhibit robust dendritic spine plasticity in vivo after input deprivation. J Neurosci 35(18): 7287–7294.

Miyamoto JJ, Honda M, Saito DN, et al. (2006). The representation of the human oral area in the somatosensory cortex: a functional MRI study. Cereb Cortex 16(5): 669–675.

Mogilner A, Grossman JA, Ribary U, et al. (1993). Somatosensory cortical plasticity in adult humans revealed by magnetoencephalography. Proc Natl Acad Sci USA 90(8): 3593–3597.

Mohajerani MH, Chan AW, Mohsenvand M, et al. (2013). Spontaneous cortical activity alternates between motifs defined by regional axonal projections. Nat Neurosci 16(10): 1426–1435.

Moore CI & Nelson SB (1998). Spatio-temporal subthreshold receptive fields in the vibrissa representation of rat primary somatosensory cortex. J Neurophysiol 80(6): 2882–2892.

Mountcastle VB (1957). Modality and topographic properties of single neurons of cat's somatic sensory cortex. J Neurophysiol 20(4): 408–434.

Mountcastle VB & Henneman E (1952). The representation of tactile sensibility in the thalamus of the monkey. J Comp Neurol 97(3): 409–439.

Mountcastle VB, Talbot WH, Sakata H, et al. (1969). Cortical neuronal mechanisms in flutter-vibration studied in unanesthetized monkeys. Neuronal periodicity and frequency discrimination. J Neurophysiol 32(3): 452–484.

Myers WA, Churchill JD, Muja N, et al. (2000). Role of NMDA receptors in adult primate cortical somatosensory plasticity. J Comp Neurol 418(4): 373–382.

Négyessy L, Pálfi E, Ashaber M, et al. (2013). Intrinsic horizontal connections process global tactile features in the primary somatosensory cortex: neuroanatomical evidence. J Comp Neurol 521(12): 2798–2817.

Nelson AJ, Blake DT & Chen R (2009). Digit-specific aberrations in the primary somatosensory cortex in Writer's cramp. Ann Neurol 66(2): 146–154.

Nelson RJ, Sur M, Felleman DJ, et al. (1980). Representations of the body surface in postcentral parietal cortex of *Macaca fascicularis*. J Comp Neurol 192(4): 611–643.

Nelson RJ & Kaas JH (1981). Connections of the ventroposterior nucleus of the thalamus with the body surface representations in cortical areas 3b and 1 of the cynomolgus macaque, (*Macaca fascicularis*). J Comp Neurol 199(1): 29–64.

Nevian T & Sakmann B (2006). Spine Ca^{2+} signaling in spike-timing-dependent plasticity. J Neurosci 26(43): 11001–11013.

Oberlaender M, Ramirez A & Bruno RM (2012). Sensory experience restructures thalamocortical axons during adulthood. Neuron 74(4): 648–655.

Ohki K, Chung S, Ch'ng YH, et al. (2005). Functional imaging with cellular resolution reveals precise micro-architecture in visual cortex. Nature 433(7026): 597–603.

Padberg J, Cerkevich C, Engle J, et al. (2009). Thalamocortical connections of parietal somatosensory cortical fields in macaque monkeys are highly divergent and convergent. Cereb Cortex 19(9): 2038–2064.

Parpia P (2011). Reappraisal of the somatosensory homunculus and its discontinuities. Neural Comput 23(12): 3001–3015.

Paul RL, Merzenich M & Goodman H (1972). Representation of slowly and rapidly adapting cutaneous mechanoreceptors of the hand in Brodmann's areas 3 and 1 of *Macaca mulatta*. Brain Res 36(2): 229–249.

Pearson PP, Li CX & Waters RS (1999). Effects of large-scale limb deafferentation on the morphological and physiological organization of the forepaw barrel subfield (FBS) in somatosensory cortex (SI) in adult and neonatal rats. Exp Brain Res 128(3): 315–331.

Pei Y-C, Denchev P V, Hsiao SS, et al. (2009). Convergence of submodality-specific input onto neurons in primary somatosensory cortex. J Neurophysiol 102(3): 1843–1853.

Penfield W & Boldrey E (1937). Somatic motor and sensory representation in the cerebral cortex of man as studied by electrical stimulation. Brain (Oxford) 60(4): 389–443.

Penfield W & Rasmussen T (1950). The cerebral cortex of man: a clinical study of localization of function. Macmillan, New York.

Peron SP, Freeman J, Iyer V, et al. (2015). A cellular resolution map of barrel cortex activity during tactile behavior. Neuron 86(3): 783–799.

Petersen CC & Sakmann B (2000). The excitatory neuronal network of rat layer 4 barrel cortex. J Neurosci 20(20): 7579–7586.

Petersen CC & Sakmann B (2001). Functionally independent columns of rat somatosensory barrel cortex revealed with voltage-sensitive dye imaging. J Neurosci 21(21): 8435–8446.

Petersen CCH & Crochet S (2013). Synaptic computation and sensory processing in neocortical layer 2/3. Neuron 78(1): 28–48.

Petersen CCH, Grinvald A & Sakmann B (2003). Spatiotemporal dynamics of sensory responses in layer 2/3 of rat barrel cortex measured in vivo by voltage-sensitive dye imaging combined with whole-cell voltage recordings and neuron reconstructions. J Neurosci 23(4): 1298–1309.

Petersen RS & Diamond ME (2000). Spatial-temporal distribution of whisker-evoked activity in rat somatosensory cortex and the coding of stimulus location. J Neurosci 20(16): 6135–6143.

Pilz K, Veit R, Braun C, et al. (2004). Effects of co-activation on cortical organization and discrimination performance. Neuroreport 15(17): 2669–2672.

Pluta S, Naka A, Veit J, et al. (2015). A direct translaminar inhibitory circuit tunes cortical output. Nat Neurosci 18(11): 1631–1640.

Polley DB, Chen-Bee CH & Frostig RD (1999). Two directions of plasticity in the sensory-deprived adult cortex. Neuron 24(3): 623–637.

Polley DB, Kvasnák E & Frostig RD (2004). Naturalistic experience transforms sensory maps in the adult cortex of caged animals. Nature 429(6987): 67–71.

Pons TP, Garraghty PE, Cusick CG, et al. (1985a). A sequential representation of the occiput, arm, forearm and hand across the rostrocaudal dimension of areas 1, 2 and 5 in macaque monkeys. Brain Res 335(2): 350–353.

Pons TP, Garraghty PE, Cusick CG, et al. (1985b). The somatotopic organization of area 2 in macaque monkeys. J Comp Neurol 241(4): 445–466.

Pons TP, Garraghty PE, Friedman DP, et al. (1987a). Physiological evidence for serial processing in somatosensory cortex. Science 237(4813): 417–420.

Pons TP, Wall JT, Garraghty PE, et al. (1987b). Consistent features of the representation of the hand in area 3b of macaque monkeys. Somatosens Res 4(4): 309–331.

Pons TP, Garraghty PE & Mishkin M (1988). Lesion-induced plasticity in the second somatosensory cortex of adult macaques. Proc Natl Acad Sci USA 85(14): 5279–5281.

Pons TP, Garraghty PE, Ommaya AK, et al. (1991). Massive cortical reorganization after sensory deafferentation in adult macaques. Science 252(5014): 1857–1860.

Pons TP, Garraghty PE & Mishkin M (1992). Serial and parallel processing of tactual information in somatosensory cortex of rhesus monkeys. J Neurophysiol 68(2): 518–527.

Pubols BH & Pubols LM (1971). Somatotopic organization of spider monkey somatic sensory cerebral cortex. J Comp Neurol 141(1): 63–75.

Qi H-X & Kaas JH (2004). Myelin stains reveal an anatomical framework for the representation of the digits in somatosensory area 3b of macaque monkeys. J Comp Neurol 477(2): 172–187.

Qi H-X & Kaas JH (2006). Organization of primary afferent projections to the gracile nucleus of the dorsal column system of primates. J Comp Neurol 499(2): 183–217.

Qi H-X, Lyon DC & Kaas JH (2002). Cortical and thalamic connections of the parietal ventral somatosensory area in marmoset monkeys (*Callithrix jacchus*). J Comp Neurol 443(2): 168–182.

Qi H-X, Preuss TM & Kaas JH (2008). Somatosensory areas of the cerebral cortex: architectonic characteristics and modular organization. In: Basbaum A, et al. (eds.), *The Senses: A Comprehensive Reference*, v. 6, pp. 143–169 (6.08).

Qi H-X, Gharbawie OA, Wong P, et al. (2011). Cell-poor septa separate representations of digits in the ventroposterior nucleus of the thalamus in monkeys and prosimian galagos. J Comp Neurol 519(4): 738–758.

Qi H-X, Kaas JH & Reed JL (2014). The reactivation of somatosensory cortex and behavioral recovery after sensory loss in mature primates. Front Syst Neurosci 8: 84.

Ramachandran VS (1993). Behavioral and magnetoencephalographic correlates of plasticity in the adult human brain. Proc Natl Acad Sci USA 90(22): 10413–10420.

Ramirez A, Pnevmatikakis EA, Merel J, et al. (2014). Spatiotemporal receptive fields of barrel cortex revealed by reverse correlation of synaptic input. Nat Neurosci 17(6): 866–875.

Randolph M & Semmes J (1974). Behavioral consequences of selective subtotal ablations in the postcentral gyrus of *Macaca mulatta*. Brain Res 70(1): 55–70.

Rausell E & Jones EG (1995). Extent of intracortical arborization of thalamocortical axons as a determinant of representational plasticity in monkey somatic sensory cortex. J Neurosci 15(6): 4270–4288.

Rausell E, Bickford L, Manger PR, et al. (1998). Extensive divergence and convergence in the thalamocortical projection to monkey somatosensory cortex. J Neurosci 18(11): 4216–4232.

Recanzone GH, Merzenich MM, Jenkins WM, et al. (1992a). Topographic reorganization of the hand representation in cortical area 3b owl monkeys trained in a frequency-discrimination task. J Neurophysiol 67(5): 1031–1056.

Recanzone GH, Merzenich MM & Jenkins WM (1992b). Frequency discrimination training engaging a restricted skin surface results in an emergence of a cutaneous response zone in cortical area 3a. J Neurophysiol 67(5): 1057–1070.

Reed JL, Pouget P, Qi H-X, et al. (2008). Widespread spatial integration in primary somatosensory cortex. Proc Natl Acad Sci USA 105(29): 10233–10237.

Reed JL, Qi H-X, Zhou Z, et al. (2010a). Response properties of neurons in primary somatosensory cortex of owl monkeys reflect widespread spatiotemporal integration. J Neurophysiol 103(4): 2139–2157.

Reed JL, Qi H-X, Pouget P, et al. (2010b). Modular processing in the hand representation of primate primary somatosensory cortex coexists with widespread activation. J Neurophysiol 104(6): 3136–3145.

Reed JL, Pouget P, Qi H-X, et al. (2012). Effects of spatiotemporal stimulus properties on spike timing correlations in owl monkey primary somatosensory cortex. J Neurophysiol 108(12): 3353–3369.

Rema V, Armstrong-James M, Jenkinson N, et al. (2006). Short exposure to an enriched environment accelerates plasticity in the barrel cortex of adult rats. Neuroscience 140(2): 659–672.

Remple MS, Henry EC & Catania KC (2003). Organization of somatosensory cortex in the laboratory rat (Rattus norvegicus): Evidence for two lateral areas joined at the representation of the teeth. J Comp Neurol 467(1): 105–118.

Rockland KS (2010). Five points on columns. Front Neuroanat 4: 22.

Roe AW, Chernov MM, Friedman RM, et al. (2015). In vivo mapping of cortical columnar networks in the monkey with focal electrical and optical stimulation. Front Neuroanat 9: 135.

Romo R, Hernández A, Zainos A, et al. (1998). Somatosensory discrimination based on cortical microstimulation. Nature 392(6674): 387–390.

Romo R, Hernández A, Zainos A, et al. (2000). Sensing without touching: psychophysical performance based on cortical microstimulation. Neuron 26(1): 273–278.

Rothschild G, Nelken I & Mizrahi A (2010). Functional organization and population dynamics in the mouse primary auditory cortex. Nat Neurosci 13(3): 353–360.

Rothemund Y, Qi H-X, Collins CE, et al. (2002). The genitals and gluteal skin are represented lateral to the foot in anterior parietal somatosensory cortex of macaques. Somatosens Mot Res 19(4): 302–315.

Ruben J, Schwiemann J, Deuchert M, et al. (2001). Somatotopic organization of human secondary somatosensory cortex. Cereb Cortex 11(5): 463–473.

Saal HP & Bensmaia SJ (2014). Touch is a team effort: interplay of submodalities in cutaneous sensibility. Trends Neurosci 37(12): 689–697.

Sakurai K, Akiyama M, Cai B, et al. (2013). The organization of submodality-specific touch afferent inputs in the vibrissa column. Cell Rep 5(1): 87–98.

Sánchez-Panchuelo RM, Besle J, Beckett A, et al. (2012). Within-digit functional parcellation of Brodmann areas of the human primary somatosensory cortex using functional magnetic resonance imaging at 7 tesla. J Neurosci 32(45): 15815–15822.

Sánchez-Panchuelo R-M, Besle J, Mougin O, et al. (2014). Regional structural differences across functionally parcellated Brodmann areas of human primary somatosensory cortex. Neuroimage 93 Pt 2: 221–230.

Sarko DK, Rice FL & Reep RL (2011). Mammalian tactile hair: divergence from a limited distribution. Ann N Y Acad Sci 1225: 90–100.

Sato K, Nariai T, Sasaki S, et al. (2002). Intraoperative intrinsic optical imaging of neuronal activity from subdivisions of the human primary somatosensory cortex. Cereb Cortex 12(3): 269–280.

Sato K, Nariai T, Tanaka Y, et al. (2005). Functional representation of the finger and face in the human somatosensory cortex: intraoperative intrinsic optical imaging. Neuroimage 25(4): 1292–1301.

Sato TR, Gray NW, Mainen ZF, et al. (2007). The functional microarchitecture of the mouse barrel cortex. PLoS Biol 5(7): e189.

Sawyer EK, Liao C-C, Qi H-X, et al. (2015). Subcortical barrelette-like and barreloid-like structures in the prosimian galago (*Otolemur garnetti*). Proc Natl Acad Sci USA 112(22): 7079–7084.

Schwartz TH, Chen LM, Friedman RM, et al. (2004). Intraoperative optical imaging of human face cortical topography: a case study. Neuroreport 15(9): 1527–1531.

Schweisfurth MA, Frahm J & Schweizer R (2014). Individual fMRI maps of all phalanges and digit bases of all fingers in human primary somatosensory cortex. Front Hum Neurosci 8: 658.

Shao YR, Isett BR, Miyashita T, et al. (2013). Plasticity of recurrent l2/3 inhibition and gamma oscillations by whisker experience. Neuron 80(1): 210–222.

Shepherd GMG, Stepanyants A, Bureau I, et al. (2005). Geometric and functional organization of cortical circuits. Nat Neurosci 8(6): 782–790.

Silva AC, Rasey SK, Wu X, et al. (1996). Initial cortical reactions to injury of the median and radial nerves to the hands of adult primates. J Comp Neurol 366(4): 700–716.

Simons DJ (1978). Response properties of vibrissa units in rat SI somatosensory neocortex. J Neurophysiol 41(3): 798–820.

Siucinska E & Kossut M (1996). Short-lasting classical conditioning induces reversible changes of representational maps of vibrissae in mouse SI cortex—a 2DG study. Cereb Cortex 6(3): 506–513.

Siucinska E & Kossut M (2004). Experience-dependent changes in cortical whisker representation in the adult mouse: a 2-deoxyglucose study. Neuroscience 127(4): 961–971.

Sripati AP, Yoshioka T, Denchev P, et al. (2006). Spatiotemporal receptive fields of peripheral afferents and cortical area 3b and 1 neurons in the primate somatosensory system. J Neurosci 26(7): 2101–2114.

Staiger JF, Bojak I, Miceli S, et al. (2014). A gradual depth-dependent change in connectivity features of supragranular pyramidal cells in rat barrel cortex. Brain Struct Funct: 1–21.

Stavrinou ML, Della Penna S, Pizzella V, et al. (2007). Temporal dynamics of plastic changes in human primary somatosensory cortex after finger webbing. Cereb Cortex 17(9): 2134–2142.

Stehberg J, Dang PT & Frostig RD (2014). Unimodal primary sensory cortices are directly connected by long-range horizontal projections in the rat sensory cortex. Front Neuroanat 8: 93.

Stent GS (1973). A physiological mechanism for Hebb's postulate of learning. Proc Natl Acad Sci USA 70(4): 997–1001.

Stern EA, Maravall M & Svoboda K (2001). Rapid development and plasticity of layer 2/3 maps in rat barrel cortex in vivo. Neuron 31(2): 305–315.

Sterr A, Müller MM, Elbert T, et al. (1998a). Changed perceptions in Braille readers. Nature 391(6663): 134–135.

Sterr A, Müller MM, Elbert T, et al. (1998b). Perceptual correlates of changes in cortical representation of fingers in blind multifinger Braille readers. J Neurosci 18(11): 4417–4423.

Stringer EA, Chen LM, Friedman RM, et al. (2011). Differentiation of somatosensory cortices by high-resolution fMRI at 7 T. Neuroimage 54(2): 1012–1020.

Stringer EA, Qiao PG, Friedman RM, et al. (2014). Distinct fine-scale fMRI activation patterns of contra- and ipsilateral somatosensory areas 3b and 1 in humans. Hum Brain Mapp 35(9): 4841–4857.

Sur M (1980). Receptive fields of neurons in areas 3b and 1 of somatosensory cortex in monkeys. Brain Res 198(2): 465–471.

Sur M, Merzenich MM & Kaas JH (1980). Magnification, receptive-field area, and "hypercolumn" size in areas 3b and 1 of somatosensory cortex in owl monkeys. J Neurophysiol 44(2): 295–311.

Sur M, Wall JT & Kaas JH (1981). Modular segregation of functional cell classes within the postcentral somatosensory cortex of monkeys. Science 212(4498): 1059–1061.

Sur M, Nelson RJ & Kaas JH (1982). Representations of the body surface in cortical areas 3b and 1 of squirrel monkeys: comparisons with other primates. J Comp Neurol 211(2): 177–192.

Sur M, Wall JT & Kaas JH (1984). Modular distribution of neurons with slowly adapting and rapidly adapting responses in area 3b of somatosensory cortex in monkeys. J Neurophysiol 51(4): 724–744.

Sur M, Garraghty PE & Bruce CJ (1985). Somatosensory cortex in macaque monkeys: laminar differences in receptive field size in areas 3b and 1. Brain Res 342(2): 391–395.

Tandon S, Kambi N, Lazar L, et al. (2009). Large-scale expansion of the face representation in somatosensory areas of the lateral sulcus after spinal cord injuries in monkeys. J Neurosci 29(38): 12009–12019.

Taoka M, Toda T, Iriki A, et al. (2000). Bilateral receptive field neurons in the hindlimb region of the postcentral somatosensory cortex in awake macaque monkeys. Exp Brain Res 134(2): 139–146.

Thakur PH, Fitzgerald PJ & Hsiao SS (2012). Second-order receptive fields reveal multidigit interactions in area 3b of the macaque monkey. J Neurophysiol 108(1): 243–262.

Timofeeva E, Mérette C, Emond C, et al. (2003). A map of angular tuning preference in thalamic barreloids. J Neurosci 23(33): 10717–10723.

Van Der Loos H (1976). Barreloids in mouse somatosensory thalamus. Neurosci Lett 2(1): 1–6.

Van der Loos H & Woolsey TA (1973). Somatosensory cortex: structural alterations following early injury to sense organs. Science 179(4071): 395–398.

Vaso A, Adahan H-M, Gjika A, et al. (2014). Peripheral nervous system origin of phantom limb pain. Pain 155(7): 1384–1391.

Vidyasagar R, Folger SE & Parkes LM (2014). Re-wiring the brain: increased functional connectivity within primary somatosensory cortex following synchronous co-activation. Neuroimage 92: 19–26.

Waite PM & Taylor PK (1978). Removal of whiskers in young rats causes functional changes in cerebral cortex. Nature 274(5671): 600–602.

Wall JT, Xu J & Wang X (2002). Human brain plasticity: an emerging view of the multiple substrates and mechanisms that cause cortical changes and related sensory dysfunctions after injuries of sensory inputs from the body. Brain Res Brain Res Rev 39(2-3): 181–215.

Wallace H & Fox K (1999). The effect of vibrissa deprivation pattern on the form of plasticity induced in rat barrel cortex. Somatosens Mot Res 16(2): 122–138.

Wallace H, Glazewski S, Liming K, et al. (2001). The role of cortical activity in experience-dependent potentiation and depression of sensory responses in rat barrel cortex. J Neurosci 21(11): 3881–3894.

Wang X, Merzenich MM, Sameshima K, et al. (1995). Remodelling of hand representation in adult cortex determined by timing of tactile stimulation. Nature 378(6552): 71–75.

Wang Z, Chen LM, Négyessy L, et al. (2013). The relationship of anatomical and functional connectivity to resting-state connectivity in primate somatosensory cortex. Neuron 78(6): 1116–1126.

Waters RS, Li CX & McCandlish CA (1995). Relationship between the organization of the forepaw barrel subfield and the representation of the forepaw in layer IV of rat somatosensory cortex. Exp Brain Res 103(2): 183–197.

Weiss T, Miltner WH, Huonker R, et al. (2000). Rapid functional plasticity of the somatosensory cortex after finger amputation. Exp Brain Res 134(2): 199–203.

Welker C (1976). Receptive fields of barrels in the somatosensory neocortex of the rat. J Comp Neurol 166(2): 173–189.

Welker E & Van der Loos H (1986). Quantitative correlation between barrel-field size and the sensory innervation of the whiskerpad: a comparative study in six strains of mice bred for different patterns of mystacial vibrissae. J Neurosci 6(11): 3355–3373.

Welker E, Rao SB, Dörfl J, et al. (1992). Plasticity in the barrel cortex of the adult mouse: effects of chronic stimulation upon deoxyglucose uptake in the behaving animal. J Neurosci 12(1): 153–170.

Welker E, Armstrong-James M, Bronchti G, et al. (1996). Altered sensory processing in the somatosensory cortex of the mouse mutant barrelless. Science 271(5257): 1864–1867.

Weller WL & Johnson JI (1975). Barrels in cerebral cortex altered by receptor disruption in newborn, but not in five-day-old mice (Cricetidoe and Muridae). Brain Res 83(3): 504–508.

Wellman CL, Arnold LL, Garman EE, et al. (2002). Acute reductions in GABAA receptor binding in layer IV of adult primate somatosensory cortex after peripheral nerve injury. Brain Res 954(1): 68–72.

Whitsel BL, Dreyer DA & Roppolo JR (1971). Determinants of body representation in postcentral gyrus of macaques. J Neurophysiol 34(6): 1018–1034.

Wilbrecht L, Holtmaat A, Wright N, et al. (2010). Structural plasticity underlies experience-dependent functional plasticity of cortical circuits. J Neurosci 30(14): 4927–4932.

Wilson SP & Bednar JA (2015). What, if anything, are topological maps for? Dev Neurobiol 75(6): 667–681.

Wilson SP, Law JS, Mitchinson B, et al. (2010). Modeling the emergence of whisker direction maps in rat barrel cortex. PLoS One 5(1): e8778.

Wimmer VC, Broser PJ, Kuner T, et al. (2010). Experience-induced plasticity of thalamocortical axons in both juveniles and adults. J Comp Neurol 518(22): 4629–4648.

Woolsey CN (1952). Patterns of localization in sensory and motor areas of the cerebral cortex. In: *Milbank Symposium: The Biology of Mental Health and Disease*. Hoeber, New York, pp. 192–206 (ch. 14).

Woolsey CN, Erickson TC & Gilson WE (1979). Localization in somatic sensory and motor areas of human cerebral cortex as determined by direct recording of evoked potentials and electrical stimulation. J Neurosurg 51(4): 476–506.

Woolsey TA & Van der Loos H (1970). The structural organization of layer IV in the somatosensory region (SI) of mouse cerebral cortex. The description of a cortical field composed of discrete cytoarchitectonic units. Brain Res 17(2): 205–242.

Woolsey TA, Welker C & Schwartz RH (1975). Comparative anatomical studies of the SmL face cortex with special reference to the occurrence of "barrels" in layer IV. J Comp Neurol 164(1): 79–94.

Wright N & Fox K (2010). Origins of cortical layer V surround receptive fields in the rat barrel cortex. J Neurophysiol 103(2): 709–724.

Wright N, Glazewski S, Hardingham N, et al. (2008). Laminar analysis of the role of GluR1 in experience-dependent and synaptic depression in barrel cortex. Nat Neurosci 11(10): 1140–1142.

Xerri C (2012). Plasticity of cortical maps: multiple triggers for adaptive reorganization following brain damage and spinal cord injury. Neuroscientist 18(2): 133–148.

Xerri C, Stern JM & Merzenich MM (1994). Alterations of the cortical representation of the rat ventrum induced by nursing behavior. J Neurosci 14(3 Pt 2): 1710–1721.

Xerri C, Merzenich MM, Peterson BE, et al. (1998). Plasticity of primary somatosensory cortex paralleling sensorimotor skill recovery from stroke in adult monkeys. J Neurophysiol 79(4): 2119–2148.

Xerri C, Merzenich MM, Jenkins W, et al. (1999). Representational plasticity in cortical area 3b paralleling tactual-motor skill acquisition in adult monkeys. Cereb Cortex 9(3): 264–276.

Xerri C & Zennou-Azogui Y (2003). Influence of the postlesion environment and chronic piracetam treatment on the organization of the somatotopic map in the rat primary somatosensory cortex after focal cortical injury. Neuroscience 118(1): 161–177.

Yang TT, Gallen C, Schwartz B, et al. (1994). Sensory maps in the human brain. Nature 368(6472): 592–593.

Yassin L, Benedetti BL, Jouhanneau J-S, et al. (2010). An embedded subnetwork of highly active neurons in the neocortex. Neuron 68(6): 1043–1050.

Yu C, Derdikman D, Haidarliu S, et al. (2006). Parallel thalamic pathways for whisking and touch signals in the rat. PLoS Biol 4(5): e124.

CHAPTER 2

Alloway KD (2008). Information processing streams in rodent barrel cortex: the differential functions of barrel and septal circuits. Cereb Cortex 18(5): 979–989.

Andermann ML & Moore CI (2006). A somatotopic map of vibrissa motion direction within a barrel column. Nat Neurosci 9(4): 543–551.

Armstrong-James M & Fox K (1987). Spatiotemporal convergence and divergence in the rat S1 'barrel' cortex. J Comp Neurol 263(2): 265–281.

Armstrong-James M, Fox K & Das-Gupta A (1992). Flow of excitation within rat barrel cortex on striking a single vibrissa. J Neurophysiol 68(4): 1345–1358.

Atencio CA & Schreiner CE (2008). Spectrotemporal processing differences between auditory cortical fast-spiking and regular-spiking neurons. J Neurosci 28(15): 3897–3910.

Avermann M, Tomm C, Mateo C, et al. (2012). Microcircuits of excitatory and inhibitory neurons in layer 2/3 of mouse barrel cortex. J Neurophysiol 107(11): 3116–3134.

Bandyopadhyay S, Shamma SA & Kanold PO (2010). Dichotomy of functional organization in the mouse auditory cortex. Nat Neurosci 13(3): 361–368.

Benjamini Y & Hochberg Y (1995). Controlling the false discovery rate: a practical and powerful approach to multiple testing. J R Stat Soc B 57(1): 289–300.

Bock DD, Lee W-CA, Kerlin AM, et al. (2011). Network anatomy and in vivo physiology of visual cortical neurons. Nature 471(7337): 177–182.

Bonin V, Histed MH, Yurgenson S, et al. (2011). Local diversity and fine-scale organization of receptive fields in mouse visual cortex. J Neurosci 31(50): 18506–18521.

Bosman LWJ, Houweling AR, Owens CB, et al. (2011). Anatomical pathways involved in generating and sensing rhythmic whisker movements. Front Integr Neurosci 5(October): 53.

Brecht M & Sakmann B (2002). Dynamic representation of whisker deflection by synaptic potentials in spiny stellate and pyramidal cells in the barrels and septa of layer 4 rat somatosensory cortex. J Physiol 543(1): 49–70.

Bureau I, Von Paul F Saint & Svoboda K (2006). Interdigitated paralemniscal and lemniscal pathways in the mouse barrel cortex. PLoS Biol 4(12): 2361–2371.

Cardin JA, Palmer LA & Contreras D (2007). Stimulus feature selectivity in excitatory and inhibitory neurons in primary visual cortex. J Neurosci 27(39): 10333–10344.

Chase SM & Young ED (2007). First-spike latency information in single neurons increases when referenced to population onset. Proc Natl Acad Sci USA 104(12): 5175–5180.

Clancy KB, Schnepel P, Rao AT, et al. (2015). Structure of a single whisker representation in layer

2 of mouse somatosensory cortex. J Neurosci 35(9): 3946–3958.

de Kock CPJ De, Bruno RM, Spors H, et al. (2007). Layer- and cell-type-speci c suprathreshold stimulus representation in rat primary somatosensory cortex. J Physiol 581(1): 139–154.

Deschênes M & Urbain N (2016). Vibrissal afferents from trigeminus to cortices. In: Prescott TJ, Ahissar E, and Izhikevich E (eds), *Scholarpedia of Touch*, Paris: Atlantis Press, pp. 657–672.

DiCarlo JJ, Lane JW, Hsiao SS, et al. (1996). Marking microelectrode penetrations with fluorescent dyes. J Neurosci Methods 64(1): 75–81.

Estebanez L, Boustani S El, Destexhe A, et al. (2012). Correlated input reveals coexisting coding schemes in a sensory cortex. Nat Neurosci 15(12): 1691–1699.

Estebanez L, Bertherat J, Shulz DE, et al. (2016). A radial map of multi-whisker correlation selectivity in the rat barrel cortex. Nat Commun 7: 13528.

Feldmeyer D (2012). Excitatory neuronal connectivity in the barrel cortex. Front Neuroanat 6: Article 24.

Feldmeyer D, Brecht M, Helmchen F, et al. (2013). Barrel cortex function. Prog Neurobiol 103: 3–27.

Garion L, Dubin U, Rubin Y, et al. (2014). Texture coarseness responsive neurons and their mapping in layer 2–3 of the rat barrel cortex in vivo. Elife 3: e03405.

Glazewski S & Fox K (1996). Time course of experience-dependent synaptic potentiation and depression in barrel cortex of adolescent rats. J Neurophysiol 75(4): 1714–1729.

Glazewski S, Barth AL, Wallace H, et al. (1999). Impaired experience-dependent plasticity in barrel cortex of mice lacking the alpha and delta isoforms of CREB. Cereb Cortex 9(3): 249–256.

Glazewski S, Giese KP, Silva A, et al. (2000). The role of alpha-CaMKII autophosphorylation in neocortical experience-dependent plasticity. Nat Neurosci 3(9): 911–918.

Harris KD & Mrsic-Flogel TD (2013). Cortical connectivity and sensory coding. Nature 503(7474): 51–58.

Hill DN, Mehta SB & Kleinfeld D (2011). Quality metrics to accompany spike sorting of extracellular signals. J Neurosci 31(24): 8699–8705.

Hofer SB, Ko H, Pichler B, et al. (2011). Differential connectivity and response dynamics of excitatory and inhibitory neurons in visual cortex. Nat Neurosci 14(8): 1045–1052.

Kanold PO, Nelken I & Polley DB (2014). Local versus global scales of organization in auditory cortex. Trends Neurosci 37(9): 502–510.

Kerlin AM, Andermann ML, Berezovskii VK, et al. (2010). Broadly tuned response properties of

diverse inhibitory neuron subtypes in mouse visual cortex. Neuron 67(5): 858–871.

Kremer Y, Léger J-F, Goodman D, et al. (2011). Late emergence of the vibrissa direction selectivity map in the rat barrel cortex. J Neurosci 31(29): 10689–10700.

Kuhlman SJ, Tring E & Trachtenberg JT (2011). Fast-spiking interneurons have an initial orientation bias that is lost with vision. Nat Neurosci 14(9): 1121–1123.

Le Cam J, Estebanez L, Jacob V, et al. (2011). Spatial structure of multiwhisker receptive fields in the barrel cortex is stimulus dependent. J Neurophysiol 106(2): 986–998.

Ludwig KA, Miriani RM, Langhals NB, et al. (2009). Using a common average reference to improve cortical neuron recordings from microelectrode arrays. J Neurophysiol 101(3): 1679–1689.

Mateo C, Avermann M, Gentet LJ, et al. (2011). In vivo optogenetic stimulation of neocortical excitatory neurons drives brain-state-dependent inhibition. Curr Biol 21(19): 1593–1602.

Moore AK & Wehr M (2013). Parvalbumin-expressing inhibitory interneurons in auditory cortex are well-tuned for frequency. J Neurosci 33(34): 13713–13723.

Oberlaender M, De Kock CPJ, Bruno RM, et al. (2012). Cell type-specific three-dimensional structure of thalamocortical circuits in a column of rat vibrissal cortex. Cereb Cortex 22(10): 2375–2391.

Ohki K, Chung S, Ch'ng YH, et al. (2005). Functional imaging with cellular resolution reveals precise micro-architecture in visual cortex. Nature 433(7026): 597–603.

Petersen CCH & Crochet S (2013). Synaptic computation and sensory processing in neocortical Layer 2/3. Neuron 78(1): 28–48.

Petersen CCH, Grinvald A & Sakmann B (2003). Spatiotemporal dynamics of sensory responses in layer 2/3 of rat barrel cortex measured in vivo by voltage-sensitive dye imaging combined with whole-cell voltage recordings and neuron reconstructions. J Neurosci 23(4): 1298–1309.

Rhoades RW, Crissman RS, Bennett-Clarke CA, et al. (1996). Development and plasticity of local intracortical projections within the vibrissae representation of the rat primary somatosensory cortex. J Comp Neurol 370(4): 524–535.

Rothschild G, Nelken I & Mizrahi A (2010). Functional organization and population dynamics in the mouse primary auditory cortex. Nat Neurosci 13(3): 353–360.

Sachidhanandam S, Sermet BS & Petersen CCH (2016). Parvalbumin-expressing GABAergic neurons in mouse barrel cortex contribute to gating a goal-directed sensorimotor transformation. Cell Rep 15(4): 700–706.

Sato TR, Gray NW, Mainen ZF, et al. (2007). The functional microarchitecture of the mouse barrel cortex. PLoS Biol 5(7): 1440–1452.

Sato TR & Svoboda K (2010). The functional properties of barrel cortex neurons projecting to the primary motor cortex. J Neurosci 30(12): 4256–4260.

Shepherd GMG (2005). Laminar and columnar organization of ascending excitatory projections to layer 2/3 pyramidal neurons in rat barrel cortex. J Neurosci 25(24): 5670–5679.

Simons DJ (1978). Response properties of vibrissa units in rat SI somatosensory neocortex. J Neurophysiol 41(3): 798–820.

Staiger JF, Bojak I, Miceli S, et al. (2014). A gradual depth-dependent change in connectivity features of supragranular pyramidal cells in rat barrel cortex. Brain Struct Funct: 1–21.

Victor JD (2002). Binless strategies for estimation of information from neural data. Phys Rev E - Stat Nonlinear, Soft Matter Phys 66(5): 1–15.

Winkowski DE & Kanold PO (2013). Laminar transformation of frequency organization in auditory cortex. J Neurosci 33(4): 1498–1508.

Woolsey TA & Van der Loos H (1970). The structural organization of layer IV in the somatosensory region (SI) of mouse cerebral cortex. The description of a cortical field composed of discrete cytoarchitectonic units. Brain Res 17(2): 205–242.

Zariwala HA, Madisen L, Ahrens KF, et al. (2011). Visual tuning properties of genetically identified layer 2/3 neuronal types in the primary visual cortex of cre-transgenic mice. Front Syst Neurosci 4: Article 162.